PHILIPS

APPLICATION BOOK

ELECTRONIC COMPONENTS AND MATERIALS DIVISION

PHOTOMULTIPLIERS

Photomultipliers

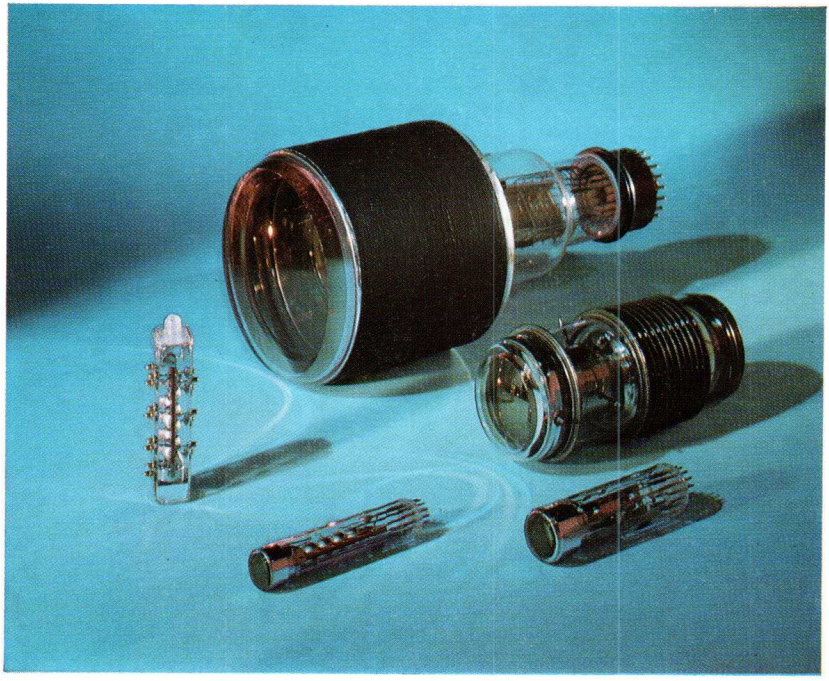

Photomultipliers

J. M. Schonkeren

Edited by H. Kater and L. J. Thompson

PUBLICATIONS DEPARTMENT
ELECTRONIC COMPONENTS AND MATERIALS DIVISION

Contents

Foreword

Everyone has heard of photomultipliers, but until recently few have had occasion to work with them — a situation that is being rapidly changed by the growth of scientific and industrial interest in weak and short-lived radiation. It is to those who have not, as it were, grown up with photomultipliers that we primarily address this book.

Mr. Schonkeren has adapted both the content and the form of the book to the needs of those who use photomultipliers, bearing in mind the questions that we, as manufacturers, are often asked. In doing so he has to some extent removed one of our most valuable sources of feed-back, but not, we hope, entirely. Constant interchange between user and manufacturer is a vital stimulus to improving the product and extending its scope. We look forward to it continuing.

Dr. P. Romberg

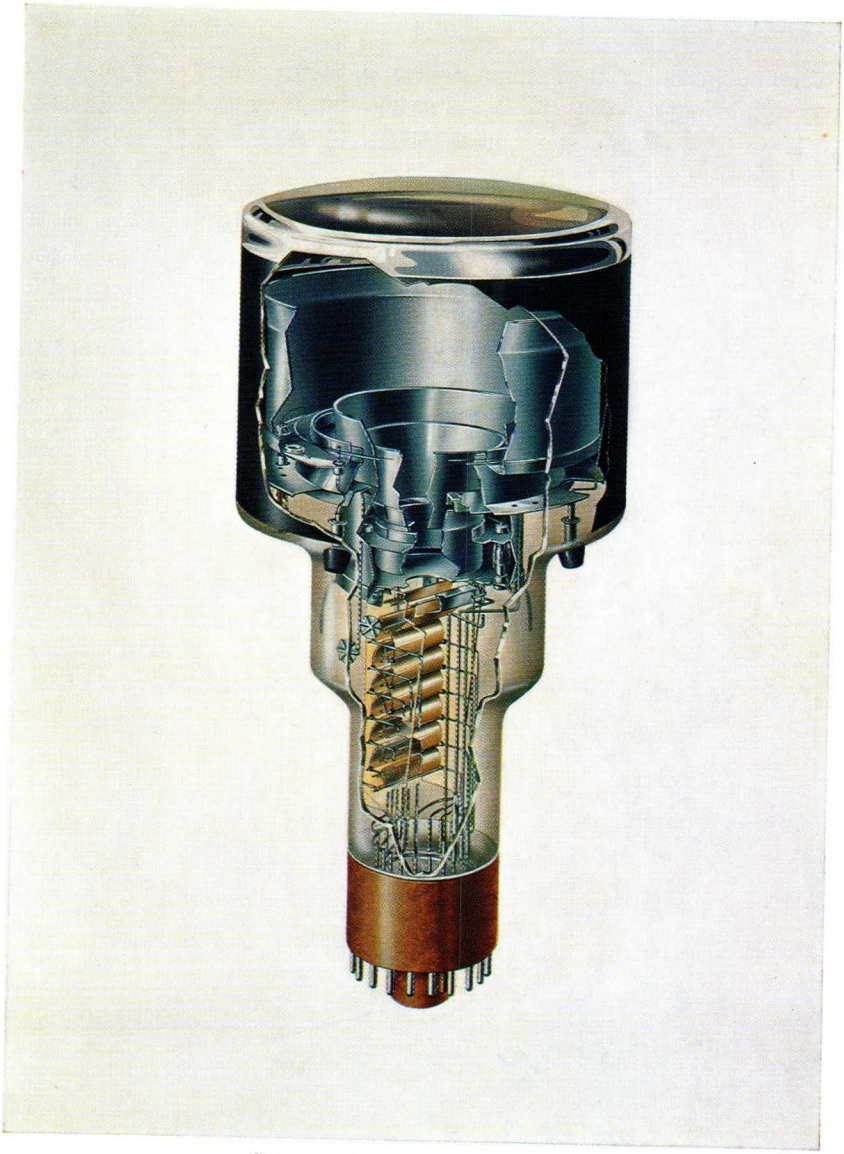

Cut-away view of a photomultiplier

Definitions of Photomultiplier Characteristics

1 Definitions of Electrical terms *

Photocurrent: current at the photocathode caused by incident radiation.

Dark current: the current flowing at the cathode (cathode dark current) or at the anode (anode dark current) in the absence of irradiation.

Equivalent dark current input: that incident radiation that would cause a d.c. output current equal to the dark current.

Equivalent noise input (ENI): the value of incident radiation which, when modulated in a stated manner, produces an r.m.s. signal output current equal to the dark current noise both in a stated bandwidth. The ENI is usually expressed in terms of luminous flux.

Noise equivalent power (NEP): as ENI, but expressed in watts of incident radiation at a stated wavelength.

Background noise pulses: frequency of dark current pulses measured in the anode above a stated threshold.
Signal noise: noise current due to random fluctuations in the electrical signal current (shot noise).
Saturation voltage: the lowest voltage that if increased produces negligible increase in photocurrent with constant illumination.

Saturation current: That output current that is only negligibly increased by an increase of either:
— illumination under constant operating conditions, or
— of operating voltage under constant illumination.

Linearity: the extent to which there is a direct proportional correspondence between illumination and output current. Usually expressed as the maximum output current at which such a correspondence (within a stated tolerance) exists.

Collection efficiency: that percentage of the electrons emitted by the photocathode that lands on the first dynode.

2 Definitions relating to Sensitivity *

Cathode radiant sensitivity (N_{kr}): the photocurrent emitted per watt of incident light flux, usually expressed in mA/W and measured at the wavelength of maximum response.

Quantum efficiency: the ratio between the number of emitted photoelectrons and the number of incident photons. Quantum efficiency (η_q) of a given wavelength (λ) for radiation is given by:

$$\eta_q = N_{kr}\,(12.4/\lambda)\,100\,\%,$$

where N_{kr} is the cathode radiant sensitivity in mA/W and λ is in Å.

Cathode luminous sensitivity (N_k): the photocurrent emitted per lumen of incident light flux, usually expressed in μA/lm.

Current amplification or gain (G): the ratio between anode signal current and cathode signal current at stated electrode voltages.

Anode sensitivity: the product of gain and cathode sensitivity: the luminous anode sensitivity $N_a = GN_k$, the radiant anode sensitivity $N_{ar} = GN_{kr}$.

Single photon detection efficiency: the proportion of single photons incident on the cathode that produces an output at the anode. Usually expressed as a percentage.

Absolute spectral sensitivity: the radiant sensitivity for monochromatic illumination at a stated wavelength, expressed in mA/W.

Absolute spectral sensitivity characteristic: the relation between wavelength and absolute spectral sensitivity.

Relative spectral sensitivity: the ratio between the radiant sensitivity at any given wavelength and the radiant sensitivity at a reference wavelength, usually the wavelength of maximum response. If the detector is nonlinear the photocurrent at both wavelengths must be equal.

Relative spectral sensitivity characteristic: the relation between wavelength and relative spectral sensitivity, in most cases normalized at a specified wavelength, usually that of maximum response.

Fatigue: a temporary change in sensitivity as may occur during the course of operation. Fatigue effects are a function of output current, history and type of materials used to form the cathode and dynodes. Two main effects can be distinguished, namely.

— *drift*, a slow change in sensitivity over a period of time
— *shift*, an abrupt change in sensitivity that results from an abrupt change in illumination.

3 Definitions of Terms involving Time *

Delta function light input: a pulse of finite integrated light flux and infinitesimal width.

Rise time: the time that the electrical output takes to rise from a stated low value to a stated higher value when the illumination is instantaneously increased. The values usually taken are at 10% and 90% of the final value.

Decay time: the time that the electric output takes to fall from a stated high value to a stated lower value when the illumination is instantaneously decreased. The values usually taken are at 90% and 10% of the original value.

Transit time: the interval between the arrival of a delta function of light pulse at the entrance window of the photomultiplier and the time at which the output pulse at the anode terminal reaches peak amplitude.

Transit time spread: the difference between the minimum and maximum transit times measured with respect to a certain point on the output pulse for a delta light function at a given point on the entrance window.

Transit time difference: a systematic relation between transit time and position of illumination on the photocathode. The reference position being usually the centre of the photocathode.

* *Note.* These definitions are, for the most part, linguistically edited versions of the definitions given in I.E.C. Document 39 (Central Office) 228 and Publication 306-1[1]. For terms not defined by the I.E.C. commonly accepted definitions have been given.

1 Construction and Operation of Photomultipliers

A photomultiplier is an electron tube with a light-sensitive element that converts incident light into an electron current, and a multiplier that amplifies the current to a useful level. The term electron multiplier phototube is preferred by some.

The parts shown in Fig. 1 are:

— The photocathode, a light-sensitive layer shown as a vacuum deposited layer on the glass envelope. Such layers, that only partly absorb incident light are known as semi-transparent cathodes. Others that are deposited on a metal base are opaque, both are illustrated in Figs. 2 and 3.

— The electron-optical input system, which ensures that as many electrons from the cathode as possible are directed towards the first dynode of the multiplier.

— The multiplier, which is a series of secondary emission electrodes called dynodes. An electron impinging on a dynode releases secondary electrons that are directed by electric fields towards the next dynode.

— The collector or anode, that collects the stream of electrons created in the multiplier and from which the output signal is taken.

In the following chapters the operation of the several parts will be discussed in detail.

1.1 The Photocathode

That metals emit electrons under the influence of light has long been known. According to Einstein, the kinetic energy of an electron released from a metal by the photoelectric effect is:

$$W_k = hv - \phi, \tag{1}$$

in which hv is the energy of the incident photon h being Planck's constant and v the frequency associated with the photon. By the laws of conservation of energy and momentum, when a photon collides with an electron in a material, the entire energy is transferred to the electron. The difference between the energy of the original photon and the energy

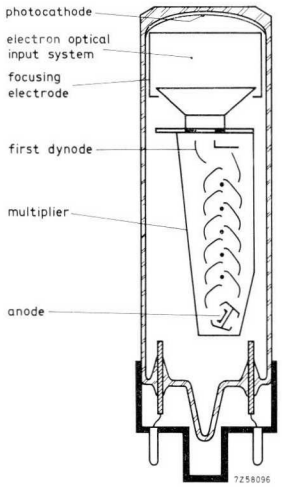

Fig. 1. Cross-section of a photomultiplier (simplified).

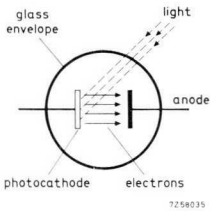

Fig. 2. Principle of operation of an opaque cathode.

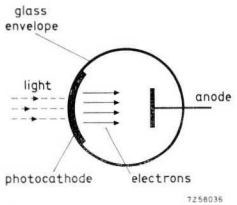

Fig. 3. Principle of operation of a semi-transparent cathode.

of the electron after it has left the material is the photoelectric work function, ϕ, the energy expended by the electron in escaping from the metal. It should be noted that as photon energy is directly related to frequency, the threshold condition is associated with the wavelength of radiation:

$$\phi = h\nu_0 = hc/\lambda_0, \tag{2}$$

ν_0 being the threshold frequency, λ_0 the threshold wavelength. If ϕ is known the threshold wavelength can be calculated. With ϕ expressed in electron volts (1 eV $= 1.6 \times 10^{-19}$ J),

$$\lambda_0 = 6.624 \times 10^{-34} \times 3 \times 10^{18} / 1.6 \times 10^{-19} \phi = 12395/\phi \text{ Å} \tag{3}$$

The photoelectric work functions of various metals are given in the table.

Table 1. Work function and threshold wavelength of various metals. *

element	ϕ	λ_0	element	ϕ	λ_0
Ag	4.7 eV	2610 Å	**Li**	2.35 eV	5300 Å
Al	4.08 eV	3560 Å	Mo	4.2 eV	2960 Å
Au	4.8 eV	2600 Å	**Na**	2.28 eV	5000 Å
Ba	2.48 eV	5000 Å	Ni	5.03 eV	2450 Å
C	4.34 eV	2850 Å	Pt	6.3 eV	1950 Å
Ca	2.70 eV	4600 Å	**Rb**	2.1 eV	5800 Å
Cs	1.80 eV	6600 Å	Sb	4.03 eV	3000 Å
Cu	4.30 eV	2900 Å	Sr	2.74 eV	4530 Å
Fe	4.6 eV	2700 Å	Ta	4.13 eV	3000 Å
Ge	4.5 eV	2750 Å	Th	3.38 eV	3670 Å
K	2.24 eV	5600 Å	W	4.53 eV	2650 Å
			Zn	3.8 eV	3720 Å

The table shows that the alkali metals (printed in bold) have the lowest work functions, and are thus of first interest for photoelectrical applications.

In photodetectors the conversion of photons into electrons should be as efficient as possible. The photo (or quantum) efficiency is determined mainly by the nature of the material of the photocathode. For those quoted in the table it is even less than 0.1 %, which means that on an average 1,000 photons are needed to release 1 electron from the cathode.

* Photoelectric work functions are difficult to measure and results differ from worker to worker. The values quoted are illustrative rather than definitive.

Quantum efficiencies of 20% or even 30% are available with semiconductors, which explains why most modern photocathodes are of semiconductor material.

To show how the photoelectric effect differs in metals and semiconductors, it will be necessary to discuss the atomic structure of the various materials with reference to the quantum theory.

1.1.1 Energy Band Theory

By present theory the electrons of an atom, within a material, occupy fixed bands about the nucleus; the bands furthest from the nucleus are those with the highest energy levels and the electrons occupying them have the loosest attachment to the nucleus. The bands represent sets of allowed, discrete, energy levels each of which, by the Pauli exclusion principle, can only be occupied by one electron. The allowed bands are separated by forbidden bands to cross which an electron must gain energy equivalent to the gap energy.

The outermost occupied band is the valence band, so called because it determines the ability of an atom to combine with others. Outside it is another allowed band — the conduction band — within which electrons are free to move under the influence of an electric field. The main difference between conductors, semiconductors and insulators is in the width of the forbidden gap separating the valence and conduction bands. As illustrated in Fig. 4, in the case of conductors, the conduction and valence bands are contiguous, in semiconductors there is a gap of about 1 eV, and in insulators an even wider gap of about 2 eV.

In general, added energy raises electrons from the valence band to the conduction band where they can travel through the material. The energy

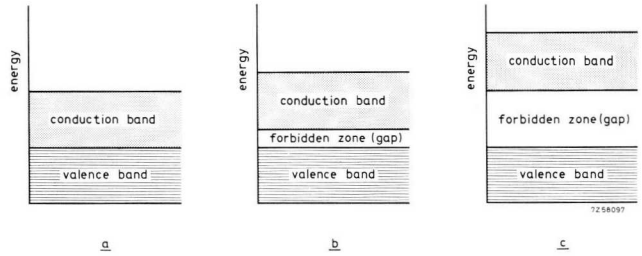

Fig. 4. Energy band diagram of (a) a conductor, (b) a semiconductor, (c) an insulator.

can be supplied in several ways: by photon bombardment (photoelectric emission), by an applied electric field (field emission), by heat (thermionic emission), or by electron bombardment (secondary emission).

In travelling through the material electrons are likely to collide with other electrons. At each collision the energy is shared between the colliding electrons and, if there are many collisions, there is little chance of an electron reaching the surface with sufficient energy to escape, bearing in mind that there is an energy barrier at the surface (electron affinity). This is the case in conductors as they have many free electrons. Semiconductors, on the other hand, have comparatively few free electrons and any collisions an excited electron may have are with the atoms of the crystal lattice. Owing to the considerable difference in mass between electrons and atoms, the electrons lose little energy and are thus much more likely to have enough energy to overcome the energy barrier at the surface.

The other point of difference between semiconductors and conductors is observed when electrons are raised from the valence band: When the electron transfers, it leaves a vacancy in the valence band of the atom concerned. With conductors this vacancy (or hole as it is known) is immediately filled by a free electron from the conduction band, but with semiconductors, because of the lack of free electrons, the hole is filled by another bound electron. This causes another hole which is again filled, so that the hole, evidenced as a positive charge, appears to move through the material.

Photoelectric emission and secondary emission are of primary importance in photomultipliers because while the first provides the initial current the second is responsible for its subsequent amplification. Thermionic emission is also of interest but in the sense of being a hindrance rather than a help.

1.1.2 Photoelectric Effect

As pointed out in sect 1.1, the quantum efficiency of metals is much lower than that of semiconductors. This is partly due to the fundamental differences in energy transfer, as explained in sect. 1.1.1. An electron excited by a photon is more likely to leave a semiconductor than a metal.

Another factor effecting quantum efficiency is the absorption of photons by the material. This may take place at the surface or in the body of the material.[2] In the first case the resultant photoemission is known as

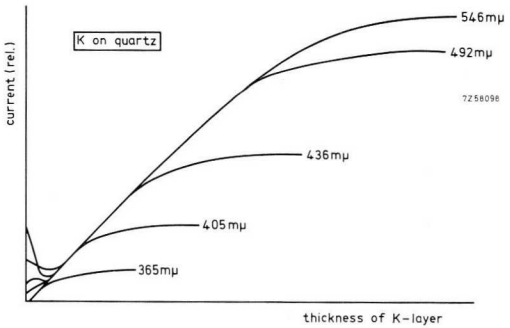

Fig. 5. Dependence of the photoelectric emission of a layer of potassium on its thickness.

"surface effect", in the second case, "volume effect". As a result of the characteristic properties of the surface no more than 10% of the photons can be absorbed here.[3] The quantum efficiency being, therefore, less than 10%, unless a volume effect is present. Experiments have confirmed this in respect of most materials investigated hitherto, as shown by the curve of Fig. 5, which was established empirically by Mayer.[4]

Spicer and Wooten have suggested a formula which indicates the fundamental quantities that determine the quantum efficiency:[2]

$$\eta_q = A\alpha_{pe}/(\alpha_{\text{tot}} + 1/l_0), \tag{4}$$

in which $\alpha_{\text{tot}} = \alpha_c + \alpha_{pe}$ denotes the total optical absorption of the material, consisting of a part α_c which gives rise to photoconduction, and a part α_{pe} which gives rise to photoemission; A is a constant approximately equal to $\frac{1}{2}$; and l_0 is the escape depth of an electron.

α_{tot} is very nearly the same for all photoemitters in which excitation takes place in the valence band. On the other hand, α_{pe} and l_0 may differ quite appreciably for different materials so that these parameters mainly determine the quantum efficiency.

The average escape depth l_0 of an electron in a semiconductor is governed by the type of energy transfer. Where the energy transfer is by the *formation of electron-hole pairs* (see section 1.1.1) l_0 is only about 10 Å to 20 Å, but, where energy transfer is by *lattice scattering* it may be as much as 200 Å to 300 Å[2] This is because a free electron excited by a photon cannct leave the material unless its energy, when it has reached the surface, exceeds the electron affinity.

On its journey from the point of excitation to the surface the electron can lose its energy in the two ways described. If the energy of the electron

is large enough it may form a second electron-hole pair, but in that case energy equal to the gap energy is lost. At such a collision a new free electron is thus created, so the total photon energy minus the lost energy (equal to the gap energy) is shared by two free electrons.

It will be clear that the escape depth of the electrons is small, considering that there is but little chance of them still having enough energy to leave the material after having travelled a long way with the risk of several collisions. With lattice scattering the excited electron loses little energy at each collision, the mass of an atom being much greater than that of an electron. Similarly, collisions with electrons rigidly bound to the atom cause little loss of energy unless an electron-hole pair is formed. This means that an excited electron can travel a much longer distance notwithstanding the greater chance of collisions, so escape depth can be correspondingly greater.

This illustrates the great advantage of using semiconductors instead of metals. With semiconductors a great escape depth is easier to obtain than with metals since a semiconductor contains much fewer free electrons and the chance of the excited electron losing energy is less.

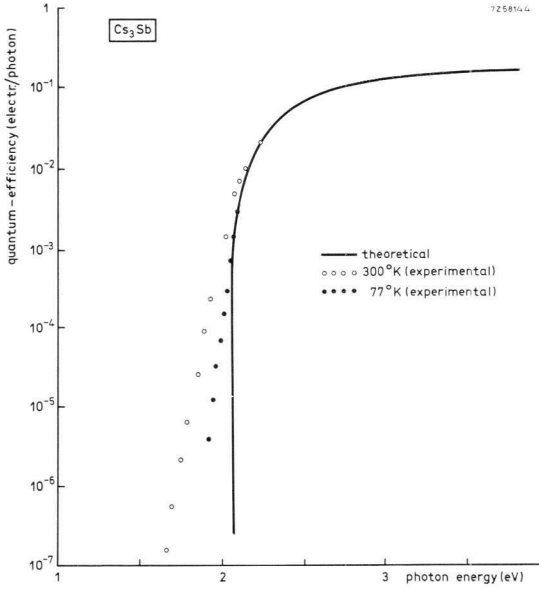

Fig. 6a. Quantum efficiency as a function of photon energy for Cs_3-Sb.[5]

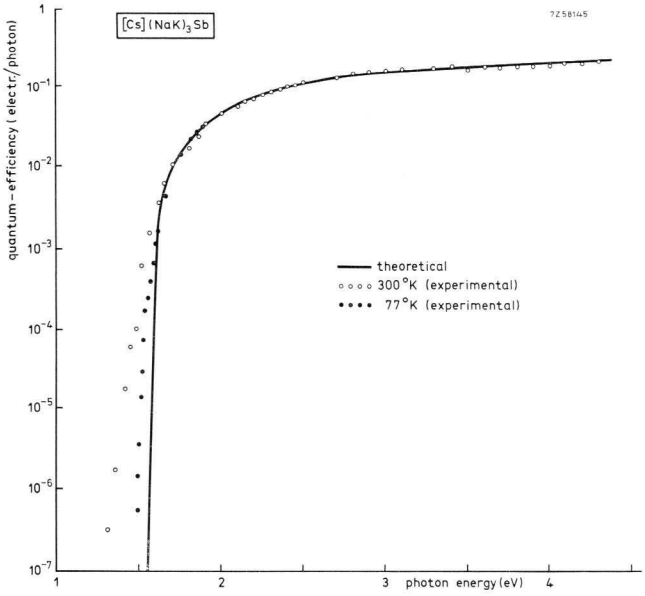

Fig. 6b. Quantum efficiency as a function of photon energy for Cs-$(NaK)_3$-Sb.[5]

The escape depth of all suitable semiconductor photoemitters is determined by lattice scattering. This implies that the electron affinity must be low compared with the gap energy so that the risk of electron-hole formation by an already excited electron is reduced to a minimum. The most suitable materials are semiconductors formed by a reaction of alkaline earth metals with antimony. Usually these semiconductors satisfy the general chemical formula m_3Sb, in which m represents one or more alkaline earth metals. Well-known photoemitters are, for example, Cs_3-Sb and Cs-$(NaK)_3$-Sb; in Fig. 6 their quantum efficiencies have been plotted as a function of photon energy.

1.1.3 Thermionic Emission

As mentioned in sect. 1.1.1, electron emission can be stimulated by heat. As far as photomultipliers are concerned such emission is unwanted and

should be kept as low as possible. According to Richardson the thermionic emission of a metal, expressed in electrons per cm^2s, is:

$$J = 7.5 \times 10^{20}\, T^2 \cdot \exp(-e\phi/kT), \tag{5}$$

where T = temperature in °K,
e = electron charge (1.6×10^{-19} C),
k = Boltzmann's constant (1.38×10^{-23} Ws/°K),
ϕ = work function of the material

Since in a metal the electrons due to photoemission and those due to thermionic emission both originate from the top of the conduction band, they have the same work function ϕ. In semiconductor photoemitters, on the other hand, the work functions for photoemission and thermionic emission differ. This is illustrated in the energy diagram of Fig. 7: photoemission originates in the valence band, whence:

$$\phi_p = W_g + W_a. \tag{6}$$

True, thermionic emission also originates in the valence band, but the required work function is smaller because the average level of the thermal electrons lies above the upper level of the valence band as a result of the thermal motion. For an intrinsic semiconductor (where the number of electrons in the conduction band equals the number of holes in the valence band),

$$\phi_t = \tfrac{1}{2} W_g + W_a. \tag{7}$$

As ϕ_p and ϕ_t are related, raising the sensitivity by reducing ϕ_p is always accompanied by increased thermionic emission. This can be reduced by refrigerating the cathode.

1.1.4 Properties of Various Cathodes

In section 1 mention has already been made of opaque and semi-transparent cathodes (see Figs 2 and 3). Semi-transparent cathodes have the advantage of more or less ideal coupling to the light source and the multiplier system. The main feature of the opaque cathode is its ability to carry high currents (up to several amperes), so that high radiant fluxes can be measured; it is moreover, the only sort that can be used in windowless photomultipliers.

The spectral sensitivity depends on the composition of the cathode and the spectral properties of the support. The graph of Fig. 8 shows the

absolute spectral sensitivities of several types of cathode. Curves of constant quantum efficiency have also been plotted according to the equation:

$$\eta_q = 100\,(12.4/\lambda)N_{kr}\,\%, \tag{8}$$

in which λ is the wavelength in Å, and N_{kr} denotes the cathode radiant spectral sensitivity in mA/W.

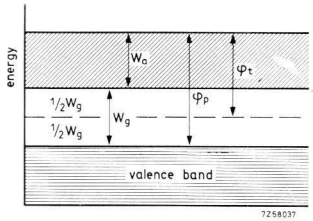

Fig. 7. Work functions for thermionic emission ϕ_t and for photoemission ϕ_p.

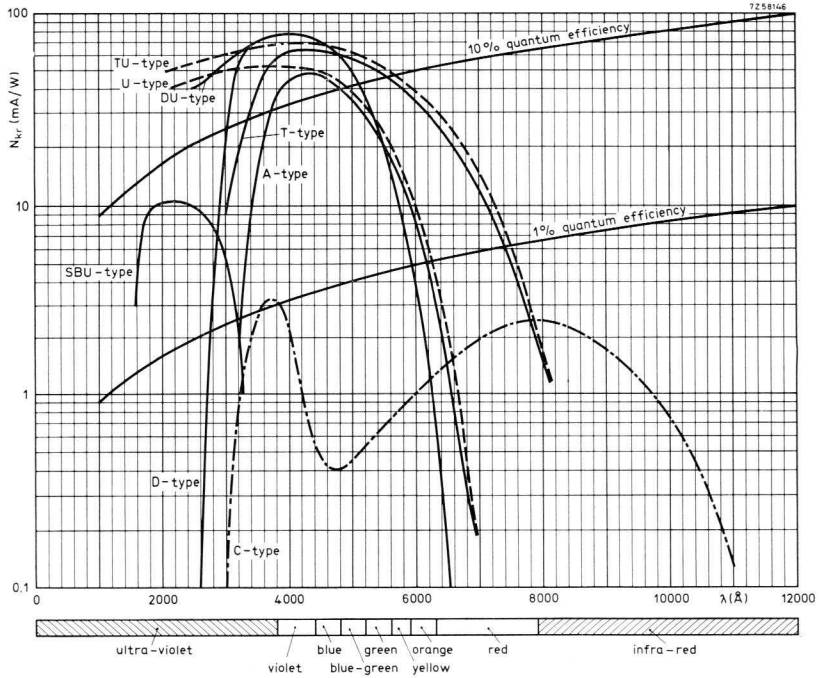

Fig. 8. Absolute spectral sensitivity of different types of cathode.

The graph clearly shows the difference between the several types. The survey below gives their characteristic properties:*

— A-type (S11), a semi-transparent Cs-Sb cathode deposited on the inner side of a polished lime glass window; spectral sensitivity lies within the visible range and is a maximum at 4200 Å.

— U-type (S13), having the same coating as the A-type, but deposited on a polished quartz window; spectral sensitivity is thus extended into the ultraviolet.

— C-type (S1), a semi-transparent Cs-O-Ag cathode deposited on a polished lime glass window; spectral sensitivity lies mainly in the red and near-infrared and is a maximum at about 8000 Å.

— T-type (S20), a semi-transparent Sb-K-Na-Cs cathode on a polished lime glass window; spectral sensitivity runs from the ultraviolet to the deep red.

— TU-type, having the same coating as the T-type, but deposited on a polished quartz window; spectral sensitivity is thus extended far into the ultraviolet.

— D-type, a semi-transparent K-Cs-Sb cathode on a glass window that is only slightly radioactive. Its specific application is in the measurement of weak β-radiation via a liquid scintillator. Spectral sensitivity lies mainly in the visible range with a maximum at about 4000 Å. This type of cathode is characterized by a low dark current and high quantum efficiency (25%).

— DU-type, a cathode with the same coating as the D-type, but deposited on a quartz window; its spectral sensitivity extends far into the ultraviolet: due to the absence of ^{40}K there is no interference by radioactive radiation.

— SBU-type, a semi-transparent CsTe cathode deposited on a polished quartz window; spectral sensitivity of this solar blind cathode lies in the ultraviolet beyond the visible spectrum.

* These types are distinguished by a capital or group of capitals. The notation between brackets conforms to the JEDEC-publication No. 50.

1.2 Electron-Optical Input System

The task of the electron-optical input system is to establish efficient coupling between the cathode and the multiplier system. In principle this coupling consists of an electric or magnetic field or both, the configuration of which focuses the electrons in such a way that they reach the first dynode of the multiplier system. For practical reasons it is customary to use only an electric field, but for very special applications — such as star tracking — a magnetic field may be used as well.

The geometry of the electric field is governed by the shape, the number, the position of, and the voltage between the electrodes. Generally the following conditions must be met:

— As many of the electrons emitted by the cathode as possible should reach the first dynode, regardless of their point of origin on the cathode. In other words, collection should be as efficient as possible.

— The transit time between the cathode and first dynode should be as independent as possible of the point at which an electron leaves the cathode.

The latter condition is very important for photomultipliers used for very fast signals, as is often the case in nuclear applications and with modulated lasers.

The construction of the multiplier (to be discussed in sect. 1.3) is also of importance in determining the shape of the field. The electron-optical input system for a Venetian blind multiplier need not be as elaborate as for a linear focus multiplier. Generally speaking, a clear distinction can be made between the normal, classic photomultiplier and the fast photomultiplier, on the construction of whose input system much more severe requirements are imposed.

1.2.1 Classic Photomultipliers

Fig. 9 shows the input system of a classic photomultiplier, with equipotential lines and a few electron paths from the cathode to the first dynode, it being assumed that the initial velocity of the electrons is zero which is not normally the case. The photocathode is deposited on the glass window of the tube.

In a linear focused multiplier system the first dynode faces the cathode

on the axis of the tube. The electron-optical system consists of an acceleration electrode, usually at the same potential as the first dynode, and a focusing electrode which is an aluminium lining to the tube and is at the same potential as the cathode.

The energy W_{el} with which an electron leaves the cathode depends on the wavelength of the incident light and on the threshold wavelength of the cathode material:

$$W_{el} \leqslant h(\nu - \nu_0). \tag{9}$$

With a threshold wavelength of, say, 6,800 Å and with radiation of 4,200 Å, the electron energy W_{el} may be as much as 1.1 eV which, considering the low electric field strength at the surface of the cathode, is by no means negligible.

As electrons may be emitted in any direction, their paths to the first dynode will differ. Fig. 10 shows the envelope of likely paths for electrons with an original energy of 1.1 eV. It is clear that not all electrons

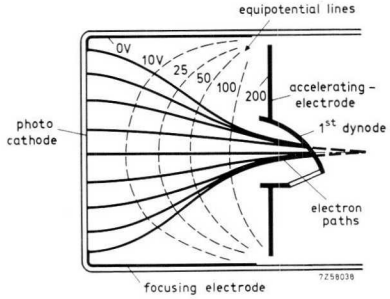

Fig. 9. Electron-optical input system of a photomultiplier.

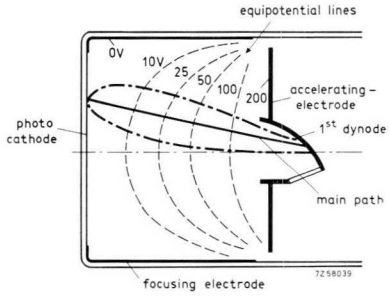

Fig. 10. Electron-optical input system showing envelope of electron paths with initial energy (W_{el}) of 1.1 eV (chain dotted line).

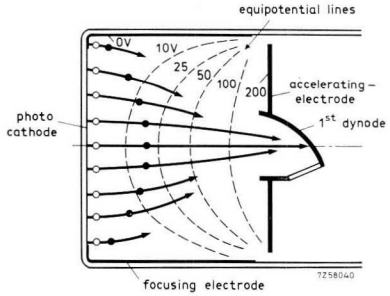

Fig. 11. Schematic representation of the transit times of electrons in the input system, assuming an initial electron speed of zero.

will reach the first dynode at the same point, every point on the cathode having a corresponding landing area on the first dynode. Efficient collection thus calls for a large first dynode or for a well-focused electron beam.

1.2.2 Fast Photomultipliers

In fast photomultipliers stringent requirements are to be met not only by the collection efficiency but also by the transit times of the electrons. We shall confine ourselves to discussing the more important effects that influence the transit time, the transit time difference, and the transit time spread.

Fig. 11 again shows the cross-section of the input system of a classic photomultiplier with equipotential lines and electron paths, it being assumed that all electrons leave the cathode at the same velocity and normal to the cathode surface. The arrow heads, dots and circles indicate points of equal transit time. At first the paths do not differ appreciably but after 15 ns the electrons that travel along the axis of the input system have already reached the first dynode, whereas those from the edge of the cathode have only covered about one-third of the distance and thus take longer to reach the first dynode. Such differences in transit time are increased by the asymmetry of the first dynode in a linear focused multiplier system. This effect is known as "*transit time difference*", and as can be seen, it is associated with the geometry of the input system.

Transit time spread, on the other hand is associated with the energy and direction of emission of the electrons. If the initial velocity is represented as a spatial vector it can be resolved into two components, W_n

normal to the cathode and W_t parallel to the cathode. To a first approximation W_n determines the transit time of the electron and W_t determines the path it will travel.

The spread in transit time can then be approximated by the expression:

$$\Delta t_n = -(2\ \mathrm{mW}_n/e^2E_0{}^2)^{1/2}, \tag{10}$$

where m = the mass of an electron (9.1×10^{-28} g),
e = the electron charge (1.6×10^{-19} C),
E_0 = the electric field strength (in V/m)
W_n = the energy component (in J) normal to the cathode.

From this expression, Δt_n is about 0.5 ns with W_n of 0.4 eV and an $E_0 = 4$ kV/m. This is the "*transit time spread*" and is quite distinct from transit time difference in that it is almost independent of the point at which the electrons leave the cathode.

The input system of fast photomultipliers is such as to minimize both transit time difference and transit time spread. The transit time difference is usually in the range from 0.2 ns to 0.5 ns, which is of the same order

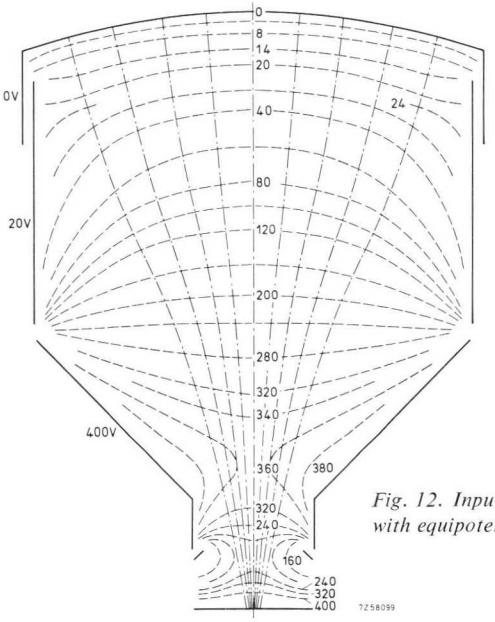

Fig. 12. Input system of photomultiplier 56AVP with equipotential lines and some electron paths.

of magnitude as the transit time spread, which stresses the need to clearly distinguish them.
Fig. 12 shows the input system of a fast photomultiplier. Transit time spread can be reduced by raising the electric field strength, as can be seen from eq. (10). Careful siting of the electrodes allows a uniform field such as that shown in Fig. 12 to be obtained in practice.

Transit time difference can be reduced by using a spherical cathode that reduces the distance between the edge of the cathode and the first dynode. The most effective way of improving the transit time difference is to progressively grade the electric field at the edges of the input system so that the "marginal" electrons are accelerated with respect to those originating from the centre of the cathode.

In most fast photomultipliers the focusing electrodes are brought out, thus giving some freedom in choosing their potential. The best adjustment is usually found by trial and error.

1.3 Multiplier System

The multiplier consists of a series of dynodes (secondary emission electrodes) ending with an anode or collector. The operation of the system is based on several clearly distinguishable phenomena, but their interaction is quite considerable. In general, the multiplier should satisfy two essential conditions:

— Sufficient secondary electrons should be produced.
— They should be effectively directed to the succeeding electrode.

1.3.1 Composition of the Dynode

The material of which the dynode is made should meet the following requirements:

— high secondary emission factor,

— stable secondary emission effect,

— low thermal emission.

The theory outlined in sect. 1.1.1 can also be applied to the secondary emission of the dynodes, the only difference being that electrons replace photons.

An incident electron transfers its energy to electrons in the material,

raising their energy to the extent that they can escape the material. In conductors most of the secondary electrons lose their energy in colliding with conduction electrons and have insufficient energy to leave the surface. In insulators or semiconductors many more electrons reach the surface of the material with sufficient energy to escape; any loss of energy being due to the production of electron-hole pairs.

Since an electric field must be applied to lead the electrons through the multiplier, the secondary emission material must be deposited on a conducting support. One way of producing thin insulating coatings is to selectively oxidize an alloy of small admixtures of an alkaline or alkaline earth metal in a more noble metal. During the process only the alkaline metal oxidizes so that a thin insulating coating is formed on a conductive support. Materials often used for this purpose are copper-beryllium, silver-magnesium and caesium-antimony. Although each has its pros and cons, preference is usually given to silver-magnesium as it offers the following advantages:

— The secondary emission factor remains constant for the life of the photomultiplier and is independent of electron current, which may reach high values when the cathode is suddenly strongly illuminated. Current densities of up to 10 mA/cm^2 are permissible for 1 ms.

— The dynodes can be well degassed by high temperature baking out while the tube is being evacuated. This is essential if a high vacuum is to be maintained.

— It is insensitive to light, and its thermionic emission is low compared to that of the cathode.

— The requisite secondary emission factor is attained at comparatively low voltages.

Copper-beryllium, which has the advantage of retaining its properties in the presence of air, is used in such special applications as windowless* multipliers.

---

* Windowless photomultipliers are not completely encapsulated. They are used in an evacuated chamber for particularly sensitive measurement. During storage and transit they are exposed to atmosphere.

1.3.2 Relation between Secondary Emission Factor, Number of Stages and Required Supply Voltage

The number of dynodes needed depends on the required gain, the dynode material and the supply voltage. The number of dynodes needed for a given gain and for a minimum supply voltage (V_b) can easily be calculated by making the following assumptions:

— That each dynode has the same voltage (V_s) with respect to the preceding one, and that the secondary emission characteristics (secondary emission factor as a function of voltage) of all dynodes are the same. This implies that the configuration and activation of all dynodes are identical.

— That the secondary emission characteristic can be represented by a straight line of slope K, passing through the origin (see Fig. 13).

The overall gain of the tube is then:

$$G = \delta^n = (KV_s)^n, \tag{11}$$

in which δ is the mean secondary emission factor of the dynodes and n their number. From eq. (11):

$$V_b = nV_s = (n/K)G^{1/n}, \tag{12}$$

and

$$\mathrm{d}V_b/dn = (1/K)G^{1/n} - (n/K)n^{-2}\,G^{1/n}\,.\,\ln G. \tag{13}$$

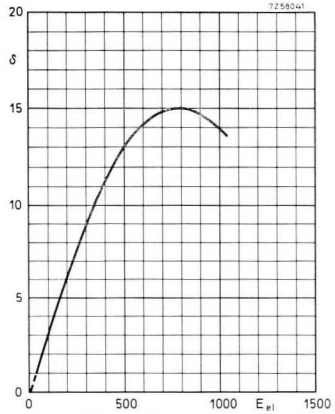

Fig. 13. Secondary emission coefficient of a silver-magnesium alloy as a function of the energy of the primary electrons.

Putting $dV_b/dn = 0$ yields:

$$n = \ln G = \ln \delta^n. \tag{14}$$

This means that V_b will be a minimum when $\delta = e$, that is, when $V_{s\,\min} = e/K$, so

$$V_{b\,\min} = (e/K) \ln G. \tag{15}$$

The comparatively low value of $\delta = e$ means that the second assumption made above can easily be satisfied; in fact this value is far below the secondary emission factor of practical dynodes. The maximum secondary emission factor thus raises no problem, the only requirement being that it should exceed 2.72.

The value of K is of greater importance: the steeper the slope of the secondary emission characteristic, the lower will be the required supply voltage. The dependence of V_b on n has been plotted in Fig. 14 for several values of gain. The actual minima are in fair agreement with the theoretical values (indicated by arrows). The voltage level is rather higher for copper-beryllium than for silver-magnesium because the last named has a higher value of K.

A low supply voltage is favourable not only for practical reasons but also because the dark current is thus kept low. However, gain and dark current are not the only factors to be considered, transit time and transit time spread, the space charge in the last stage and, finally, the number of pins that can be accommodated on the tube base must also be considered and these usually lead to a higher supply voltage than that indicated.

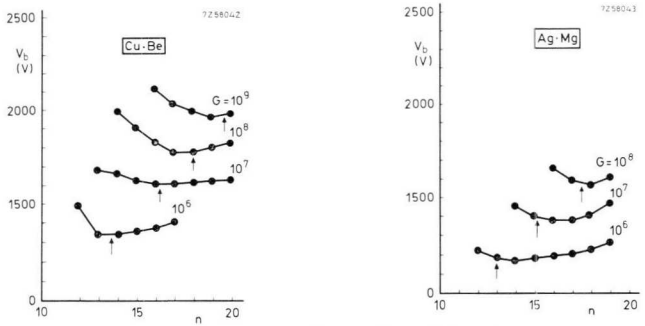

Fig. 14. Dependence of the gain (G) on the number of dynodes (n) and on the overall supply voltage (V_b).

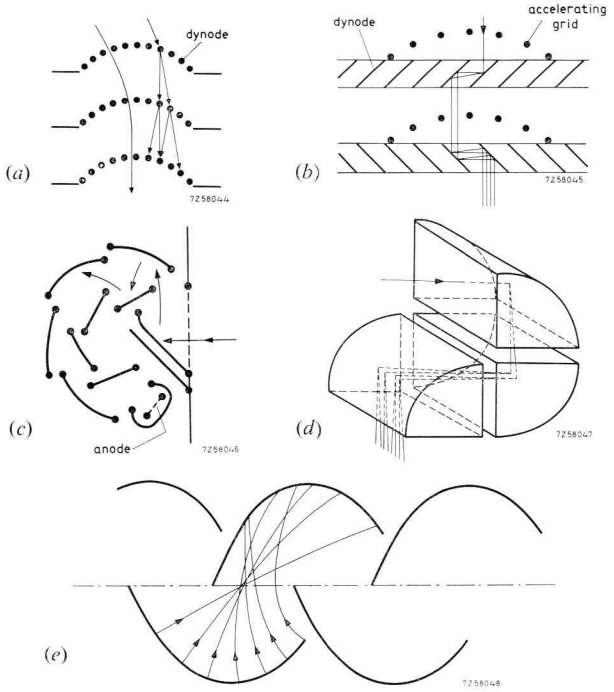

Fig. 15. Configurations and electron paths of (a) sieve dynodes, (b) Venetian blind dynodes, (c) circular cage dynodes, (d) box dynodes, (e) linear focus dynodes.

1.3.3 Dynode Configurations

Fig. 15 shows several electrostatically focused dynode systems; magnetic focussing is of little practical significance because of its cost and complexity. Two sorts of electrostatically focused photomultipliers can be distinguished, those where the dynodes form a sieve or a Venetian blind through which the electrons pass, and those in which the dynodes are reflecting elements.

The sieve dynode (Fig. 15*a*) is the simplest and offers the following advantages:

— it is easier to put the dynodes in line;
— all electrons emitted by even a large photocathode can be made to impinge on the first dynode;
— the dimensions are not critical;

— the dynodes can be large, and successive dynodes can be close together to increase electric field strength.

A drawback of the sieve dynode is the impossibility of preventing some primary electrons from passing straight through; this results in a comparatively low gain and considerable variation in transit time.

Venetian blind dynodes (Fig. 15*b*), which are metal strips (with an emissive coating) placed at an angle of 45° to the axis of the tube, share the advantages of the sieve type of dynode. They also share their drawbacks, though to a lesser extent.

Although reflecting dynodes, such as in the photomultipliers described here, do not suffer from these disadvantages, they are not ideal. They can be arranged in three ways: as a circular cage (Fig. 15*c*), as a box (Fig. 15*d*), and in linear cascade (Rajchman) (Fig. 15*e*).

Linear cascade has the following advantages:

— the potentials in the tube can be so distributed that no high potential differences occur between adjacent points, thus minimizing dark current;

— cathode and anode can be sufficiently well isolated to minimize the risk of feedback;

— all the available space in a tube can be used; the dynodes can be as large as the tube diameter permits;

— it is easy to incorporate a large number of dynodes.

Linear cascade dynodes are about three times as long as they are wide, so boundary effects and the influence of the insulating supports can be ignored.

The first dynode should not only collect all electrons emitted by the cathode, thus acting as a coupling between the input system and multiplier, but it should also deflect them so that they land at a favourable angle on the next dynode.

If the voltage between successive dynodes is below a certain value (about 80 V for linear systems), the collection efficiency of the electron-optical systems between the dynodes drops considerably; moreover the detrimental effect of the space charge between the dynodes increases and the anode current ceases to be proportional to the luminous flux incident on the cathode.

1.3.4 Fast Multiplier System

The principal conditions to be met by fast photomultipliers are high gain and fairly uniform transit time. Gain could be made high by using many stages with an appropriate voltage distribution between the dynodes. However, this would not necessarily mean that the variation in transit time would be minimized. The factors that influence gain also influence the transit time and the paths travelled by the electrons.

We shall confine ourselves here to giving a short description of the functions of the main parts of the multiplier system, namely:

— the transition zone,

— the intermediate zone,

— the collection zone.

The two or three dynodes in the *transition zone* differ from the other dynodes which form the intermediate zone of the multiplier. Their purpose is — apart from multiplication — to adapt the beam of electrons to the average angle of incidence and to the angular aperture required by the intermediate zone.

In the *intermediate zone* the dynodes progressively focus the beam of electrons. To this end special rod-shaped focusing electrodes are mounted between all stages.

The *collection zone* is the terminal region of the multiplier. The geometry of the dynodes is unlike the preceding stages because their purpose, apart from multiplication, is:

— to collect all electrons;

— to reduce space charge phenomena even at the maximum expected pulse level;

— to equalize and reduce transit times in the last interdynode space;

— to reduce the coupling between the anode and its adjacent electrodes and with the electron beams, except the coupling to the last dynode which produces the useful signal.

These aims are partly compatible, but limit the choice of geometrical structure. The collector proper can best be in the form of a grid mounted as close as possible to the last dynode.

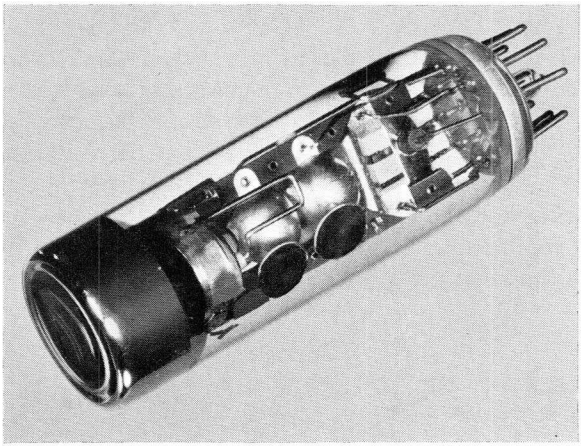

Photomultiplier type XP1113 (approx. full size).

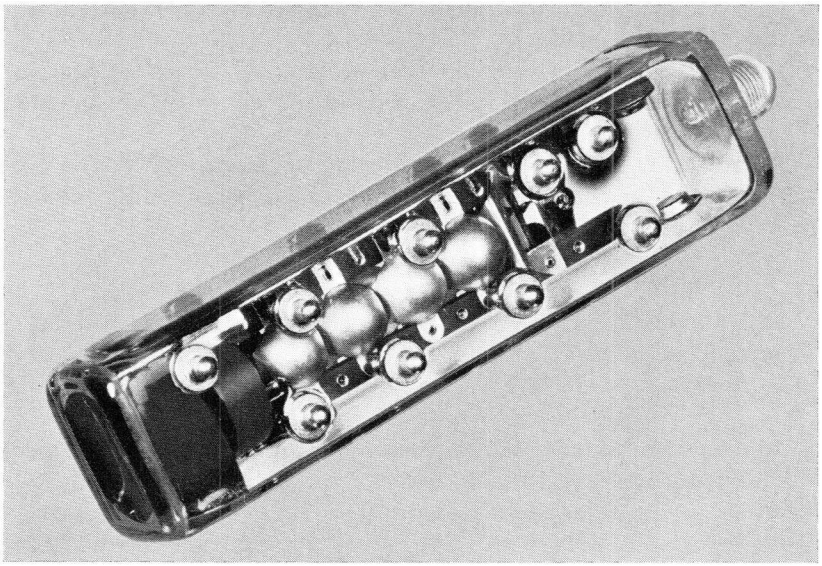

Photomultiplier XP1220 (approx. full size).

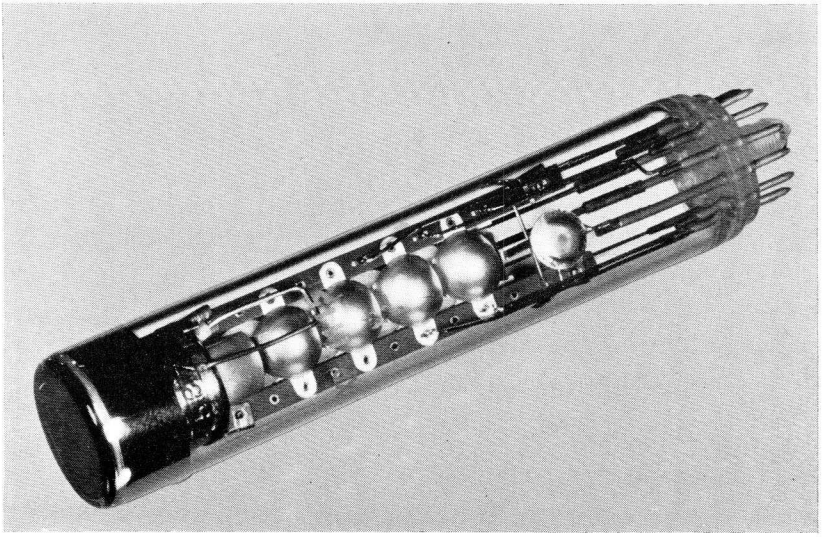

Photomultiplier type XP1110 (approx. full size).

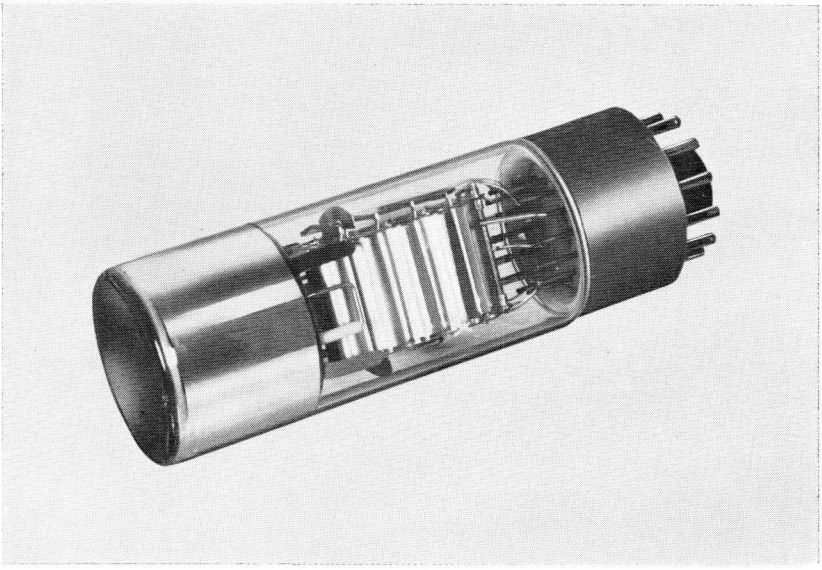

Photomultiplier type XP1010 (approx. 2/3 full size).

2 Operational Considerations

Photomultipliers are very sensitive, but damage is not the only consequence of careless operation; it can also lead to misleading results. Some common causes of misinterpretation are:

— not allowing the photomultiplier time to stabilize after excessive illumination;

— allowing ambient temperature to influence operation;

— insufficiently stabilizing the supply voltage;

— operating in the non-linear part of the characteristics;

— allowing the signal current to affect the dynode voltages;

— allowing external magnetic fields to interfere;

— improper earthing.

Taking these in the order given.

2.1 Influence of Excessive Illumination [6]

Excessively illuminating a photomultiplier may cause the current through the final dynodes and the anode to exceed their maximum permissible dissipation. At the least this may give rise to serious fatigue effects (see section 3.2.1), and, at worst, may destroy the photomultiplier. In some cases the tube can be revived by storing it for a long period in darkness. The effects on the tube are difficult to predict because they depend largely on the type of tube and its history, that is, the sort of treatment it has had in the past. The most distinct effect of excessive illumination is usually a considerable increase in dark current. This will also happen if the tube is excessively illuminated when *not* in operation, but then the dark current will gradually drop to a stable value after the tube has been put into operation; how long this will take depends on the strength of the illumination.

To illustrate the effects of excessively illuminating an inoperative photomultiplier we include the results of some measurements. They were made

on tubes with U-type cathodes which were exposed to radiation of a given intensity and wavelength for a given time. The supply was switched on 1 s after irradiation ceased, and 3 s later the number of electrons per second emitted by the cathode were counted.

The behaviour of the dark current appears to depend on the following factors:

— the radiant flux,

— its wavelength,

— the exposure time.

Figs 16, 17 and 18 shows the relative number of electrons per second as a function of the time elapsed after the radiation had ceased. The number of electrons per second still being emitted by the cathode after the stable condition has been reached is taken as unity.

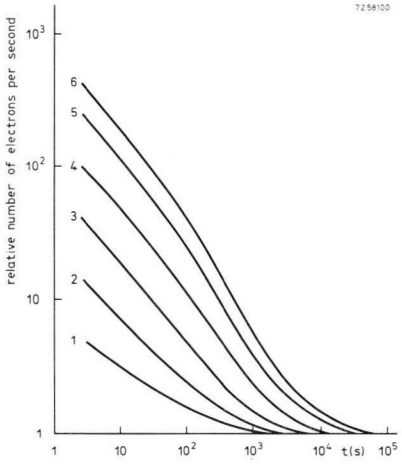

Fig. 16. Decay of the dark current of a U-type cathode (S13) at a temperature of 0 °C after exposure for 100 s to radiation of a wavelength (λ) of 3660 Å:

curve number	1	2	3	4	5	6	
radiant flux	1.11	4.45	13.3	40	120	240	μW

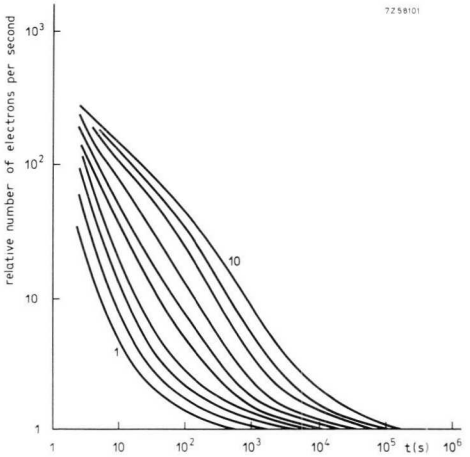

Fig. 17. Decay of the dark current of a U-type cathode (S13) at 0 °C after exposure to radiant flux of 120 μW at a wavelength λ of 3660 Å:

curve number	1	2	3	4	5	6	7	8	9	10	
exposure time	0.4	1	2	4	10	20	40	100	200	400	s

Apparently the total number of additional electrons emitted by the cathode after it has been irradiated is related to the radiant flux ϕ (Fig. 16). This total number of additional electrons being those emitted during the interval between termination of the irradiation and the time at which the cathode has become stable, i.e. emits a constant number of electrons per second. This relation can be expressed by the formula:

$$N_e = A_\lambda \phi^{0.96}, \tag{16}$$

in which N_e is the total number of electrons, A_λ a constant depending on the wavelength, and ϕ the radiant flux. The constant A_λ varies exponentially with the reciprocal of the photon energy:

$$A_\lambda = B \cdot \exp(-C/h\nu), \tag{17}$$

where B and C are constants, and $h\nu$ is the photon energy.

Eq. (17) shows that the number of dark current electrons very rapidly increases as the wavelength of the radiation decreases.

In addition to the radiant flux, the exposure time τ has great influence

on the dark current, see Fig. 17. One might expect that the total number of electrons N_e would be constant for constant energy, that is that $\phi\tau = N_e = \text{constant}$, but this is not the case. More electrons are emitted after heavy irradiation for a short period than after weak irradiation for a long period. In the first case the number of electrons emitted immediately after irradiation is important, in the second case the tail of the curve has more influence (Fig. 19, curve 2). In practice this means that excessive irradiation for a short period results in a fairly high dark current that drops rapidly back to a stable value, whereas although moderate irradiation for a long period increases the dark current less, the cathode takes very much longer to recover. Short wavelength irradiation increases both the dark current and the time to reach stability more than long wavelength irradiation.

Fig. 18 shows the behaviour of a U-type cathode exposed to radiation of different wavelengths but of a constant number of photons:

$$N_p = (\phi/hc)\lambda, \tag{18}$$

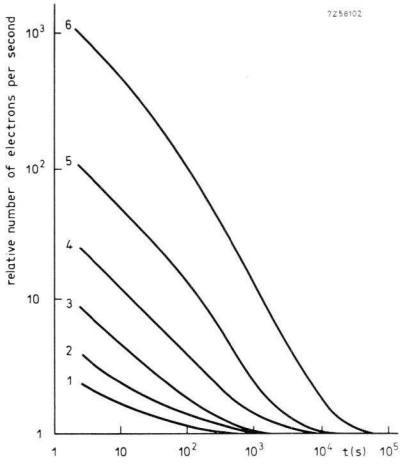

Fig. 18. Decay of the dark current of a U-type cathode (S13) at 0 °C after it has been exposed for 100 s to different wavelengths, the number of photons being the same in every case.

curve number	1	2	3	5	5	6	
wavelength	5500	4375	4075	3660	3140	2537	Å
radiant flux	6.25	7.80	8.40	9.35	10.9	13.3	μW

in which N_p again denotes the number of photons. Very similar curves are obtained if constant radiant flux is taken as parameter instead of the number of photons. For any wavelength the ratio of the total number of electrons N_{e1} after irradiation by a constant radiant flux ϕ_1 (or photons N_{p1}), to the total number of electrons N_{e2} after irradiation by a constant radiant flux ϕ_2 (or photons N_{p2}), is:

$$N_{e1}/N_{e2} \simeq \phi_1/\phi_2. \tag{19}$$

N_e may be said to vary linearly with the number of photons impinging on the cathode during irradiation.

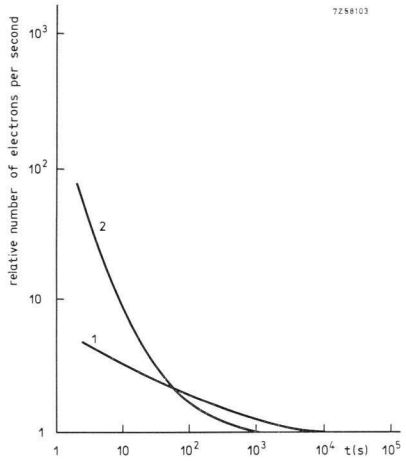

Fig. 19. Decay of the dark current of a U-type cathode (S13) at 0 °C after it has been exposed to radiation of 3660 Å; curve 1 applies to an exposure of 100 s with a radiant flux of 1.2 μW, curve 2 to an exposure of 1 s with a radiant flux of 120 μW.

Because of its very low work function (about 1 eV), the dark current of a C-type cathode is about 20 times greater than that of U- A- and D-type cathodes, although the curves are generally similar. The T-type cathode is about 30 times more sensitive to excessive illumination than the U-type.

2.2 Influence of Ambient Temperature

The influence of temperature on the characteristics of photomultipliers and the advantages of refrigeration will be dealt with in detail in section 4.2. We shall here discuss the influence of ambient temperature fluctuations.

When the equipment in which photomultipliers are used develops heat the rise in temperature must be allowed for. The anode signal will vary because:

— cathode sensitivity is a function of temperature;

— dark current is a function of temperature.

2.2.1 Influence of Ambient Temperature on Cathode Sensitivity

The temperature dependence of cathode sensitivity is not the same for all kinds of light but is a function of wavelength and, moreover, depends on the type of cathode. Generally speaking in the range 25 °C to 50 °C with light of a colour temperature of 2854 °K, the cathode sensitivity of A-type cathodes falls by about 0.5%/degC with rising temperature. This decrease is to be attributed to variation in spectral sensitivity. Fig. 16 shows the temperature coefficient as a function of wavelength for the temperature range 20 °C to 55 °C.

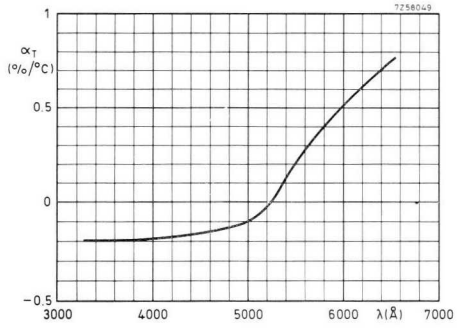

Fig. 20. Temperature coefficient of an A-type cathode (S11) expressed in per cent per degC, as a function of the wavelength of the incident radiation. Valid for the temperature range +25 °C to +55 °C.

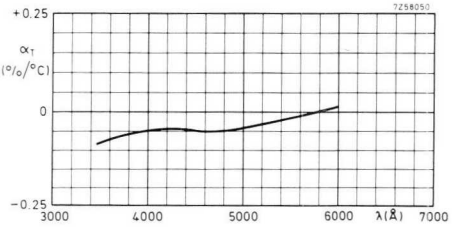

Fig. 21. As Fig. 20, but for a T-type cathode (S20).

For T-type cathodes (*S*20) the temperature coefficient is much smaller, namely −0.1 %/degC for light of a colour temperature of 2854 °K. Fig. 21 is the curve, corresponding to Fig. 20, for T-type cathodes.

2.2.2 Influence of Ambient Temperature on Dark Current

Temperature variations have considerable influence on dark current. The table below shows the temperature change needed to change anode dark current by a factor of 10:

Table 2

type of cathode	C (S1)	T (S20)	A (S11)
temperature change	15 degC	25 degC	40 degC

It should be recognized that the above figures are the average of many measurements. In practice other effects (see section 3.3) may contribute to a larger extent to dark current, and may obscure the dependence of the dark current on temperature.

2.2.3 Influence of Temperature on Gain

The temperature dependence of the gain has been studied by several investigators, but the results have been unreliable because of errors introduced in measuring the gain. As a rule the gain variation does not exceed a few tenths of a percent per degC and may be either positive or negative. See section 4.2.3.

2.3 Supply

The supply voltages for photomultipliers can be obtained in several ways, each of which has its advantages and disadvantages; the choice depends on the application. Small variations in voltage may cause considerable variations in gain since, as shown in section 1.3.2, the gain is given by eq. (11):

$$G = \delta^n = (KV_s)^n.$$

Differentiation with respect to V_s and substitution of this expression yields:

$$dG/G = n \cdot dV_s/V_s. \tag{20}$$

Hence, if a gain stability of, say, 1 % is required and a ten-stage multiplier is used ($n = 10$), the dynode voltages alone must be stable within 0.1 %, disregarding all other possible causes of instability.

The distribution of the voltages over the several stages sets another limit to the choice of the voltage source. Generally the tube data quote a voltage distribution with which the circuit design is optimum for certain properties (see section 2.3.2). Fig. 22 shows by way of example the voltage distribution for an XP1110 photomultiplier with which the gain is a maximum for a given overall voltage V_b.

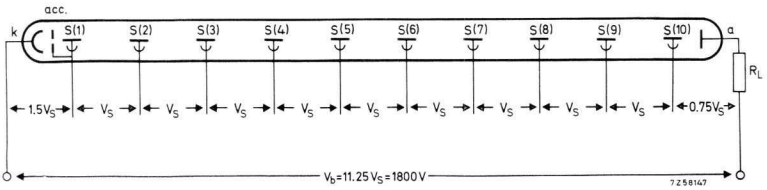

Fig. 22. Optimum voltage distribution of an XP1110 for maximum gain at a given overall supply voltage V_b.

In principle the requisite voltages could be obtained by using stable batteries, for example mercury cells. However, the number of cells needed to obtain the high voltage will usually be prohibitive, although excellent stability could thus be ensured. Instead of batteries, controlled supply units can be used, allowing individual adjustment of each multiplier stage, but this is again expensive and too complicated for most purposes.

Where optimum voltage setting is not essential voltage stabilizing tubes or voltage regulator (zener) diodes can be used in combination with an unstabilized high voltage supply unit, as shown in Fig. 23. The maintaining voltage or zener voltage of the tubes or diodes must correspond to the desired adjustment of each stage. The series resistor R_1 must be of such a value as to provide the preferred current of the tubes or diodes.

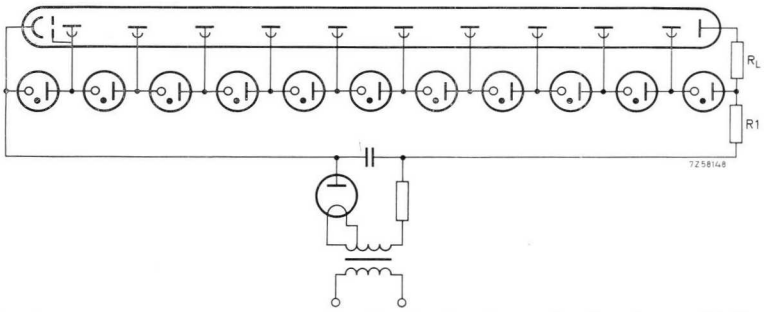

Fig. 23. Using voltage stabilizing tubes for the dynode supply of a photomultiplier.

The current must, moreover, be large with respect to the anode current of the photomultiplier (see section 2.3.2). This type of supply has the advantage of ensuring a fairly good stabilization, and allowing a simple and inexpensive high voltage supply unit to be used. However, fixed voltages do not allow optimum adjustment of the photomultiplier.

The most common method is to use a stabilized high voltage supply unit in combination with a voltage divider (bleeder), as shown in Fig. 24. The resistors can conveniently be chosen to meet the interelectrode voltage requirements for optimum operation of the photomultiplier. The supply unit can be adjustable, so that the gain of the photomultiplier can be controlled by adjusting the overall voltage, without affecting the ratio between the electrode voltages. If the overall voltage cannot be controlled, a variable resistor between two successive multiplier stages can be used to vary gain as indicated by the broken lines in Fig. 24; the variable resistor should be substituted for the fixed resistors across the stages $S(3)$-$S(4)$ and $S(4)$-$S(5)$. In this way gain can be controlled over a range of about 1 : 100, depending on the type of tube. In Fig. 25 gain has been plotted as a function of the voltage variation ($\Delta V_{S(4)}$) with respect to the nominal voltage $\Delta V_{S(4)}$.

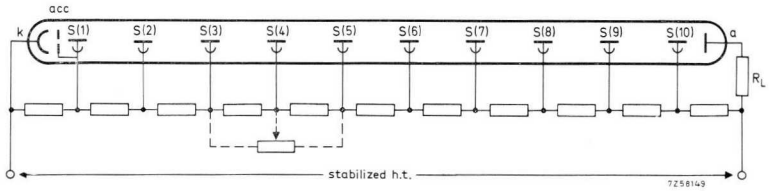

Fig. 24. Supply system using a stabilized h.t. voltage and a voltage divider. The gain can be adjusted if two resistors are replaced by a potentiometer.

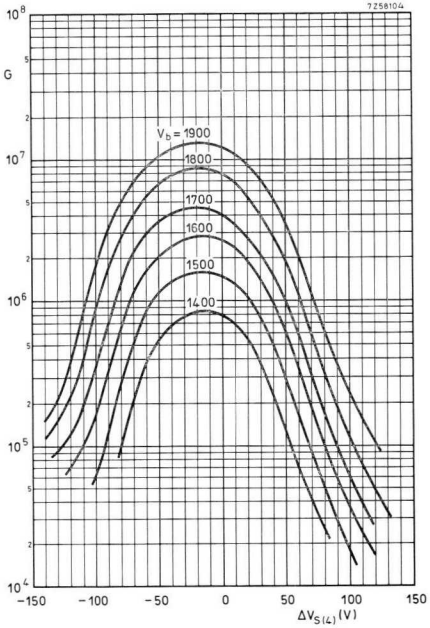

Fig. 25. Gain of a photomultiplier as a function of the variation $\Delta V_{S(4)}$ of the nominal supply voltage $V_{S(4)}$, with the overall supply voltage V_b as parameter.

2.3.1 Electrode Currents

The electrode current (whether of photocathode, interstage, or anode) should always be in the region of saturation to ensure good proportionality between it and the cathode illumination over the whole operating range. The upper limits of the electrode current are determined by considerations of dissipation, and of fatigue and aging effects.

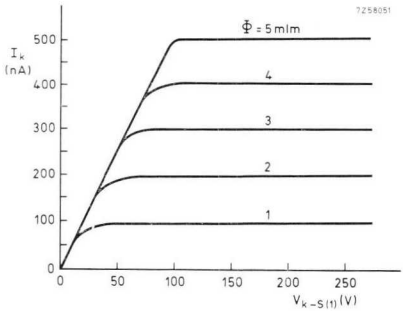

Fig. 26. Cathode current I_k as a function of the voltage $V_{k-S(1)}$ between cathode and first dynode, with the luminous flux Φ as parameter.

Fig. 26 shows the cathode current as a function of the voltage $V_{kS(1)}$ with the radiant flux as parameter. The upper limit of the cathode current density is about 100 nA/cm^2.

The resistance of the photocathode has great influence on the characteristics. However carefully the transparent conductive supporting layer is evaporated, the cathode resistance will be of the order of some tenths of a megohm. This means that the emission of photoelectrons will modify the surface potential of the photoemissive layer, and hence the potential difference between the cathode and first dynode, thus impairing the collection efficiency. It will be clear that this potential difference should lie on the flat part of the characteristic to ensure a linear relationship between radiant flux and cathode current.

Similar conditions apply to the dynode system. The voltage between two stages should be such that the interstage current, too, lies in the saturation range. In practice this is usually the case as the voltage required for good focusing (80 V) is much higher than that at which saturation occurs. Provided the tube data are observed, there is no risk of the interstage current dropping below saturation.

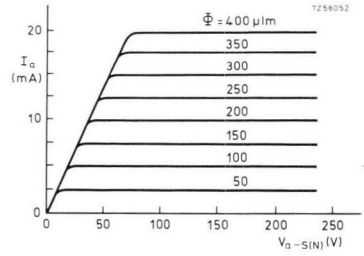

Fig. 27. Anode current I_a as a function of the voltage $V_{a-S(N)}$ between anode and last dynode, with a luminous flux Φ as parameter.

The anode saturation current characteristics are plotted in Fig. 27 as functions of the voltage between the last dynode and the anode. The anode current produces a voltage drop across the load resistance connected in series with the anode, causing the anode voltage to fall as anode current rises. The anode voltage should therefore be high enough to ensure saturation at the highest output current. In other words:

$$V_{a-S(N)} - V_{\text{out}} > V_{\text{min}} > 80 \text{ V}, \tag{21}$$

where $V_{a-S(N)}$ = voltage between anode and last dynode in the absence of a signal,

V_{out} = output signal amplitude measured across the load resistance,

V_{min} = minimum voltage between the last dynode and anode.

2.3.2 Bleeder Current

The voltage divider of a photomultiplier must be such as to prevent excessive potential variations during operation. Unless the dynode currents are low compared with the total bleeder current through the voltage divider when the cathode is dark, the dynode voltages between the last stages will be seriously reduced. If the supply voltage remains constant, the voltages of the first few stages will increase thus raising their secondary-emission factors. If this rise exceeds the fall in secondary-emission factor of the last stages, the overall gain will increase. The extent of the change in gain is dependent on the number of stages affected, the interstage voltage, the magnitude of the voltage variations, and the secondary emission characteristics of the dynode material.

The operating conditions can best be investigated by illuminating the cathode with a constant luminous flux. The currents may then flow as shown in Fig. 28. To give an insight into the relation between the gain, the anode current and the bleeder current, we shall derive the relative variation of the gain caused by a varying anode current.

Assume that the photomultiplier has N stages and that the electrodes are fed by a bleeder of $N + 1$ identical resistors of value R. The electrodes and electrode currents are denoted as in Fig. 29, I being the bleeder current in the absence of anode current and ΔI the change caused by anode current.

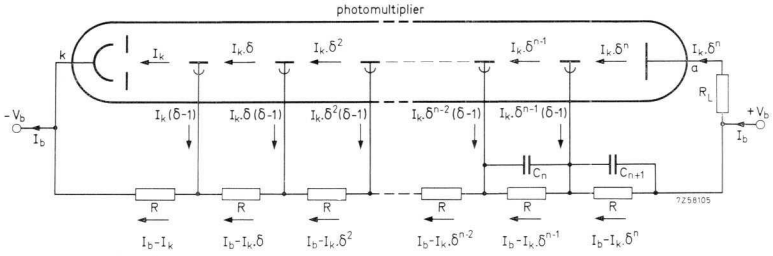

Fig. 28. The currents through a photomultiplier and its voltage divider.

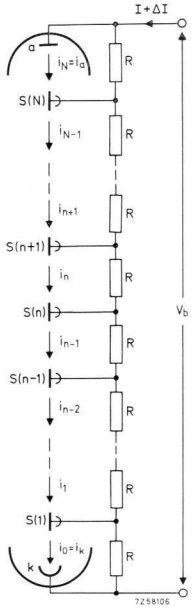

Fig. 29. Notation of the various electrodes and currents of a photomultiplier as used in the derivation below.

As the overall voltage remains constant the sum of the changes in the dynode voltages must be zero, hence:

$$\Delta I(N+1)R = (i_0 + i_1 + \ldots + i_a)R, \tag{22}$$

or

$$\Delta I = (i_0 + i_1 + \ldots + i_a)/(N+1). \tag{23}$$

The gain δ_n of the nth dynode is a function of the velocity with which the primary electrons impinge on the dynode; it therefore depends on the voltage $V_{S(n-1)-n}$ between the dynodes $S(n)$ and $S(n-1)$. Hence:

$$\delta_n = K\{V_{S(n-1)-n}\}^b, \tag{24}$$

in which K and b are constants. For dynodes of Ag-Mg-O-Cs, b is unity. If the stage gain with negligible anode current is denoted by δ_0, we get:

$$\frac{\delta_n}{\delta_0} = \frac{K(I + \Delta I - i_{n-1})R}{KIR} = 1 + \frac{\Delta I - i_{n-1}}{I}. \tag{25}$$

The ratio of the overall gain G with an anode current i_a to the gain G_0 at negligible anode current is thus given by the product:

$$\frac{G}{G_0} = \prod_{N=1}^{n=N} \left(1 + \frac{\Delta I - i_{n-1}}{I}\right). \tag{26}$$

Taking terms of the first order, we get:

$$G/G_0 = 1 + \{\Delta IN - (i_0 + i_1 + \ldots + i_{N-1})\}/I. \tag{27}$$

Substitution of eq. (23) yields:

$$\begin{aligned} G/G_0 &= 1 + \{(i_0 + i_1 + \ldots + i_N)N/(N+1) - \\ &\qquad - (i_0 + i_1 + \ldots + i_{N-1})\}/I \\ &= 1 + \frac{1}{I}\left(\frac{N}{N+1} \cdot i_N - \frac{i_0 + i_1 + \ldots + i_{N-1}}{N+1}\right) \end{aligned} \tag{28}$$

Defining the relative gain variation as:

$$\Delta G/G_0 = (G - G_0)/G_0 = G/G_0 - 1, \tag{29}$$

thus yields:

$$\Delta G/G_0 = \frac{i_N}{I}\left\{\frac{N}{N+1} - \frac{i_0 + i_1 + \ldots + i_{N-1}}{i_N(N+1)}\right\}. \tag{30}$$

The term between brackets is almost independent of δ, so we may put:

$$i_n/i_{n-1} = \delta_n = \delta. \tag{31}$$

From eqs (30) and (31):

$$\frac{\Delta G}{G_0} = \frac{i_N}{I}\left\{\frac{N}{N+1} - \frac{1}{N+1}(1 + \delta + \delta^2 + \ldots + \delta^{N-1})/\delta^N\right\}. \tag{32}$$

Substituting:

$$1 + \delta + \delta^2 + \ldots + \delta^{N-1} = (1 - \delta^N)/(1 - \delta), \tag{33}$$

yields:

$$\frac{\Delta G}{G_0} = \frac{i_N}{I} \cdot \frac{N}{N+1}\left\{1 - (1/N\delta^N - 1/N)/(1 - \delta)\right\}, \tag{34}$$

which, considering that $1/N\delta^N \ll 1/N$, may be reduced to:

$$\frac{\Delta G}{G_0} = \frac{i_N}{I} \cdot \frac{N(1 - \delta) + 1}{(N + 1)(1 - \delta)}, \tag{35}$$

or, since $i_N = i_a$:

$$\frac{\Delta G}{G_0} = \frac{i_a}{I} \cdot \frac{N(1 - \delta) + 1}{(N + 1)(1 - \delta)}. \tag{36}$$

By eq. (36) increasing the anode current from a low value to 10% of the bleeder current causes the gain to rise by 10%. In general, for the system to be linear within 1%, the bleeder current must be at least 100 times the maximum anode current.

From the above argument changes in gain due to voltage changes are to be attributed mainly to voltage variations across the bleeder resistors of the last stages, the dynode currents of the first stages have so little influence that they may be disregarded. In principle it would suffice if the bleeder current of the final stages only were fairly high, and in applications where high signal currents occur, this circumvents the necessity of a powerful high voltage unit. Fig. 30 shows a supply system in which an additional low-voltage heavy current supply is used for the bleeder resistors of the final stages.

Where pulses are encountered, for example in scintillation counters, such high peak anode currents (e.g. 300 mA with the 56AVP) may occur that separate supply units alone will not solve the problem. The voltages across the dynodes can then be kept constant for the pulse duration by

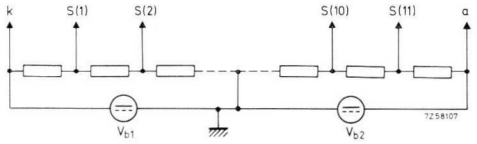

Fig. 30. Basic photomultiplier supply using two separate voltage sources; V_{b1} is a low-current, high-voltage supply, V_{b2} a high-current, low-voltage supply.

capacitors shunted across the bleeder resistors of the last stages, where they have the greatest effect (see Fig. 28). Calculations on capacitively stabilized voltage dividers are very complicated and will not be dealt with here. The minimum capacitance needed depends on the peak anode current and the pulse duration.

The value of C_{n+1} (Fig. 28) can be approximated if it is assumed that the charge Q_c that C_{n+1} should supply during the anode current pulse is much greater than the charge Q_a transported by the pulse:

$$Q_a = \int i_a \cdot \mathrm{d}t. \tag{37}$$

If the voltage across the last stage must be stable within 1 %, that is, $\Delta V/V_{S(N)} = 1/100$, and if the influence of the bleeder resistor R across the capacitor is neglected, then $Q_c = 100\ Q_a$, whence:

$$C_{n+1} = \frac{Q_c}{V_{S(N)}} = \frac{100\ Q_a}{V_{S(N)}} = \frac{100}{V_{S(N)}} \int i_a \cdot \mathrm{d}t. \tag{38}$$

As the current through the preceding stage is a factor δ lower, its bypass capacitance can be a factor δ smaller:

$$C_n = C_{n+1}/\delta. \tag{39}$$

Bypass capacitors reduce the required bleeder current quite considerably and greatly reduce voltage variations, but it should be borne in mind that they do make the time constant of the bleeder circuit very long. With high pulse rates, that is, when the intervals between successive pulses are short, the capacitors will not fully discharge and the pulse effects will add up until the amplitude of the voltage fluctuations has become quite appreciable. The error thus produced is a function of the pulse frequency, and for high pulse frequencies, where a short time constant is obligatory, a high bleeder current must be accepted.

Normally the resistors in the bleeder chain are not equal as we have assumed, but are graded according to the voltage distribution recommen-

ded in the photomultiplier data sheets. Two types of bleeder are commonly used.

— A-type, in which the resistors are graded to ensure maximum gain with a given overall supply voltage;
— B-type, in which the resistors are graded to meet the conditions of high linear output current and the best possible time characteristics.

With the overall voltage and the bleeder current known it is easy to calculate the individual resistor values.

Fig. 31 shows the two bleeders recommended for the XP1000 photomultipliers. In the B-type bleeder the voltage across the final stages is successively increased to prevent them becoming prematurely saturated, linearity is thus improved. The time characteristics are also improved by making the voltage between the cathode and first dynode higher, which reduces transit time differences and spread.

With several types of photomultiplier it is advisable to make the voltage on the accelerator electrode (between the cathode and first dynode) adjustable to obtain either optimum collection efficiency or optimum time response. With fast photomultipliers particular care should be paid to correct voltage distribution because of the need for optimum time characteristics.

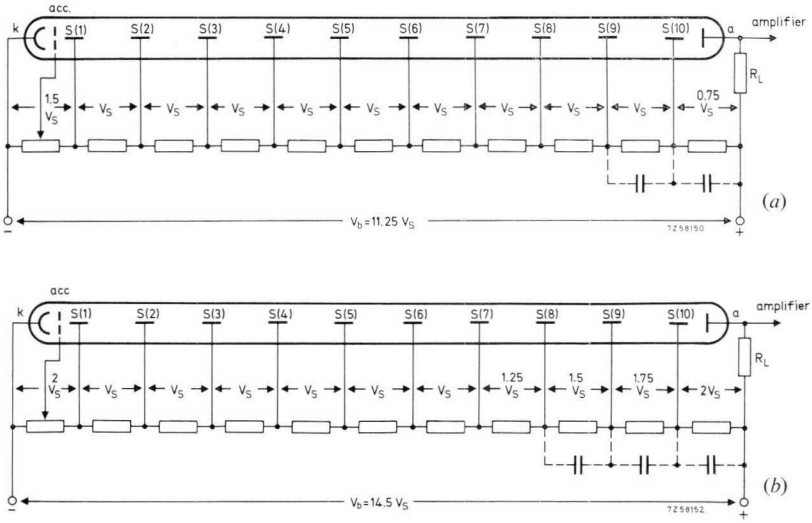

Fig. 31. (a) A-type bleeder, and (b) B-type bleeder for the XP1000 photomultiplier.

2.3.3 Influence of the Earthing Point of the Supply Unit

In view of the high supply voltage used with photomultipliers (in excess of 1000 V) it is of interest to consider which is the best point of the circuit to earth. There are three possibilities, the most suitable of which depends partly on the associated equipment:

— the cathode may be earthed (positive supply voltage);

— one of the dynodes may be earthed (floating supply voltage);

— the anode may be earthed (negative supply voltage).

The second method is usually adopted if separate supply units are used (cf. Fig. 30). The anode is often earthed if it is coupled direct to other signal-handling equipment (no coupling capacitor being used). However, it should be borne in mind that this may temporarily raise the dark current. The high potential difference between the cathode and adjacent parts at earth potential, for example, a Mumetal screen or the shield of the photomultiplier, may give rise to scintillations in the glass envelope that increase the cathode dark current and thus also the anode dark current. As can be seen in Fig. 32, after a time the dark current returns to its normal value.

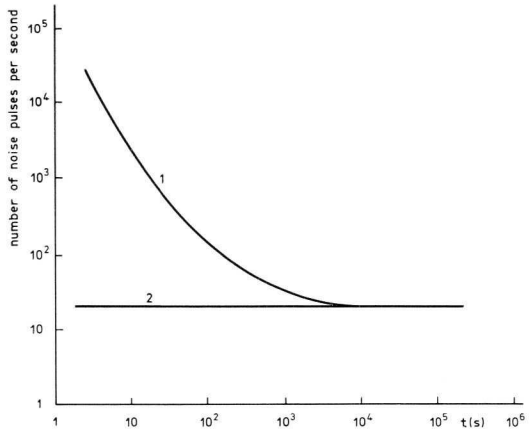

Fig. 32. Decay of the noise pulses after switching-on the photomultiplier. Curve 1 is with the anode earthed, curve 2 with the cathode earthed.

2.4 Magnetic Fields

Magnetic fields affect the behaviour of photomultiplier tubes; gain, for example, may vary markedly under the influence of even the terrestrial magnetic field. Rotating a tube on its axis may cause considerable variation in anode current if there is a magnetic field normal to the axis. This is because of the asymmetry of the first dynode and its location in relation to the cathode and to the focusing and accelerating electrodes.

Because of the distance an electron must travel between the cathode and the first dynode the electron-optical input system is the most sensitive region. Under the influence of magnetic and electric fields electrons may be deflected so much that they never reach the first dynode. This reduces collection efficiency, and hence output current.

To show how magnetic fields influence anode current, we shall first discuss the results of some tests.

2.4.1 Measured Results

Measurements were on an unscreened XP1000 photomultiplier, subjected to a magnetic field the magnitude and direction of which were adjustable. The principal axes are indicated in Fig. 33; the arrows point in the positive direction.

Figs 34*a*, *b* and *c* show the relative anode current as a function of the magnetic flux density B along each of the three principal axes.

Experiments on several tubes justify the following conclusions:

— In general, anode current decreases as magnetic flux density increases.

— The influence of the magnetic field is least along the axis of the tube (Z direction).

— The quantitative results obtained from a single tube are not representative of the type, but the curves have the same general appearance.

— The curves of tubes with large cathodes have more peaks than those of tubes with small cathodes.

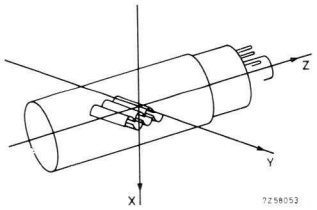

Fig. 33. Defining the axes X, Y, Z.

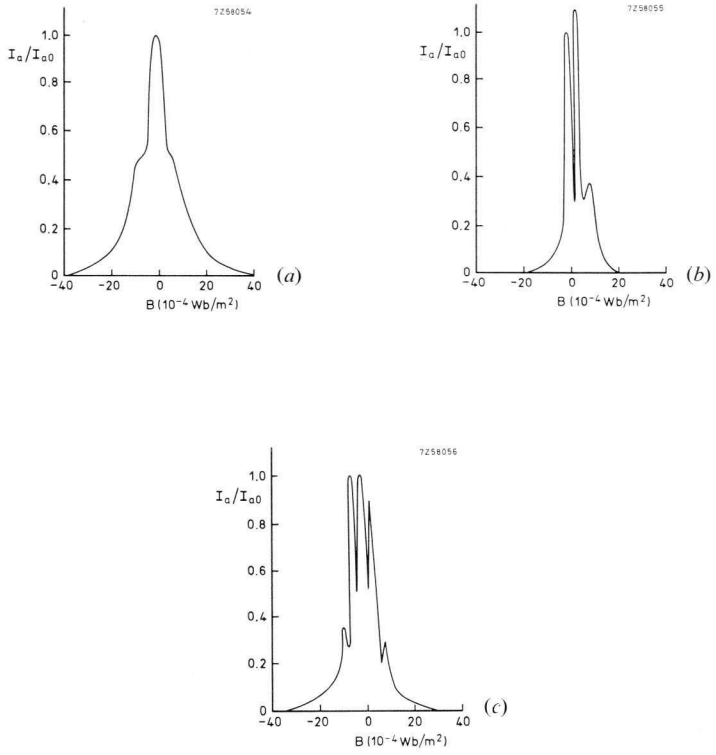

Fig. 34. Effect of a magnetic field on the anode current of an unscreened XP1000 photomulitplier with (a) the field in the Z-direction, (b) in the Y-direction and (c) in the X-direction.

Figs 35 and 36 show the influence of a magnetic field when the tube is rotated with respect to it. This has been plotted in Fig. 35 as a function of the angle, in the plane Y-Z, between the magnetic field and the Z-axis (see Fig. 33); in Fig. 36 it has been plotted as a function of the angle, in the plane X-Y, between the magnetic field and the X-axis.

The graphs reveal that a photomultiplier is so sensitive to magnetic fields as to make magnetic screening essential. As a rule cylindrical screens matched to the type of photomultiplier are available. It is usually sufficient if the upper rim of the screen is at the same height as the cathode of the photomultiplier but screening is better if the screen extends about half its diameter above the photocathode (see below).

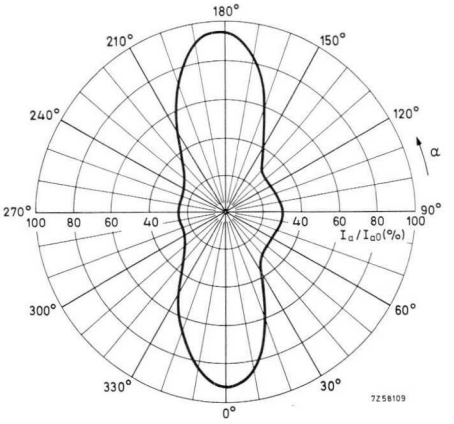

Fig. 35. Relative anode current as a function of the angle between the magnetic field ($B=2\times10^{-4}\,Wb/m^2$) and the X axis in the plane Y-Z.

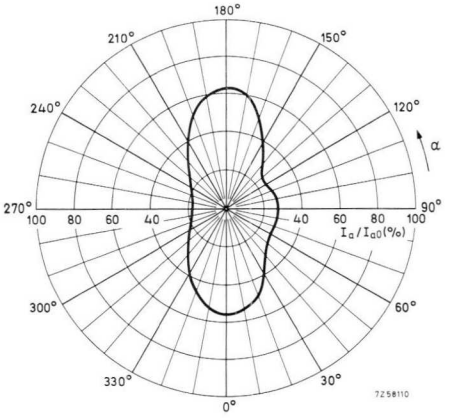

Fig. 36. Relative anode current as a function of the angle between the magneticfield ($B=2\times10^{-4}\,Wb/m^2$) and the X-axis in the plane X-Y.

2.4.2 The Influence of Mumetal Screens

The effect of Mumetal screens on magnetic interference is illustrated by Figs 37*a*, *b* and *c*.These curves give the relative anode current of an XP1000 photomultiplier as a function of the magnetic flux in the four cases illustrated in Fig. 38, namely:

1. unscreened;
2. with the recommended screen (type 56128);
3. with the same screen extending 25 mm above the photo cathode;
4. with a screen Type 56130, 20 mm longer than Type 56128, which screens the entire tube even when it extends beyond the cathode.

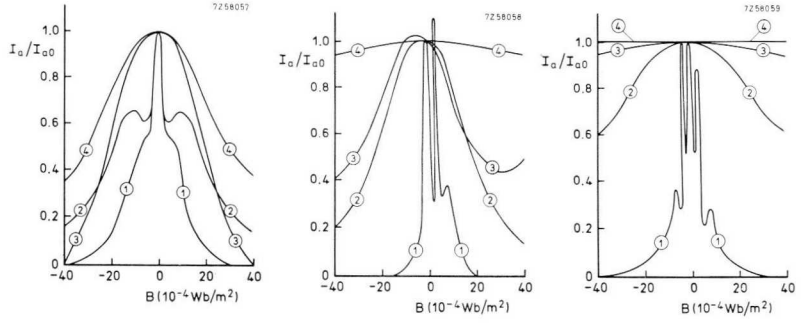

Fig. 37. Effect of a magnetic field on the anode current of an XP1000 photomultiplier with a Mumetal screen; with (a) the field in the Z-direction, (b) in the Y-direction and (c) in the X-direction. The numbers 2, 3 and 4 relate to the position of the screen (see Fig. 38), number 1 is with the photomultiplier unscreened.

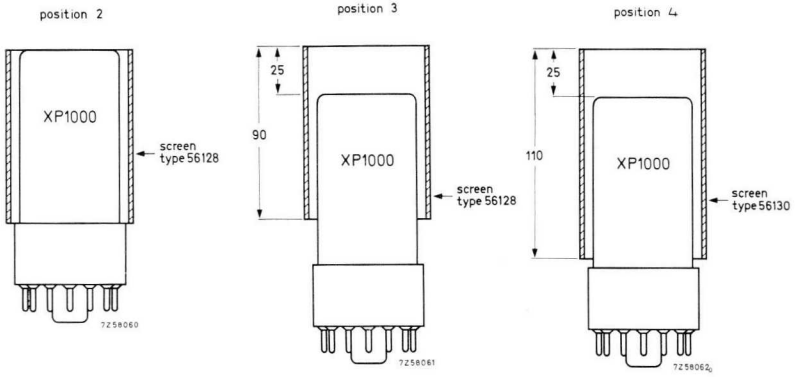

Fig. 38. Positions of the screens used in plotting Fig. 37.

The graphs clearly show that while the screening is most effective in the last case, considerable improvement is obtained by shifting the normal screen upwards.

Where photomultipliers must be used in the presence of extremely strong magnetic fields, a supplementary soft iron screen, shown in Fig. 39, may be necessary.

2.4.3 Properties of Mumetal Screens

Fig. 40 shows the screening factor of several Mumetal screens in respect of a 50 Hz magnetic flux. The screening factor S is defined as the ratio of the applied magnetic field H_a to the magnetic field H_i in the centre of the screen:

$$S = H_a/H_i. \tag{40}$$

The graph clearly shows that the screening factor depends largely on the ratio of the length l to the internal diameter d of the cylindrical screen. The steep fall-off of the curves is caused by the saturation of the Mumetal and is a function of the composition and thickness of the material. Some materials with a saturation point higher than that of "Mumetal" are "Permenorm", soft iron, and "Vacaflux", which are better in this respect than Mumetal by factors of 1.9, 2.5 and 3.0.

Fig. 41 plots the screening factor of several Mumetal screens as a function of frequency. The applied field strength was 80 A/m. The screening factor of screen Type 56136, which has an l/d ratio of almost 4,

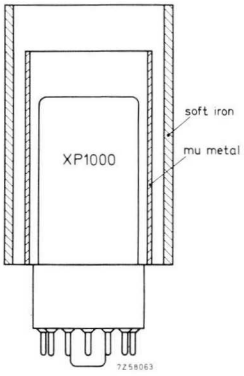

Fig. 39. Photomultiplier with both a Mumetal and a soft iron screen as protection against very strong magnetic fields.

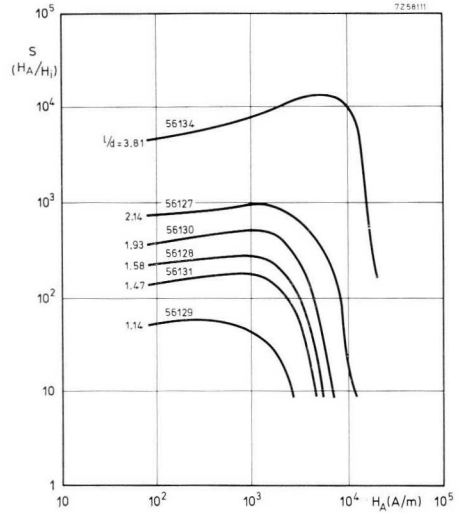

Fig. 40 Screening factor S as a function of the strength H_a of a magnetic field of frequency 50 Hz with screens of different ratio l/d. The magnetic field was normal to the axis of the cylinder.

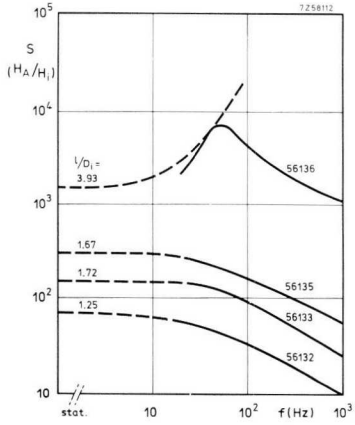

Fig. 41. Screening factor as a function of the frequency of the magnetic fields.[7]

initially rises with frequency, due to decreased penetration into the screen, passes through a maximum and then falls again. At high frequencies a field normal to the axis of the cylinder penetrates further into the cylinder because the ratio l/d is finite; this counteracts the rise and leads eventually to a decrease in the screening factor. The maximum shifts rapidly to lower frequencies as the ratio l/d is decreased. With short cylinders of relatively large diameter there is no maximum and the curves gradually fall off with frequency.

Since permeability depends on temperature, the screening factor is also a function of temperature. Fig. 42 shows the change in relative permeability μ_T/μ_{20} and relative screening factor S_T/S_{20} as functions of temperature t of a type 56135 screen. The screening factor is seen to depend less on temperature than on the permeability of Mumetal. Because the screen is of large diameter the properties of the material have comparatively little influence.

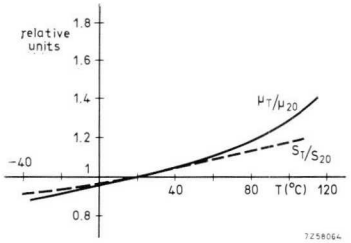

Fig. 42. Relative screening factor S_T/S_{20} and relative permeability μ_T/μ_{20} as functions of temperature, referred to a temperature of 20 °C.[7]

2.4.4 Magnetization of Parts in the Photomultiplier

When working in the neighbourhood of strong magnetic fields there is a risk of some parts of the photomultiplier becoming magnetized. In particular, if parts close to the electron-optical input system are magnetized, collection efficiency might be seriously impaired. Tubes can be demagnetized by placing them in an alternating magnetic field and then slowly removing them. As a rule a magnetic induction of about 10^{-2} Wb/m^2 at 50 Hz, in the centre of a cylindrical coil is sufficient.

2.5 Method of Illuminating the Photocathode

Since the photocathode is formed by vacuum-depositing several materials, its surface may not be perfectly uniform. This causes the cathode sensitivity to vary over its area. A luminous spot moving over the cathode surface will produce a varying output signal. Other factors that influence the uniformity, as presented to the anode, are:

— non-uniform collection efficiency of the electron-optical input system;
— variation of the secondary emission coefficient of the first stage as a function of the angle of incidence of the electrons;
— the wavelength (or photon energy) of the light incident on the cathode.

Collection is not always equally efficient for every point or area of the cathode, deviations can be caused by local disturbances in the radially symmetrical field that directs the electrons from the cathode to the first dynode, perhaps by the parts supporting the electron-optical input system, or perhaps by slight local magnetization. (See section 2.4.4.)

Differences in the secondary emission coefficient of the first stage may so alter the gain of the photomultiplier that anode current varies according to which part of the cathode is illuminated.

For photons of different energy the initial energy of the emitted electrons will also be different and so, too, will the collection efficiency for particular points on the cathode, depending on their position with respect to the first dynode.

It will thus be clear that other factors may influence the output signal to an even greater extent than non-uniformities of the cathode itself. Generally speaking, the cathode uniformity, measured at the anode, is determined mainly by the three factors mentioned above. Photomultipliers with a large diameter cathode and a comparatively small multiplier system are particularly affected by these factors. In photomultipliers with a small diameter cathode and with a multiplier system in a narrow envelope (such as the XP1110 or XP1115) non-uniformity is due mainly to asymmetry of the first dynode with respect to the cathode. Photomultipliers with a cathode 30 mm to 50 mm diameter (such as the 150AVP and XP1000 series), are most uniform.

The degree of non-uniformity can be expressed in several ways, for example in terms of the ratio of the maximum to the minimum sensitivity; in terms of the maximum percentage deviation with respect to the average sensitivity; or in the form of a map of the cathode on which lines of constant sensitivity are traced.

Measurements must always be made with only a given part of the cathode illuminated, the sensitivity of the parts being then compared. The size of the spot is of paramount importance, the smaller it is, the better the definition.

It will be clear that providing reliable information about uniformity is extremely difficult; there is, moreover, a fair chance that the information supplied is of little value in certain applications. It is always better to illuminate so that the part illuminated is independent of the shape and/or position of the light source. A good way is to use an objective with a so-called field lens, as shown in Fig. 43, positioned so that the field lens projects the image of the objective onto the cathode; if the light source is moved the position of the spot on the cathode will not be affected.

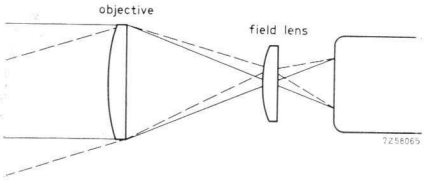

Fig. 43. Optical system with objective lens and field lens to prevent effects due to non-uniformity of the cathode.

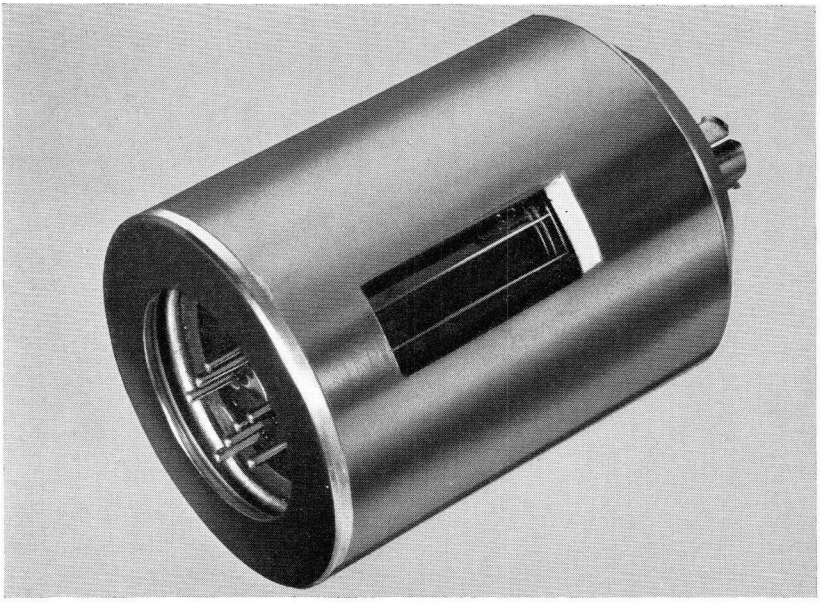

Photomultiplier type XP1143 (approx. half full size).

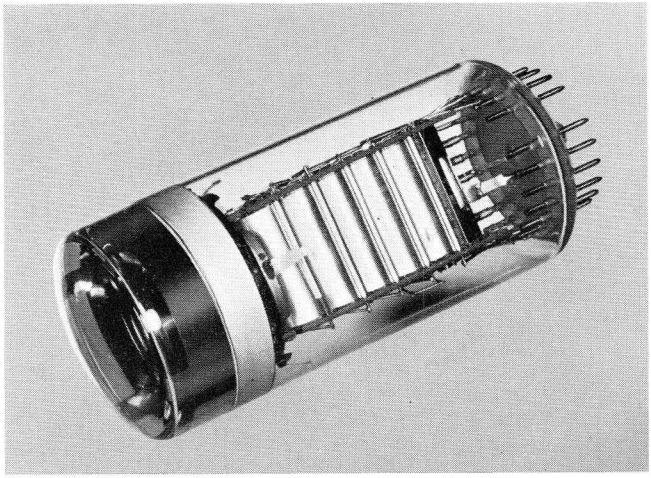

Photomultiplier type PM2003 (approx. half full size).

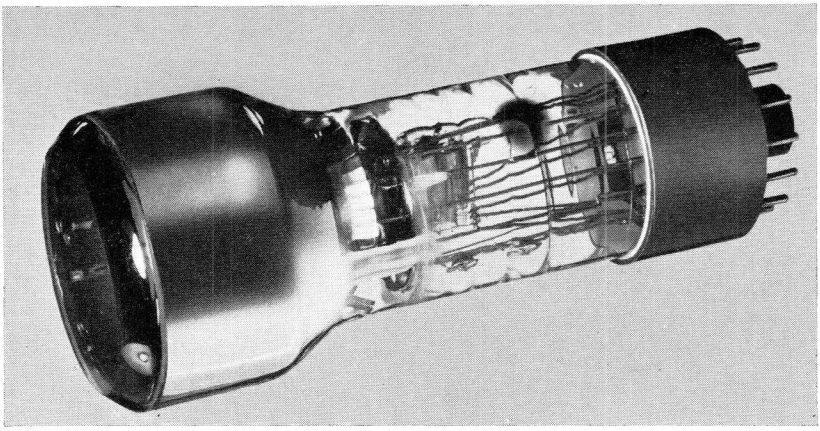

Photomultiplier type XP1033 (approx. half full size).

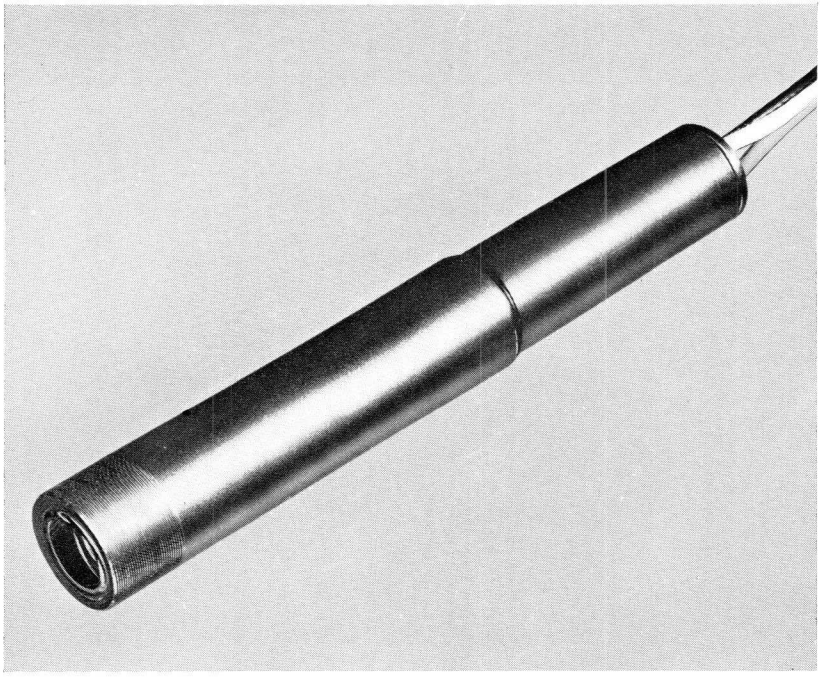

Photomultiplier type PS1520 (approx. 2/3 full size).

3 Photomultiplier Characteristics

In the following sections we shall deal with the photomultiplier characteristics defined earlier. We shall also deal with the causes and consequences of characteristics properties wherever this is of practical interest.

3.1 Cathode Sensitivity

If a radiant power of P watts impinges on a photo cathode, the photoemissive current will be:

$$I_k = \eta_q(\lambda) \cdot (P/h\nu)e, \tag{41}$$

where $\eta_q(\lambda)$ is the quantum efficiency as a function of the wavelength λ,
$h\nu$ is the energy of a photon,
ν is the frequency c/λ,
e is the electron charge (1.6×10^{-19} C),
h is Planck's constant (6.624×10^{-34} Js).

This gives for the radiant cathode sensitivity:

$$N_{kr}(\lambda) = I_k/P = \eta_q(\lambda) \cdot e\lambda/hc, \tag{42}$$

or,
with N_{kr}, λ and η_q in terms of mA/W, Å and % respectively:

$$N_{kr}(\lambda) = \eta_q(\lambda) \cdot \lambda/1240. \tag{43}$$

Since the radiant cathode sensitivity depends on the wavelength, the wavelength must be quoted. Usually it will be the wavelength associated with maximum radiant sensitivity. Complete information concerning the sensitivity of a photocathode would need a characteristic representing the absolute sensitivity in mA/W as a function of wavelength. However, it would be too laborious to do this for every photomultiplier, so it is usual to publish these curves for each type of cathode only (see Fig. 8).

Another way of defining the sensitivity of a photocathode is to measure the photocurrent resulting from accurately specified illumination. Provided the spectral characteristic of the source and its luminous flux are

known, the cathode sensitivity can be expressed in terms of A/lm. The luminous flux, in lm, is given by:

$$\Phi = 682 \int_0^\infty P(\lambda) \cdot V(\lambda) \cdot \mathrm{d}(\lambda), \tag{44}$$

in which $P(\lambda)$ is the spectral characteristic of the light source and $V(\lambda)$ the luminosity function; the factor 682 accounts for the luminosity equivalent in lm/W.

Of the several standard light sources laid down in the International Lighting Vocabulary (3rd edition), the "white A standard" is used for measurements of photosensitive devices. It has a spectral characteristic corresponding to a black body at 2854 °K and is best approximated by an incandescent lamp with a tungsten filament. This gives for the cathode current in mA:

$$I_k = \int_0^\infty N_{kr}(\lambda) \cdot P(\lambda) \cdot \mathrm{d}(\lambda), \tag{45}$$

and for the sensitivity in μA/lm:

$$N_k = \frac{I_k}{\Phi} = \frac{10^3 \int_0^\infty N_{kr}(\lambda) \cdot P(\lambda) \cdot \mathrm{d}(\lambda)}{682 \int_0^\infty P(\lambda) \cdot V(\lambda) \cdot \mathrm{d}(\lambda)}, \tag{46}$$

In practice the luminous flux Φ is determined by measuring the illumination E in the plane of the photocathode to be investigated. If its surface area A is known, the flux is given by:

$$\Phi = AE, \tag{47}$$

in which A is in m^2 and E in lx. The light source is adjusted to a colour temperature of 2854 °K by calibrating it against a standard light source, which makes measurement easy and accurate.

Comparison of eqs (42) and (46) shows that the first calls for the radiant power to be measured, whereas the second calls for the luminous flux at a colour temperature of 2854 °K to be measured. Cathode current can be measured in the same way in both cases and can by conventional means be determined within 1 %.

The radiant power P must be measured with a thermopile or with a photocell calibrated against a thermopile. Since the process of measuring

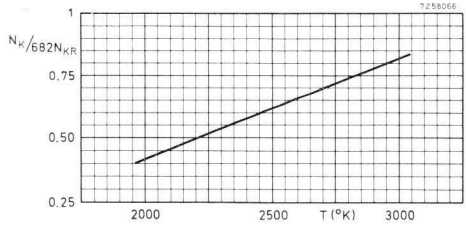

Fig. 44. Influence of the colour temperature T of the light source on the ratio N_{kr}/K for a photomultiplier with an A-type cathode (S11).

with thermopiles is very delicate, because of their fragility, and calls for much experience, routine measurements are usually carried out with a calibrated photocell. However, the limit to absolute accuracy is then set by the calibration of the photocell, which will seldom be better than 5% to 10%.

The accuracy of the luminous sensitivity measurement is governed by the calibration of the light source at 2854 °K and by the measurement of the luminous flux. At present the calibration of colour temperature and the manufacture of standard light sources of a given colour temperature is such that accuracies of 0.5% are practicable. The luminous flux can be measured by means of a photocell provided with a filter that ensures that its spectral sensitivity corresponds to the standardized luminosity function. Such measurements can be performed with an accuracy of within 1%. This means that the accuracy of the luminous sensitivity measurement is roughly an order of magnitude better than that of the radiant sensitivity measurement. It should nevertheless be remembered that introducing the luminosity function obscures to some extent the information regarding the absolute spectral sensitivity.

Fig. 44 illustrates the influence a shift in colour temperature has on the luminous sensitivity measurement, according to the expression:

$$N_k = \frac{N_{kr} \int_0^\infty R(\lambda) \cdot P(\lambda) \cdot \mathrm{d}(\lambda)}{682 \int_0^\infty P(\lambda) \cdot V(\lambda) \cdot \mathrm{d}(\lambda)}, \qquad (48)$$

where N_{kr} is the maximum absolute cathode sensitivity of an A-type cathode (S11), expressed in A/W,

$R(\lambda)$ is the relative spectral sensitivity of an A-type cathode,

N_k is the luminous sensitivity, expressed in A/lm.

If the colour temperature of the light source changes, $P(\lambda)$ will also change so that an error is introduced in the measurement of N_k. Since N_{kr} may be considered as a constant, we may write:

$$N_{kr}/682 = K. \tag{49}$$

In Fig. 44 the ratio N_k/K has been plotted as a function of the colour temperature T. Within the range 2000 °K to 3000 °K the function satisfies the expression:

$$N_k/K = 3.9 \times 10^{-4}\, T - 0.36. \tag{50}$$

It follows that at 2854 °K a change in colour temperature of 1% results in an error in the measured luminous sensitivity of about 1.5%.

It is stressed that these figures apply exclusively to A-type cathodes. For other types of cathode the dependence of the colour temperature will be slightly different.

3.1.1 Relation between Radiant and Luminous Sensitivity

As mentioned before, the luminous sensitivity is a quantity which is often difficult to handle. In particular for measurements of monochromatic light sources the radiant sensitivity provides more direct information. Fortunately it is possible to derive from eq. (48) a conversion factor C that allows luminous sensitivity to be converted into radiant sensitivity:

$$N_{kr} = CN_k, \tag{51}$$

in which by eq. (48), the factor C, expressed in lm/W, amounts to:

$$C = \frac{N_{kr}}{N_k} = \frac{682 \int_0^\infty P(\lambda) \cdot V(\lambda) \cdot \mathrm{d}(\lambda)}{\int_0^\infty R(\lambda) \cdot P(0\lambda) \cdot \mathrm{d}(\lambda)} \tag{52}$$

The relative curves $P(\lambda)$, $V(\lambda)$ and $R(\lambda)$ are all known, so that the conversion factor can be evaluated for any type of cathode by numerical integration. The values for the several types of cathode are entered in the table below.

type of cathode	A (S11)	U (S13)	T (S20)	TU	C (S1)	D	DU
factor C (lm/W)	916	946	440	433	88	1236	1226

3.2 Gain and Anode Sensitivity

Once the cathode sensitivity is known, the anode sensitivity can be calculated from:

$$N_a = GN_k, \tag{53}$$

the gain G being given by:

$$G = I_a/I_k. \tag{54}$$

Since the gain is usually very high ($> 10^6$) it is seldom possible to measure both the anode current and cathode current under the same conditions. With most photomultipliers the maximum permissible anode current is about 1 mA which, with a gain of 10^6, corresponds to a cathode current of 1 nA. Considering the high voltage involved, measurement of such small currents is apt to be considerably influenced by leakage currents between the base connections and in the measuring set-up. In practice it is, therefore, customary to measure the gain in two or more steps, advantage being taken of the following properties:

— a direct linear relationship exists between incident luminous flux and cathode current, anode current and dynode currents;

— gain is independent of the luminous flux and of the wavelength of the light.

The photomultiplier is connected as shown in Fig. 45. With the dynodes $S(5)$ and $S(6)$ connected to the negative terminal of the high voltage source via earth, the electron current flowing through the multiplier system will not reach the anode. Luminous flux can be increased until the cathode current (in the order of 0.1 μA) is high enough for leakage currents to be neglected.

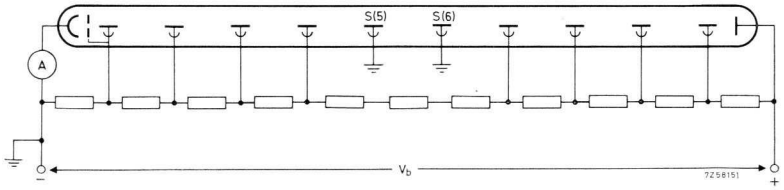

Fig. 45. Circuit for measuring the cathode current of a photomultiplier when finding its gain.

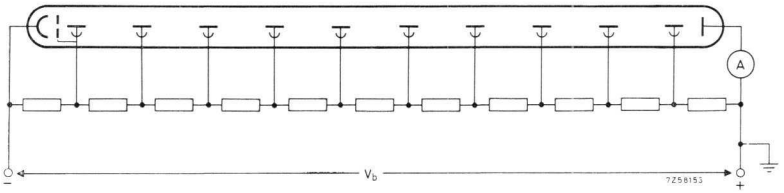

Fig. 46. Circuit for measuring the anode current of a photomultiplier when finding its gain.

To measure the anode current the photomultiplier is connected as shown in Fig. 46. The luminous flux is then reduced by neutral filters until the anode current corresponds to the value encountered in practice (< 100 μA).

The gain is now given by:

$$G = I_a A / I_k, \tag{55}$$

in which the factor A accounts for the attenuation by the neutral filter. If the gain of the photomultiplier is extremely high, it is advisable to measure it in steps, for example from the cathode to the nth dynode and from the nth dynode to the anode. In this way there is no need for such a dense neutral filter, which is difficult to calibrate.

Errors caused by the filter not being quite neutral are avoided by using monochromatic light, obtained by placing an interference filter between the light source and the photocathode.

This method of measuring the gain is to be preferred to another in which the photomultiplier is connected as a diode to measure cathode current (see Fig. 47). This entails the risk that the electric fields in the input system of the photomultiplier are not those obtaining normally, with the result that the saturation characteristics of the input system when the anode current is measured will differ from that when the cathode current is measured.

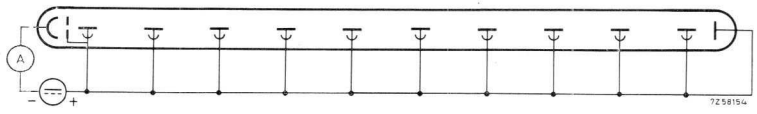

Fig. 47. Photomultiplier connected as a diode.

3.2.1 Gain Variations

In practice the sensitivity of a photomultiplier may fluctuate during operation. Investigations have shown that these are caused mainly by gain fluctuations originating somewhere in the multiplier system. Although this phenomenon has been studied by many investigators, it is not yet clear what the causes of the instability actually are. There are distinct differences in the behaviour of the various types of photomultiplier and even of different specimens of the same type.

Generally speaking, distinction can be made between two types of sensitivity variation:

— shift, which is characterized by a rapid change in gain immediately after the current through the tube has changed as a result of a change in luminous flux;
— drift, which is characterized by a change in gain as a function of time without any change in luminous flux.

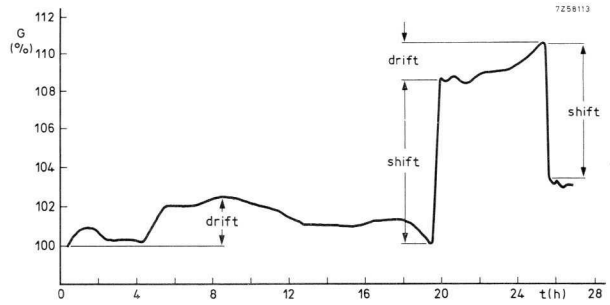

Fig. 48. Relative gain variation of a 53AVP photomultiplier as a result of drift and shift.

Both types of instability are represented in Fig. 48. The shift was measured after the current through the photomultiplier had been raised by increasing the luminous flux. In the present case the gain was shifted in the positive direction, but occasionally a negative shift may be experienced.

Although opinions differ in many respects, there seems to be general agreement that drift and shift can be attributed to the following causes:

— Effects related to insulating materials in the tube being charged so that the electrons may or may not be additionally deflected.
— Changes in the properties of some materials in the tube as a result of chemical reactions, for example the dynode material reacting with residual gases in the tube.

— Caesium atoms being scattered from the dynodes as a result of the electron bombardment, or caesium ions being released from the dynodes by the electric field. Since secondary emission effects reaches a maximum with a certain quantity of caesium, the gain will increase or decrease, depending on the amount of caesium present on the dynodes.

All phenomena related to the instability of a photomultiplier are usually called "fatigue". Fatigue appears to be dependent on such parameters as temperature, voltage, and current through the tube. Some photomultipliers are extremely stable and do not suffer from fatigue, provided the current remains below a given value. Since it is a factor of paramount importance for some applications, tubes are often selected in respect of stability.

Because of the importance of stability in nucleonic research where photomultipliers are used in measuring radiation (via scintillation crystals —see section 4.1.2), selection for stability is usually based on this application. We shall now briefly discuss the procedures used to ascertain shift and drift, and the conditions to be met by selected photomultipliers.

To measure its stability the photomultiplier is used as a scintillation counter in conjunction with a ^{137}Cs source, a pulse height analyser selects the pulses appearing at the anode of the photomultiplier. The distance between the source and the scintillator (plus photomultiplier) is adjustable, so that the number of pulses per second and hence the anode current can be varied.

As the pulse height depends exclusively on the energy of the source and on the anode sensitivity of the photomultiplier, the position of the pulses in an energy spectrum as a function of time is a measure of the gain variation, provided the cathode sensitivity is constant. Drift is measured over a long period at a count rate of 1,000 counts per second, corresponding to an anode current of about 10 nA. Shift is measured by reducing the distance between the source and the scintillation counter so that the count rate rises very rapidly to 10,000 counts per second, corresponding to about 100 nA. During these measurements the ambient temperature is kept constant within $\pm$ 0.5 degC.

The measuring cycle is as follows. After 3 hours operation at a count rate of 1,000 counts per second the position of the energy peak in the energy spectrum is determined once an hour for, say, 20 hours. The *drift* of the photomultiplier is defined as:

$$D = \left(\sum_{i=1}^{n} |\bar{P} - P_i| 100\% \right) / n\bar{P}, \tag{56}$$

where P_i denotes the ith measurement out of a series of n measurements at a count rate of 1,000 counts per second, and $\bar{P}$ the arithmetical average of n measurements. The drift D should not exceed 1%.

The count rate is then increased within a few seconds to 10,000 counts and the position of the energy peak in the spectrum is recorded every 10 minutes, four measurements being made. The *shift SH* of the photomultiplier is then calculated from the expression:

$$SH = \left(\sum_{i=n+1}^{n+4} |P_i - P_n| 100\% \right) / 4P_n, \tag{57}$$

in which P_n is the last measurement of the series carried out at the low count rate (1,000 counts per second); the shift should not exceed 1% either.

It will be clear that the results need interpreting with care since they are related to specific conditions of temperature, voltage and current, other conditions may give different results. In general, however, a photomultiplier selected by this procedure will also be stable under other conditions.

3.2.2 Gain Stabilization by External Means

As mentioned above, stability is of particular interest in nuclear research, which explains why several investigators in this field have essayed designs of feedback circuits to compensate gain variations. These circuits are usually based on the following principle.

In addition to the signal to be detected the photomultiplier is fed with a reference signal from a radioactive source or light source. The two signals from the photomultiplier are separated and the reference is used to drive a system that compensates the gain variation of the photomultiplier, by modifying, for example, the supply voltage or some part of the circuit.

The signal to be detected may in some cases be used as reference. This procedure is often followed in nuclear spectrometry (see section 4.1.2); the multiplier signal then consists of pulses whose amplitudes depend on the energies occurring in the spectrum to be measured. Pulses of a given amplitude or shape can be separated from the signal by discrimination and subsequently serve as reference pulses.

Depending on the advantages and disadvantages to specific applications, the stabilization systems may differ as regards the reference signal or the manner in which the gain variation of the photomultiplier is compensated. In choosing a system due attention should be paid to the influence of the stabilization system on the results.

3.3 Dark Current

The dark current is the current that flows even when the cathode is unilluminated; it has several components, originating from:

— thermionic emission,

— leakage currents,

— ionization phenomena.

— light phenomena,

— field emission.

3.3.1 The Origin of the Several Dark Currents

Thermionic emission is caused by the thermal motion of the electrons in a material (see section 1.1.3). The principal dark current is due to thermionic emission from the cathode and — to a lesser extent — from the first dynode. The total contribution of the thermionic emission to the anode dark current is given by:

$$I_{a0} = I_{k0}\delta^n + I_{s(1)0}\delta^{n-2} + I_{s(2)0}\delta^{n-2} + \ldots ; \qquad (58)$$

of which only the first two terms are significant.

Thermionic emission from the photocathode can be reduced by refrigeration, see sections 2.2.2 and 4.2.1. Thermionic emission from the first dynode can be kept low by using the right material (AgMg) and by making the area as small as practicable. By these means dark current, which is mainly thermionic in origin, can be kept to a reasonable level.

The electrode supports are of insulating materials specially chosen to minimize leakage currents. However, with an insulation resistance of $10^{12}\ \Omega$, the leakage current is no less than 1 nA, which is of the same

order of magnitude as the anode dark current caused by cathode thermionic emission.

The requirements to be met by the insulation are therefore extremely severe. The tube base with its pins are the major source of leakage currents and should be protected when photomultipliers are used under conditions where contamination is likely. It should also be recognized that reducing the atmospheric pressure also reduces the breakdown voltage until, for a given spacing between the pins, the minimum breakdown voltage is reached.

Leakage currents give little trouble unless they flow towards the pin from which the output signal is taken, usually the anode pin. With some tubes the anode connection has a guard ring at roughly the same potential as the anode to prevent leakage currents flowing through the load resistance (see Fig. 49).

The influence of leakage currents on the total dark current is greatest at low voltages, that is, at low gain when there is little amplification of the cathode thermionic dark current.

However carefully a photomultiplier is degassed, some residual gas always remains, so electrons may form ions. Being positive the ions will move in the opposite direction to the electrons, and on reaching the dynodes and cathode may release secondary electrons that will contribute to the dark current.

Another effect that may be caused either by electrons or ions impinging on the glass is fluorescence in the glass envelope. If the resulting scintillations reach the cathode, new electrons will be emitted to add to the dark current. This phenomenon occurs particularly with high gain, and hence high current densities. Apart from raising the dark current, it may give rise to after-pulses, thus introducing errors in pulse applications.

Photomultipliers whose electrode structure is prone to this phenomena are protected by a collar-shaped screen that intercepts both ions and scintillations.

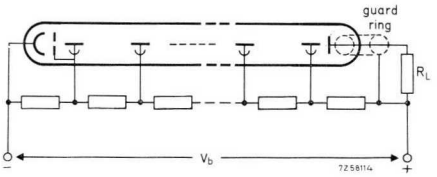

Fig. 49. Photomultiplier provided with a guard ring surrounding the anode pin.

3.3.2 Optimum Ratio between Signal and Dark Current

The anode dark current, like the gain, depends on the supply voltage V_b. The gain and the dark current characteristics of photomultiplier 56TVP have been plotted in Fig. 50. It is customary to plot the d.c. component of the dark current, but because the anode dark current consists of random bunches of electrons of varying amplitude there are also a.c. components.

The d.c. component can be compensated by external circuits, but not the a.c. The supply voltage of the photomultiplier must be so chosen that the ratio between signal and dark current is as high as possible, as will be the case when the ratio of the dark current I_{a0} to the gain is a minimum. This ratio, derived from the characteristics of the 56TVP, has also been plotted in Fig. 50.

If the dark current originated entirely in the cathode, the ratio I_{a0}/G would be a linear function of the supply voltage. However, at low supply voltages the leakage current predominates, causing the $I_{a0} = f(G)$ curve to rise. This also occurs at high voltages when the high electric field strength may cause field emission, and ionization and scintillation phenomena may cause random fluctuations in the dark current.

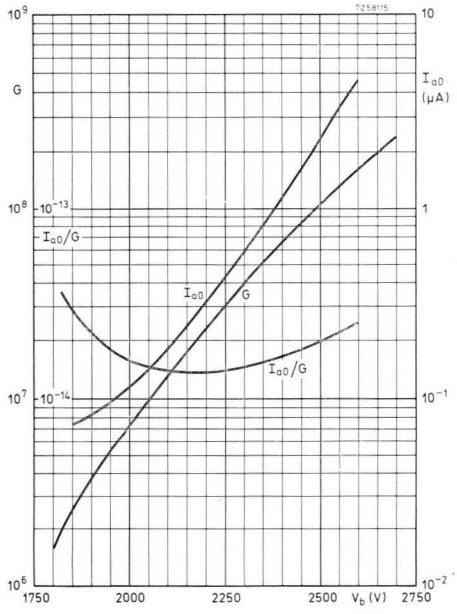

Fig. 50. Gain G, dark current I_{a0} and their ratio as functions of the supply voltage V_b of a 56TVP photomultiplier.

The trend of the curve $I_{a0} = f(G)$ is not the same for all types of photomultiplier, depending as it does on their construction. In many cases the curve does not pass through a minimum and may either rise or fall as the supply voltage increases.

3.3.3 Amplitude Distribution of the Dark Current

The anode dark current can be measured in several ways. Depending on the measuring procedure, the dark current is observed as a d.c. current or as a pulsatory current of varying amplitude.

A current meter with a long time constant will read the average value or the d.c. component of the dark current. If the time constant is very short, as when a wide-band oscilloscope is used, the dark current will appear to consist of random unidirectional current pulses of varying amplitude. (It should be noted that the current pulses are often called "dark current noise" in view of their shape; this is, however, deprecated as it may lead to confusion with the noise component of the d.c. dark current, to which the term dark current noise should be reserved.

It will be clear that in pulse applications (e.g. photon counting) the amplitude distribution and the frequency of the unidirectional dark current pulses determine the lowest signal that can be detected. With a pulse-height analyser, that sorts the pulses according to their amplitude, the amplitude distribution of the dark current pulses can be investigated. Fig. 51 gives an example of such measurements, showing that the spread

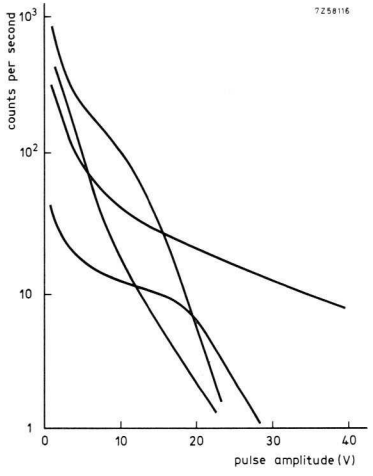

Fig. 51. Number of counts per second in the interval $V + \delta V$ as a function of the pulse amplitude V. The curves were obtained with different photomultipliers.

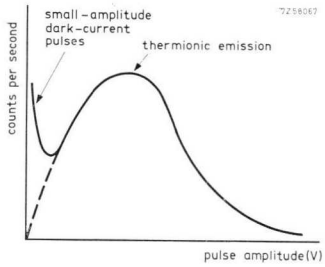

Fig. 52. Amplitude distribution of dark-current pulses caused mainly by thermionic emission.

of the distribution curves can be quite considerable. It is, moreover, seen that the dark current contains many pulses of low amplitude that are attributable to electrons that have not been fully amplified by the multiplier system. This means that they either do not originate from the cathode or, if they do, they did not reach the anode via the multiplier system.

The thermionic dark current pulses which have been fully amplified by the multiplier system are represented in the distribution curve. Since the gain of the multiplier system displays statistical spread, the amplitudes of the thermionic dark current pulses will be statistically distributed (see section 3.4.3).

Signal electrons cannot be distinguished from thermionic electrons, their amplitude distributions being identical. The difference between dark current pulses and the lowest signal pulses depends on the least perceptible difference in count rate of pulses of the same average amplitude as the thermionic dark current pulses. Not only must the difference in count rate be ascertained, electrons originating from the cathode must be distinguished from those originating from other points in the tube.

By taking great care in the construction of the photomultiplier the frequency of dark current pulses of low amplitude can be kept low. The amplitude distribution of the dark current pulses will then be similar to the graph shown in Fig. 52.

3.4 Noise [8]

Noise is a generic name given to disturbances caused by fluctuations in the transport of electric charges. If these fluctuations are treated as random phenomena, probability theory allows reliable quantitative data on noise to be obtained. All statistical fluctuations that may occur during the handling of the signal must be considered in photomultipliers:

— those occurring while the photocathode converts light into electrons,
— those introduced during amplification by the secondary emission system.

The variance, that is the mean square of the signal deviations with respect to the mean signal value, is a measure of the noise. Once the probability distribution of the signal fluctuations is known, the r.m.s. or effective value of the noise in the signal can be derived.

3.4.1 Noise in Vacuum Photocells

The input system of a photomultiplier is comparable to a saturated photodiode; noise theories applicable to photodiodes are also valid for photomultipliers. The number of electrons that light releases from the cathode is subject to fluctuations due to two statistical phenomena:

— fluctuations caused by the statistical distribution of the number of photons;
— fluctuations in the conversion of photons into electrons depending on whether or not an electron is liberated by a photon.

The statistical distribution of the photons incident on the cathode can be described by Poisson's equation:

$$P(N_p) = (\bar{N}_p{}^{Np}/N_p!) \cdot \exp(-\bar{N}_p), \tag{59}$$

in which $P(N_p)$ denotes the chance that N_p photons reach the cathode within a given time interval, and $\bar{N}_p$ is the average number of photons per time interval.

The statistical distribution of the photoelectric phenomenon can be described by a binomial probability distribution:

$$P(N_e) = \frac{N_p!}{N_e!(N_p - N_e)!} \cdot p^{Ne}(1-p)^{Np-Ne}, \tag{60}$$

where $P(N_e)$ is the probability that N_e electrons are liberated from the cathode in a given time interval if N_p photons impinge on the cathode during this interval, and p denotes the probability of one electron being liberated from the cathode by one photon, thus corresponding to the quantum efficiency η_q, which can be expressed by:

$$p = \eta_q = N_e/N_p = \bar{N}_e/\bar{N}_p. \tag{61}$$

During a given interval τ, the deviation in the number of electrons emitted by the cathode with respect to the average number of electrons is deter-

mined by the sum of the fluctuations due to the photon statistic and to the conversion statistic:

$$(N_e - \bar{N}_e)_{\text{tot}}{}^2 - (N_p - \bar{N}_p)\eta_q + (N_e - \bar{N}_e). \tag{62}$$

the total variance thus becomes:

$$\overline{(N_e - \bar{N}_e)_{\text{tot}}{}^2} = \overline{(N_p - \bar{N}_p)^2}\eta_q{}^2 + \overline{(N_e - \bar{N}_e)^2}. \tag{63}$$

The variance of a Poisson distribution (eq. (59)) can be expressed by:

$$\overline{(N_p - \bar{N}_p)^2} = \bar{N}_p, \tag{64}$$

and that of a binomial distribution (eq. (60)) by:

$$\overline{(N_e - \bar{N}_e)^2} = \bar{N}_e(1 - p). \tag{65}$$

From eqs (61) and (65):

$$\overline{(N_e - \bar{N}_e)^2} = \bar{N}_p\eta_q(1 - \eta_q). \tag{66}$$

The total variance is obtained by substituting eqs (64) and (66) in Eq. (63):

$$\overline{(N_e - \bar{N}_e)_{\text{tot}}{}^2} = \bar{N}_p\eta_q{}^2 + \bar{N}_p\eta_q - \bar{N}_p\eta_q{}^2 = \bar{N}_p\eta_q = \bar{N}_e. \tag{67}$$

If, during interval τ, N_e electrons are emitted by the cathode, the current averaged over this time interval will thus be $N_e \cdot e/\text{t}$, in which e denotes the electron charge. The d.c. cathode current will be the average of this value, that is, $I_k = \bar{N}_e \cdot e/\tau$. The deviation of the current during interval τ therefore amounts to:

$$i_\tau = (N_e - \bar{N}_e)e/\tau, \tag{68}$$

for which, according to the above argument, we may write:

$$i_\tau{}^2 = (N_e - \bar{N}_e)_{\text{tot}}{}^2 \cdot e^2/\tau^2 = \bar{N}_e \cdot e^2/\tau^2 = I_k \cdot e/\tau. \tag{69}$$

Eq. (69) shows that $\overline{i_\tau{}^2}$ is inversely proportional to the time interval τ during which the measurement is carried out. Since τ depends on the bandwidth of the measuring circuit which records the noise current, it is obviously necessary to allow for this bandwidth in eq. (69). If τ is the interval during which the measuring circuit can record just one signal fluctuation, it can be derived that τ is related to the bandwidth Δf by:

$$\tau = 1/2\Delta f.$$

Substituting this in eq. (69) yields the shot-noise equation:

$$\overline{i_n{}^2} = 2eI_k\Delta f. \tag{70}$$

Considering that the cathode current I_k is composed of a signal current I_{ks} and a thermal dark current I_{k0}, the effective noise I_{kn} in the cathode signal can be expressed by:

$$I_{kn} = \{2e(I_{ks} + I_{k0})\Delta f\}^{1/2}. \tag{71}$$

Since with the purely random phenomena considered here the contribution of each electron results in an infinitely rapid disturbance, all frequencies will be equally represented. The frequency limitation depends on the minimum time an electron takes to acquire the photon energy and be emitted, but this is so short as to imply no practical frequency limit so the frequency spectrum may be taken to be uniform.

The relative variance of the conversion distributional characteristic is a measure of the signal-to-noise ratio at the input to the photomultiplier. In a general form the relative variance is given by the square of the standard deviation of the mass divided by the square of the average of the mass. Applying this to eq. (66) yields for the relative variance of the number of electrons.:

$$v_e = \bar{N}_p\eta_q(1 - \eta_q)/(\bar{N}_p\eta_q)^2 = (1 - \eta_q)/\bar{N}_p\eta_q. \tag{72}$$

This equation shows that to obtain a high signal-to-noise ratio at the input to the photomultiplier, the average number of photons $\bar{N}_p$ and/or the quantum efficiency η_q should be as high as possible. It is therefore important for the window of the photomultiplier to have a good transmission.

The signal-to-noise ratio depends not only on the factors discussed above, the construction of the electron-optical input system of the photomultiplier has also considerable influence. Collection should be as efficient as practicable and be substantially the same for any point on the cathode. It can be calculated that the total relative variance v_{tot} at the output of a photomultiplier is given by:[9]

$$v_{\text{tot}} = v_p + (1 - \eta_c\eta_q + v_s)/N_p\eta_c\eta_q, \tag{73}$$

where $\bar{N}_p$ is the average number of photons incident on the cathode,
v_p is the relative variance of the number of photons,
η_c is the collection efficiency of the electron-optical input system,
η_q is the quantum efficiency,
v_s is the relative variance of the single electron spectrum, that is, the statistic of the multiplier system.

3.4.2 Noise Contribution of the Multiplier System

The output signal of a photomultiplier of n stages, each with a secondary emission factor δ, is given by:

$$I_a = I_k \delta^n. \tag{74}$$

If the multiplier system contributed no noise, the output noise could be determined in a similar way, that is, by:

$$i_{an} = \delta^n (2eI_k \Delta f)^{\frac{1}{2}} \qquad \text{or} \qquad \overline{i_{an}^2} = 2eI_k \delta^{2n} \Delta f, \tag{75}$$

assuming the dark current I_{k0} to be negligible with respect to I_k and the collection efficiency of the input system to be 100%.

Since, however, δ depends on such factors as the penetration of the primary electron, the total gain δ^n is subject to fluctuations that add to the noise in the output signal. The first stage introduces a noise current i_1 which is multiplied by $n-1$ stages, the second stage a noise current i_2 multiplied by $n-2$ stages, and so on. If we denote the probability of a primary electron releasing m secondary electrons by $P(m)$, we may put the part of the primary current I_k which liberates m electrons per primary electron as:

$$I_{k(m)} = P(m) \cdot I_k. \tag{76}$$

The statistical fluctuations derived in section 3.4.1 for shot noise will also be present in the current $I_{k(m)}$, whence:

$$\overline{I_{k(m)}^2} = 2eI_{k(m)} \Delta f. \tag{77}$$

Now

$$\sum_{m=0}^{\infty} P(m) = 1, \qquad \sum_{m=0}^{\infty} m \cdot P(m) = \delta, \qquad \sum_{m=0}^{\infty} m^2 \cdot P(m) = \beta\delta, \tag{78}$$

in which β is a proportionality constant. If all secondary electrons land on the following dynode, the variance of the secondary current is given by:

$$\overline{i_s^2} = \sum_{m=0}^{\infty} 2I_{k(m)} m \Delta f.e \tag{79}$$

From eqs (76), (78) and (79):

$$\overline{i_s^2} = 2eI_k \beta \delta_1 \Delta f, \tag{80}$$

in which δ_1 denotes the secondary emission factor of the first stage. If each primary electron liberates δ_1 secondary electrons, the noise current due to the secondary electrons of the first stage is, according to eq. (75):

$$\overline{i_{sn}^2} = 2eI_k\delta_1^2\Delta f. \tag{81}$$

The difference between eqs (81) and (80) is the noise contribution of the first stage:

$$\overline{i_1^2} = 2eI_k\delta_1(\beta - \delta)\Delta f. \tag{82}$$

Similarly, the noise contribution of the second stage will be:

$$\overline{i_2^2} = 2eI_k\delta_2^2(\beta - \delta)\Delta f. \tag{83}$$

For a multiplier with n stages and $\delta_1 = \delta_2 = \ldots = \delta_n$ the total noise is found by summing all noise contributions, which gives:

$$\overline{i_{an}^2} = 2eI_k\Delta f\delta^{2n} + 2eI_k\delta(\beta - \delta)\Delta f\delta^{2n-2} + \\ + 2eI_k\delta^2(\beta - \delta)\Delta f\delta^{2n-4} + \ldots . \tag{83a}$$

The second and following terms form a descending geometric progression with argument $1/\delta$. If $n \gg 1$ and $\delta > 1$ then $0 < 1/\delta < +1$, this yields

$$\overline{i_{an}^2} = 2eI_k\Delta f\delta^{2n}(\beta - 1)/(\delta - 1). \tag{84}$$

Although not always strictly true, the secondary emission effect is often assumed to have a Poisson distribution. This means that the noise contribution per stage, as given by eq. (82). consists of shot noise, $\beta - \delta$ being unity. Introducing this into eq. (84), we find for the noise at the output of a photomultiplier with n stages:

$$\overline{i_{an}^2} = 2eI_k\Delta f\delta^{2n}\delta/(\delta - 1). \tag{85}$$

Substitution of eq. (74) in eq. (85) yields:

$$\overline{i_{an}^2} = 2eI_a\delta^n\Delta f\delta/(\delta - 1). \tag{86}$$

If we compare this result with eq. (75), we see that the multiplier system increases the noise by a factor $\delta/(\delta - 1)$. The calculated noise output according to eq. (86) proves to be in fair agreement with the measured values, as is evidenced by Fig. 53. The larger the value of δ, the smaller

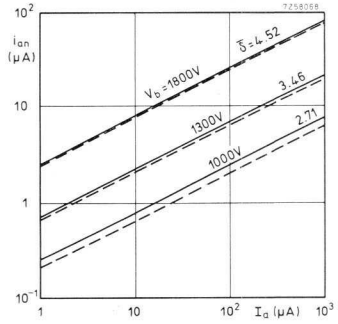

Fig. 53. Effective noise i_{an} as a function of the signal I_a. The curves in full line show the measured results, those in broken line the calculated results. They apply to an XP1000 photomultiplier with an A-type bleeder; $\Delta f = 4$ MHz.

the difference between the calculated and measured values seems to be. One reason for discrepancy is probably that the statistic of the multiplier is not always Poisson as assumed, but for practical purposes eq. (86) can be used.

3.4.3 The Single-Electron Spectrum

The statistically fluctuating amplifying process of a multiplier system can best be judged by a single-electron spectrum. If one electron enters the multiplier system the resulting current pulse at the anode will have a shape that depends on two quantities that are independently subject to statistical fluctuations:

— the gain of the multiplier system, which depends on the secondary emission factor and the mutual collection efficiency of the multiplier stages;
— the electron transit times which, not being identical for all electrons, give pulses of finite width instead of lines.

The pulse width is not the same for every electron, so the spread in transit time also causes the amplitude of the output signal to vary. The ratio of the charge arriving at the anode to the charge of the single electron is a measure of the gain. Since the charge at the anode corresponds to the area of the output pulse, integration will yield a defined pulse whose amplitude corresponds to the gain of the amplifier. The number of pulses with amplitudes ranging from V_i to $V_i + \Delta V_i$ during a time interval Δt then provides the statistical distribution of the output pulses caused by single electrons (see Fig. 54).

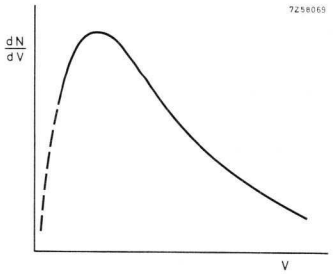

Fig. 54. Example of a single-electron spectrum.

Section 3.3.3 described in brief the method of recording the amplitude distribution of the dark current pulses. The same method is used to record a single-electron spectrum, with the difference, however, that there is a greater probability of the spectrum referring exclusively to single electrons.

This may be explained as follows. If the photocathode is illuminated by a monochromatic luminous flux that is so weak that there is but little chance of an electron being emitted, the probability is great that the spectrum is caused by single electrons. The luminous flux must be monochromatic because otherwise the secondary emission factor of the first dynode might be influenced by differences in the initial energy of the released electrons.

In section 3.4.1 the photons were assumed to be emitted according to a Poisson distribution. The conversion of photons into electrons and the collection of the electrons by the multiplier input system are statistical processes with but one alternative so the distribution of the electrons at the input of the multiplier system is also characterized by a Poisson distribution. As for eq. (59) we may write:

$$P(N_e) = (\bar{N}_e{}^{Ne}/N_e!) \cdot \exp(-\bar{N}_e). \tag{87}$$

Assuming the average number of electrons $\overline{N_e}$ per time interval $\Delta\tau$ to be 0.1 yields:

$$P(0) = 90\%, \quad P(1) = 9\%, \quad P(2) = 0.4\%.$$

The probability of an output signal being caused by *at least one* electron is therefore:

$$1 - P(0) = 10\%.$$

The ratio $P(1)/\{1-P(0)\}$ defines the proportion of the output signal caused by single electrons. For $\bar{N}_e = 0.1$ this ratio thus is $0.09/0.1 = 90\%$. Assuming the collection efficiency to be 100%, the current in the first dynode will equal I_k whence:

$$N_e = I_k \Delta\tau/e = I_k/2\Delta fe. \tag{88}$$

If the system has a bandwidth of 1 MHz and $\bar{N}_e = 0.1$, eq. (88) yields a cathode current of $I_k = 3.2\times10^{-14}$ A. With a gain of 10^6 this results in an anode current of 3.2×10^{-8} A. A cathode sensitivity of about 60 mA/W at 4000 Å thus requires a radiant power of:

$$P = 3.2\times10^{-14}/6\times10^{-2} = 5.3\times10^{-13} \text{ W}.$$

The above figures give an impression of the order of magnitude of the currents, the level of radiation and the bandwidth of the system needed to record a single-electron spectrum. It will be clear that whether or not such a spectrum can be plotted depends on the dark current characteristics of the photomultiplier (see section 3.3.3). The dark current spectrum must be such that the signal electrons and the thermionic electrons can be clearly distinguished.

To reduce the influence of the dark current pulses on the single-electron spectrum either of two measuring methods can be used. In one use is made of a continuous light source (incandescent lamp). The dark current is measured separately and then subtracted from the single electron measurement. Unfortunately this method can be used only if the dark current is sufficiently low with respect to the signal current, which according to eq. (88) is proportional to the bandwidth of the measuring system. The greater the bandwidth, the larger the permissible dark current will be. In practice the maximum permissible dark current is about 10^{-16} A/cm^2, corresponding to 1000 electrons per second.

The other method makes use of a pulsed light source with a pulse duration of a few ns and a pulse repetition frequency ranging from 5 kHz to 10 kHz. The measuring equipment is controlled by electric pulses synchronized with the light pulses to record only signals that coincide with the light pulses. In this way the majority of the dark current pulses are eliminated. The difference between the two spectra can now be ascertained under much more favourable conditions than with the previous method. Pulsed operation has one drawback: that it takes longer to plot a given spectrum.

Apart from being influenced by dark current pulses and phenomena related to the flow of electrons through the tube (e.g. scintillations in the glass envelope), the single-electron spectrum may be affected by non-uniformity of the dynodes. This may be explained as follows[10].

Let us assume that the secondary emission process obeys a Poisson distribution, but that the effective secondary emission factor varies for different points of the dynode due to variation in the average number of emitted electrons and the differing probabilities of them reaching the next dynode. The *local average value* of the secondary emission coefficient thus differs from place to place, obeying a Laplace distribution. The relative variance of the distribution of all secondary electrons which reach the next dynode is thus larger than would be the case if the statistical spread were characterized exclusively by a Poisson distribution. Experiments have shown that the statistic of the multiplier system can be better described by a Polya distribution (also called negative-binomial or compound-Poisson distribution).

If a single electron reaches the input system, the probability of N_e electrons being produced after n stages of amplification (where $N_e \geqslant 1$ and $n \geqslant 1$) is given by:

$$P_n(N_e) = \frac{\delta \sum_{i=0}^{i=Ne-1} P_n(i) \cdot P_{n-1}(N_e - i)\,\{N_e + i\,(b-1)\}}{N_e[1 + b\delta\,\{1 - P_{n-1}(0)\}]}, \quad (89)$$

and

$$P_n(0) = [1 + b\delta\{1 - P_{n-1}(0)\}]^{-1/b}, \quad (90)$$

in which δ denotes the average secondary emission factor per stage and b the relative variance of the Laplace distribution.

It follows from the single-electron requirement on the first dynode that:

$$P_0(1) = 1 \quad \text{and} \quad P_0(0) = 0. \quad (91)$$

Taking this expression as a starting point, all possible probabilities can be calculated by means of eqs (90) and (89).

The relative variance of the Polya distribution after the electrons have been amplified in n stages is given by:

$$v = (b + \delta^{-1})(1 + \delta^{-1} + \delta^{-2} + \ldots + \delta^{-n+1}) \quad (92)$$

or

$$v = (b\delta + 1)/(\delta - 1). \quad (93)$$

Several distributions calculated from eqs (89), (90) and (91) have been plotted in Fig. 56. These curves have been normalized to make their averages unity. The Polya distribution appears to be representative for several forms of single electron spectra. When $b = 0$, that is, when the secondary emission factor is uniform for the whole surface area of the dynodes, the distribution is Poisson. When $b = 1$ the distribution becomes exponential, and when b exceeds 0.5 the distribution clearly assumes a quasi-exponential character (see Fig. 56).

As mentioned before, b is a measure of the spread of the average local secondary emission factor over the surface of the dynode. A relative standard deviation of 10% corresponds to $b = 0.01$. Fig. 57 compares the results of measurements on photomultipliers with linear focus and with Venetian blind dynode systems with the calculated single-electron spectra for two values of b. The agreement between the measured and calculated values appears to be excellent.

Comparison of the geometry of the linear focus and the Venetian blind systems suggests that b is larger in the latter case. In fact, linear focus systems are designed to keep the electrons well focused during their travel

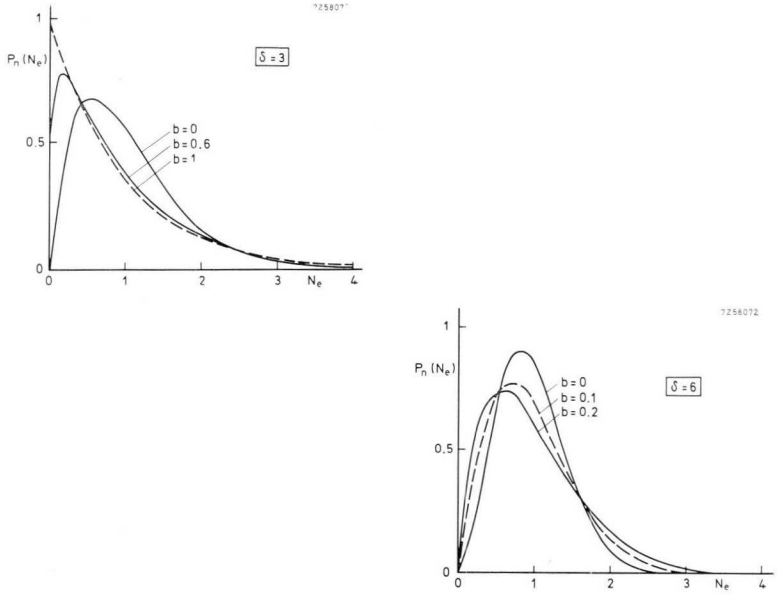

Fig. 56. Calculated single-electron spectra for different values of δ and b.

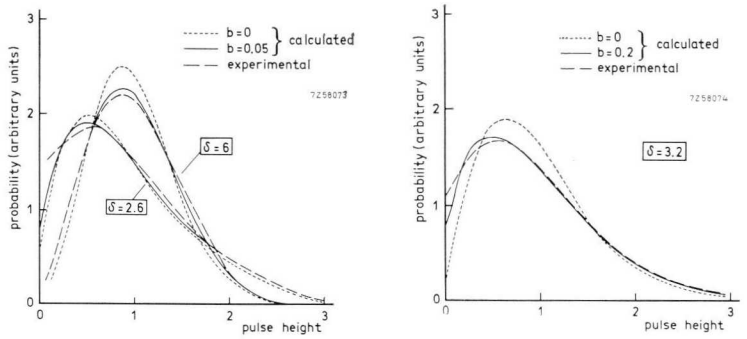

(*a*) (*b*)

Fig. 57. Comparison of calculated and experimental single electron spectra, (a) for a linear focus multiplier and (b) for a Venetian blind multiplier.

through the tube, so non-uniformities of the dynode play a much smaller part.

It should be recognized that the above comments are not sufficient proof that the widening of the single-electron spectrum is exclusively due to non-uniformities of the dynodes. Other causes, such as a non-Poissonian behaviour of the secondary emission process itself, might also contribute.

Investigations with single-electron spectra have been a great help in improving the noise properties of multiplier systems by designing special tube constructions.

The derivation of the noise contribution given in section 3.4.2 shows that the noise contribution of the multiplier system is governed mainly by the first stage. The signal-to-noise ratio is favourably influenced by giving the first stage a high value of δ (see eqs (82), (83) and (83*a*)).

With very low light levels, for example in photon counting, it is of prime importance that the number of low-amplitude pulses be kept small. It follows from the above comments and from Fig. 57 that this can be achieved with a high average value of δ and a multiplier construction that ensures the best possible focussing of the electron beam.

3.4.4 Noise Definitions

To calculate the minimum signal that can be detected, the noise properties of the photomultiplier must be known. The form in which the noise

properties are specified should, however, be such that a user can calculate the minimum detectable signal obtaining in his particular field. This explains why several noise definitions are used.

In general the noise can be expressed in terms of the following quantities:

— the r.m.s. or the peak output noise current, expressed in A,
— the equivalent noise input, expressed in lm,
— the noise equivalent power in terms of radiant power in W,
— the background noise, that is, the number of noise and dark current pulses per second at the output of the photomultiplier.

All these expressions for the noise properties refer exclusively to the noise the photomultiplier introduces in the absence of a signal. The additional noise produced as a result of a signal being present (shot noise) can be closely approximated by eq. (85) or eq. (86).

A less familiar method is to specify the single-electron detection efficiency. Since this characteristic is used almost exclusively in such special applications as liquid scintillation counting it is published only for photomultipliers used in this field.

In publishing the noise properties the conditions of measurement (e.g. supply voltages, temperature and bandwidth) should also be quoted unless they are commonly known.

In choosing the anode load of the photomultiplier, the Johnson or thermal noise voltage V_T of the load resistance should be taken into account. This is given by:

$$V_T = (4kT\Delta f R)^{\frac{1}{2}} , \tag{94}$$

in which R is the resistance, k the Boltzmann constant, and T the absolute temperature.

The combination of the shot noise as given by eq. (86) and the Johnson noise given by eq. (94) results in a noise voltage across the load resistance of:

$$\begin{aligned} \overline{V_{an}{}^2} &= 2eR^2 I_a \Delta f \delta^n \cdot \delta/(\delta - 1) + 4kTR\Delta f \\ &= eR\Delta f \{2\delta^n R I_a \cdot \delta/(\delta - 1) + 4kT/e\}. \end{aligned} \tag{95}$$

At an ambient temperature of 300 °K, $4kT/e \simeq 0.1$. To ensure that the signal is not drowned by the Johnson noise the following condition must be met:

$$2\delta^n R I_a \cdot \delta/(\delta - 1) > 0.1.$$

Neglecting $\delta/(\delta - 1)$ and substituting G for δ^n

$$RI_a > 0.05/G. \tag{96}$$

Reverting to the photocell analogy where $RI_a > 0.05$, we can see that the load resistance of the photomultiplier can be reduced by a factor G. In addition to the advantage of the lower Johnson noise, this also means that because the cut-off frequency is determined by the product of load resistance and capacitance across it, it is easier to design the output circuit of the photomultiplier so that high frequency signals are not attenuated.

Equivalent Input Noise

As mentioned above, the noise properties of a photomultiplier are often quoted in such a way that they are directly applicable to a specific field of application. To determine the minimum detectable signal, the effective (or peak) value of the noise current at a given bandwidth would often be impractical, which is why the "equivalent noise input" (E.N.I.) and the "noise equivalent power" (N.E.P.) have been introduced for the photometric and spectrometric fields. Both expressions have been defined earlier and are based on a measurement frequently occurring in photometry. These quantities are found in the following way[11].

The luminous flux incident on the cathode is periodically intercepted by a mechanical chopper so that a square wave voltage appears at the anode of the photomultiplier. It is customary to choose a chopper frequency of about 100 Hz and to use either a light source with a colour temperature of 2854 °K or in the case of N.E.P. measurements, monochromatic light.

A low-pass filter is used to limit the equivalent noise band-width, $\Delta f_{eq} = 1.57\ \Delta f_{3db}$, to 1 kHz. The effective value of the output signal is measured by an r.m.s. instrument. Fig. 58 shows the block diagram of the set-up.

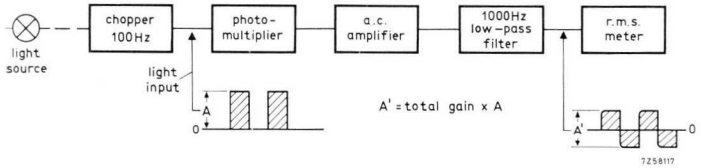

Fig. 58. Measuring set-up for establishing the equivalent noise input (E.N.I.).

Two measurements are made in succession: one with the light source switched on, as indicated in Fig. 58, the other with the light source switched off so that only the effective value of the noise V_n is measured. If the luminous flux Φ is known, the E.N.I. for a bandwidth of 1 Hz, Φ_{ENI}, can be derived from the ratio of the two measurements according to:

$$\Phi_{ENI} = \Phi V_{n(1\text{ Hz})}/V_{s(1\text{ Hz})}, \tag{97}$$

in which $V_{n(1\text{ Hz})}$ denotes the noise voltage and $V_{s(1\text{ Hz})}$ the signal voltage, both at a frequency of 1 Hz. The signal for a bandwidth of 1 Hz is the effective value of the *fundamental* of the square wave signal.

In the set-up of Fig. 58 $V_{s(1\text{ Hz})}$ can be calculated from the reading E of the r.m.s. meter. For a 100 Hz symmetrical square wave voltage and a system with an equivalent noise bandwidth of 1 kHz ($f_{3db} = 1000/1.57 = 637$ Hz), Fourier analysis shows that the square wave voltage is:

$$V_{s(1\text{ Hz})} = 0.945\ E. \tag{98}$$

The effective noise at a noise bandwidth of 1 Hz is given by:

$$V_{n(1\text{ Hz})} = V_n/\sqrt{1000}. \tag{99}$$

The E.N.I. can now be derived by substituting eqs (98) and (99) in eq. (97):

$$\Phi_{ENI} = (\Phi/0.945\sqrt{1000})V_n/E, \tag{100}$$

in which Φ denotes the luminous flux, V_n the measured effective noise, and E the measured effective signal, the latter two at $\Delta f_{eq} = 1$ kHz.

The N.E.P., P_{NEP}, can be measured in the same way as the E.N.I., the only difference being that the light source must be monochromatic and that in eq. (100) the radiant power in watts must be substituted for luminous flux.

By the argument followed in section 3.1.1, the relation between E.N.I. and N.E.P. can be shown to be:

$$P_{NEP} = C \cdot \Phi_{ENI}. \tag{101}$$

The conversion factor C is identical to that quoted in the table in section 3.1.1 for the wavelength at which the spectral sensitivity of the photocathode is a maximum. This implies that the N.E.P. calculated by eq. (101) applies to only that wavelength. For other wavelengths it must be multiplied by the relative value of the spectral sensitivity applicable to the wavelength under consideration.

Background Noise

Where the signal to be detected is pulse-shaped, the amplitude distribution is of interest and the frequency of the dark current signal with respect to it (see section 3.3.3). The number of pulses per time unit that exceed a given threshold may be quoted instead of a dark current spectrum. The amplitude distribution above the threshold need not be known, it being of little interest to most users. It is more important to specify the threshold value at which the pulses were recorded.

Since the amplitude of the anode current pulses depends amongst other things on the transit time spread of the electrons in the tube (see section 3.4.3), it is usually integrated over a time such that the amplitude of the signal voltage depends only on the transported charge. This is why the threshold is defined as the minimum detectable charge, expressed in coulombs.

The variation of the pulsatory voltage can be calculated as a function of time according to the expressions:

$$V(t) = (Q/C_L) \cdot \exp(-t/R_L C_L) \tag{102}$$

and

$$V_{max} = Q/C_L, \tag{103}$$

in which Q denotes the charge transported by the current pulse, R_L the load resistance and C_L the integration capacitance. If in eq. (103) Q is equal to the threshold value and C_L is known, the threshold voltage V_{max} can be calculated.

The integration time $R_L C_L$ must short enough not interfere with resolution at the expected count rate. On the other hand, because the influence of transit time spread on the output pulse increases as the integration time becomes shorter, $R_L C_L$ must be large compared with the transit time spread. Usually $R_L C_L$ is between 1 μs and 200 μs. In view of the anode capacitance of the photomultiplier and the stray capacitances, the minimum capacitance cannot be made much less than 20 pF, so R_L must be about 100 kΩ.

If the background noise, the threshold, the quantum efficiency and the collection efficiency of a photomultiplier are known, the minimum detectable radiant flux, measured under conditions dictated by the threshold value, can be determined. Since, however, the product of the two efficiencies, $\eta_q \eta_c$, may vary from tube to tube and depends moreover on the voltage adjustment of the tube, it is usual to quote, in addition to the

background noise, the single-photon detection efficiency η_{sp}. This quantity gives the ratio between the number of pulses caused by single electrons and the number of photons impinging on the cathode. It can be expressed as:

$$\eta_{sp} = N_s/N_p = \eta_q \eta_c. \tag{104}$$

Single-photon detection efficiency is measured under the same conditions as background noise with a monochromatic radiant flux so weak that the probability of single photons impinging on the cathode is great (see section 3.4.3). If the radiant flux is known, the number of photons striking the cathode can be calculated from:

$$N_p = (\Phi/hc)\lambda, \tag{105}$$

in which Φ is the radiant power in watts.

The number of signal pulses N_s is obtained by subtracting the background pulses N_0 from the total number of pulses N_{tot}.

$$N_s = N_{tot} - N_0. \tag{106}$$

Fig. 59 shows how N_0 and N_s depend on the voltage applied to the photomultiplier. The block diagram of the measuring circuit is shown in Fig. 60.

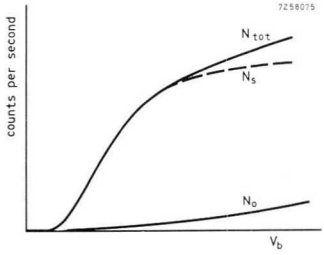

Fig. 59. Signal N_s and background N_0 as functions of the total supply voltage V_b.

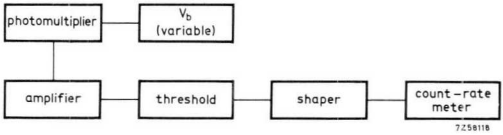

Fig. 60. Set-up for measuring the background and single-electron detection efficiency

Allowing for statistical error in detection the minimum detectable signal can now be ascertained. Usually the calculation will be based on the measurement of the background and of the signal plus background (see eq. (106)). The number of pulses measured in a given interval has a Poisson distribution, so the background noise measured in an interval t_0 is given by $N_0 \pm \sqrt{N_0}$. In other words, the background per unit time amounts to:

$$N_0/t_0 \pm \sqrt{N_0}/t_0 = \nu_0 \pm \Delta\nu_0, \tag{107}$$

where ν is the number of pulses per unit time. Similarly, the signal plus background measured during interval t_1 is given by $N_{\text{tot}} \pm \sqrt{N_{\text{tot}}}$, which gives per unit time:

$$N_{\text{tot}}/t_1 \pm \sqrt{N_{\text{tot}}}/t_1 = \nu_{\text{tot}} \pm \Delta\nu_{\text{tot}} \tag{108}$$

The signal per unit time is thus given by:

$$\nu_s \pm \Delta\nu_s = \nu_{\text{tot}} - \nu_0 \pm \sqrt{\{(\Delta\nu_0)^2 + (\Delta\nu_{\text{tot}})^2\}}. \tag{109}$$

Substituting $\sqrt{(N_0)}/t_0$ for $\Delta\nu_0$ and $\sqrt{(N_{\text{tot}})}/t_1$ for $\Delta\nu_{\text{tot}}$ yields:

$$\nu_s \pm \Delta\nu_s = \nu_{\text{tot}} - \nu_0 \pm \sqrt{(\nu_0/t_0 + \nu_{\text{tot}}/t_1)}. \tag{110}$$

Putting the total interval of the two measurements as:

$$t = t_1 + t_0, \tag{111}$$

gives a relative standard deviation σ_{rel} of:

$$\Delta\nu_s/\nu_s = \delta_{rel} = \frac{\sqrt{\{\nu_0/t_0 + \nu_{\text{tot}}/(t - t_0)\}}}{\nu_{\text{tot}} - \nu_0}. \tag{112}$$

t can be so divided between t_1 and t_0 that σ_{rel} is a minimum. By differentiating σ_{rel} with respect to t_0 and equating to zero we get:

$$t_1/\sqrt{(\nu_{\text{tot}})} = t_0/\sqrt{\nu_0} = t/(\sqrt{(\nu_{\text{tot}})} + \sqrt{\nu_0}), \tag{113}$$

and

$$\sigma_{rel\ \min} = 1/(\sqrt{\nu_{\text{tot}}} - \sqrt{\nu_0})\sqrt{t}. \tag{114}$$

The factor $(\sqrt{\nu_{\text{tot}}} - \sqrt{\nu_0})$ can be written:

$$\sqrt{\nu_{\text{tot}}} - \sqrt{\nu_0} = \sqrt{(\nu_s + \nu_0)} - \sqrt{\nu_0} = \sqrt{\nu_0} \cdot \{\sqrt{(1 + \nu_s/\nu_0)} - 1\} \simeq \nu_s/2\sqrt{\nu_0}. \tag{115}$$

By substituting eq. (115) in eq. (114) we get for the minimum detectable signal:

$$\nu_{s\ \min} = 2\sqrt{\nu_0}/\sigma_{rel\ \min}\sqrt{t}, \tag{116}$$

It follows from eq. (116) that the minimum detectable signal is set by:
— the background and the corresponding threshold,
— the desired accuracy, $\sigma_{rel\ min} = \Delta\nu_s/\nu_s$,
— the time available for measuring the background and the signal plus background; proportioned in accordance with eq. 113.

3.4.5 Signal-to-noise Ratio and Ways to improve it

It can be derived from eq. (85) that, when the photomultiplier is operated in the (so-called) d.c. mode, the signal-to-noise ratio is given by:

$$\frac{S}{N} = \frac{I_{as}}{i_{an}} = \frac{I_{ks}}{\{2e\Delta f\ (I_{ks} + I_{k0})\delta/(\delta - 1)\}^{1/2}}, \qquad (117)$$

where I_{as} is the d.c. anode current caused by the signal,
i_{an} is the anode noise current,
I_{ks} is the d.c. cathode current caused by the signal.
I_{k0} is the cathode dark current.

It follows from eq. (117) that the signal-to-noise ratio can be improved by:
— reducing the bandwidth Δf of the measuring circuit,
— reducing the dark current,
— increasing the secondary emission factor δ.

It was mentioned in section 3.4.3 that the signal-to-noise ratio is improved more by increasing the secondary emission factor of the first stage than by increasing the others. Raising the secondary emission factor of all stages by raising the overall voltage, will increase the risk of excessive noise being caused by the high current density in the last stages (see section 3.3.3).

The cathode thermionic dark current I_{k0} can be reduced by refrigerating the cathode (see section 2.2.2 andd 4.2). It should be recognized that reducing the dark current also reduces the shot noise caused by it, so the limit of the minimum detectable signal, set by noise, is thus lowered.

Another way to reduce cathode dark current is to reduce the active area of the cathode. The cathode may be made only locally sensitive, for example in the centre, by external magnetic fields. Thermionic electrons originating from other parts of the cathode are thus deflected away from the multiplier system. Concentrating the incident luminous flux to the sensitive centre of the cathode, improves the signal-to-noise ratio, but only if the anode dark current originates mainly at the cathode.

The most effective method of improving the signal-to-noise ratio is to reduce the bandwidth Δf of the measuring circuit. In practice this can easily be done by using a sensitive measuring instrument in the anode circuit. The equivalent noise bandwidth is given by $\Delta f = 1/4\tau$, in which τ denotes the time constant of the instrument. Where the signal is integrated over a time interval, the bandwidth is given by $\Delta f = 1/t$. With both methods, as with similar ones, the d.c. component of the dark current must be compensated but if the signal is small with respect to the dark current, this is impracticable because of the dark current's unstable character.

In photometry mechanical light choppers are often used in combination with a narrow-band a.c. amplifier (bandwidth about 1 Hz). Since a.c. amplification is very selective, only the fundamental of the signal is amplified. The measurement of the equivalent input noise described in section 3.4.4 is based on this principle.

A.C. coupling has the advantage that dark current compensation can be dispensed with as the d.c. component is automatically eliminated.This obviously does not apply to the shot noise caused by the dark current, which is normally amplified by the selective amplifier. If the signal I_{ks} is small with respect to the dark current I_{k0}, the shot noise depends exclusively on the dark current.

If the luminous flux is modulated (chopped) (see Fig. 61), the r.m.s. value of the fundamental of I_{ks} is given by:

$$\overline{I_{ks}{}^2}^{\frac{1}{2}} = (\sqrt{2}/\pi) I_{ks}. \tag{118}$$

Taking the unmodulated luminous flux at the cathode to be Φ and the cathode sensitivity to be N_k, then:

$$I_{ks} = \Phi N_k \tag{119}$$

Combining eqs (117), (118) and (119) yields:

$$S/N = \Phi N_k/\pi \{e I_{k0} \Delta f \cdot \delta/(\delta - 1)\}^{\frac{1}{2}}, \tag{120}$$

I_{k0} being much larger than I_{ks}.

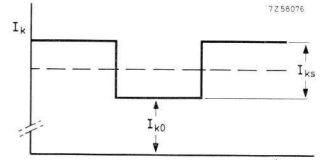

Fig. 61. Oscillogram of the cathode current when the luminous flux is periodically intercepted (pulsed operation). I_{k0} is much larger than I_{ks}.

It will be clear that I_{k0} can be minimized not only by refrigeration but also by reducing the active area of the cathode, and its effect can be reduced by modulating the light source.

The signal-to-noise ratio with pulsed operation will be:

$$S/N = \{(N_s + N_0) - N_0\}/(N_s + 2N_0)^{\frac{1}{2}} , \qquad (121)$$

where N_0 is the number of background pulses measured in an interval t, and $N_s + N_0$ the number of signal and background pulses measured in an identical interval.

Apart from the dark current pulses originating at the cathode, there are others of much smaller or much larger amplitude. The signal-to-noise ratio will be optimum if only pulses originating at the cathode are measured. In practice thresholds are incorporated in the measuring circuit to prevent pulses of too small or too large an amplitude reaching the measuring circuit.

Fig. 62 shows schematically how these thresholds should be chosen with a view to getting the optimum signal-to-noise ratio. In this graph the integral pulse height spectrum has been plotted on a double logarithmic scale. In the area between D_1 and D_2 the two spectra coincide and the signal-to-noise ratio may be taken to be optimum. The threshold values must therefore be so chosen that pulses smaller than D_1 and larger than D_2 are not measured.

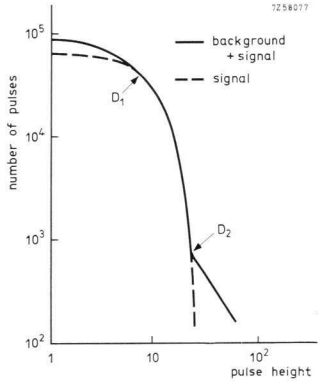

Fig. 62. Adjustment of the thresholds for optimum signal-to-noise ratio.

In the preceding we have assumed the output pulses to be random, which they will be in such applications as photon and scintillation counting. Where a pulsed luminous flux is measured, it is sometimes possible to make the photomultiplier inoperative during the dark intervals. A switching pulse is derived from the light pulse and used to switch the photomultiplier on (see section 4.1.1). While the photomultiplier is inoperative the dark current noise is not recorded, so the signal-to-noise ratio is improved.

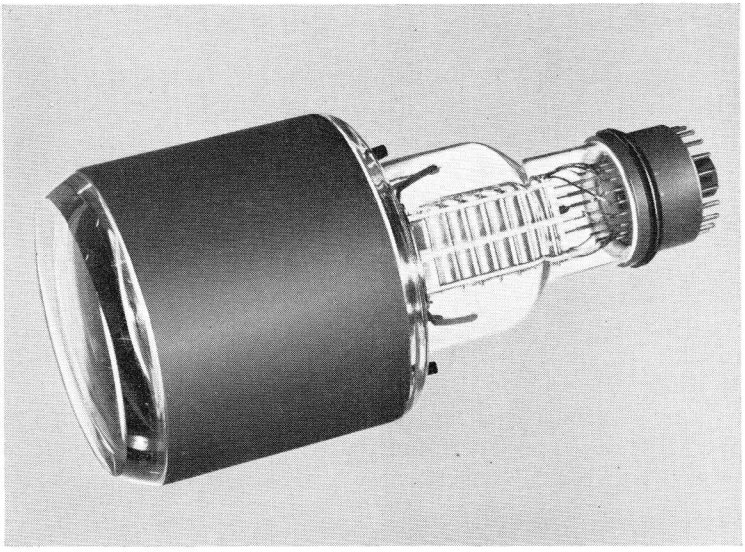

Photomultiplier type 58AVP (approx. 1/3 full size).

4 Photomultipliers in Practice

Photomultipliers are mainly used to measure very low light levels in the range of about 10^{-17} W to 10^{-4} W. Higher levels are likely to damage photomultipliers, one can better use photocells. In general, three groups of applications can be distinguished:

— measuring low light intensities,
— studying the time dependency of fast luminous phenomena,
— investigating nuclear phenomena through, for example, scintillation counters.

The sort of measuring circuit following the photomultiplier depends on the kind of information wanted. Bearing in mind that electrons leaving the photocathode will give rise to bunches of electrons at the anode, it will be clear that the investigations usually amount to answering one of the following questions:

— How many bunches of electrons does the signal contain?
— How many electrons does each bunch contain?
— How many "anode electrons" are there per unit time?

If one of these questions can be answered and the characteristics of the photomultiplier are known, it is usually possible to derive the radiant or luminous flux incident on the cathode. To answer these questions, the circuit must be capable of either counting a number of pulses, of analysing the amplitude of the pulse, or of measuring the anode current, and must therefore have specific properties. It is these properties we shall first discuss.

4.1 Comparison of the Different Measuring Circuits

If a continuous radiant or luminous flux impinges on the cathode, the number of electrons during an interval Δt will not be constant, but will fluctuate around an average value. Provided the measuring time is long with respect to this interval, the average value will be measured.

If, on the other hand, the flux is so weak that the average number of electrons during the measuring time is very small, it is most improbable that two electrons leave the photocathode simultaneously. The bunches

of electrons at the anode are thus separate and can be counted (see. section 3.4.3).

4.1.1 D.C. Current Measuring Circuits

The anode current of a photomultiplier can be measured with a sensitive galvanometer or by measuring the voltage drop across a high resistance (1 MΩ to 10 MΩ). The resistance should not be so high that with the highest signal current the voltage drop across it reduces the potential between the last dynode and the anode below the saturation value (see section 2.3.1). Since the time constant of a measuring instrument is long compared to the average time between pulses, the meter will read the average value of current.

If the dark current of a photomultiplier cannot be neglected with respect to the signal current it must be compensated or subtracted from the measured value. Figs 63 to 67 show several circuit diagrams, based on the d.c. current measurement principle, in which dark current is compensated.

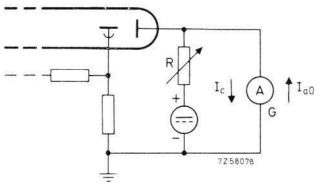

Fig. 63. Simple circuit for dark current compensation using a battery and variable resistor.

In the circuit of Fig. 63 the variable resistor R and the battery voltage B allow the compensation current I_c flowing through the galvanometer G to be made equal to I_{a0}. With the meter thus zeroed current caused by a given luminous flux can be read off.

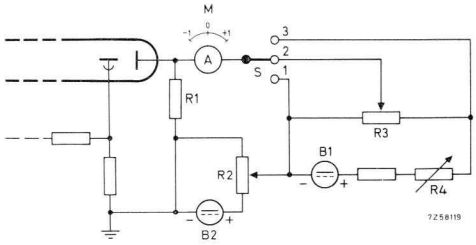

Fig. 64. Circuit for dark current compensation by adjustment of the voltage drop across load resistor R_1.

In the circuit of Fig. 64 the voltage drop across the load resistance R_1 is measured by zeroing the indicator M. With switch S in position 1 and the photomultiplier dark, the dark current is compensated by adjusting resistor R_2 until the indicator is zeroed. The luminous flux is then measured with the switch in position 2 by adjusting R_3 so that the indicator is again zeroed. The position of R_3 is then a measure of the luminous flux. Position 3 of the switch is for measuring the ratio of two light values. The higher value is measured with the switch in position 3, the indicator being zeroed by adjusting R_4. Then with the switch in position 2 the lower value is measured by adjusting R_3 until the indicator is zeroed again. The ratio R_4/R_3 corresponds to the ratio of the luminous fluxes. The circuit can be made more or less sensitive by varying, for example, the value of R_1.

Sometimes the total radiant energy produced in a given time is wanted. With the circuit of Fig. 65 the signal can be integrated over the period involved. The anode current charges the dynamic capacitance C' until the voltage reaches:

$$V = (1/C') \int_0^t i_a \cdot \mathrm{d}t. \tag{122}$$

The dynamic capacitance C' is usually an operational amplifier with capacitive feedback. Such amplifiers usually have a high input impedance, so the circuit may be considered an ideal integrator. The dynamic input capacitance is given by;

$$C' = (1 + A_0)C + C_w, \tag{123}$$

in which A_0 is the open-loop gain of the operational amplifier and C_w the wiring capacitance. The switch has the following functions:
position 1: all input capacitances are discharged and the meter is zeroed;
position 2: tle signal is integrated;
position 3: the voltage across the input capacitance is measured.

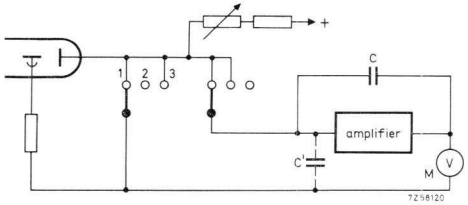

Fig. 65. Circuit with integrator.

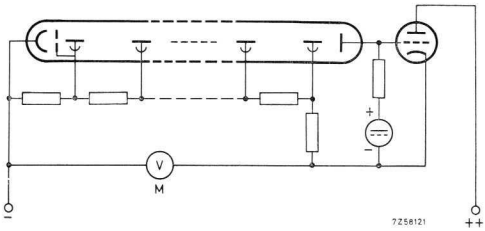

Fig. 66. Circuit with feedback to keep the anode current constant.

The dark current is compensated by variable the resistor with the switch at position 2. The meter should be at zero when the switch is set to position 3.

Fig. 66 shows in principle a circuit in which anode current is kept constant by a feedback circuit. [12] The bleeder voltage, which is a measure of the luminous flux, is indicated by the voltmeter *M*. When the luminous flux increases, anode current will rise and grid voltage of the controlling tube will go more negative. As a result, the voltage drop across the tube will increase and sensitivity will decrease. Since the anode sensitivity of a photomultiplier is a semi-logarithmic function of the supply voltage, the change in meter reading as a function of the luminous flux will also be semi-logarithmic. For measuring quantities, such as the density of filters, which range over many decades, this is an advantage since they can be read from a linear scale.

Because the feedback circuit provides for a constant anode current, the photomultiplier is automatically safeguarded against excessive currents due to an intense luminous flux. The upper measuring limit is set by the cut-off point of the controlling tube. For low light intensities the circuit is limited either by the dark current or by the grid of the controlling tube becoming positive so that it is fully conducting. The voltage across the photomultiplier then reaches its maximum value.

With the principles underlying d.c. measuring circuits out of the way, we can deal with two particular types of circuit, sampling and wide-band circuits.

Sampling Measuring Circuits

As mentioned in section 3.4.5, when the dark current is of the same order of magnitude as the signal current, it is difficult to compensate, particularly if the dark current fluctuates. But it was also shown that with the chopping method, a.c. coupled circuits can be used that automatically elimi-

nate the d.c. component of the dark current. Only the shot noise and non-periodic fluctuations of the dark current not eliminated by the a.c. coupling may still cause trouble. It is thus mainly rapid fluctuations that set a limit to the performance of the photomultiplier.

If the signal to be detected is periodic, the measuring circuit can be so designed that it operates only when the signal is at maximum. By repeating the measurement over many periods and integrating the results, reliable information is obtained that is scarcely affected by noise or rapid fluctuations in the dark current because these occur mostly outside the actual measuring time. This gives a much higher signal-to-noise ratio than other methods.

Fig. 67 shows the block diagram of a circuit often used in photometry for measuring continuous luminous flux. The light chopper converts the continuous signal into a periodic one. An additional light source and photocell produce a reference signal whose phase can be adjusted with respect to the measuring signal. The reference signal is used to open a gate at the correct instant for the signal to be integrated by the succeeding circuit.

In spectrometry the variation with time of a pulsatory luminous flux is often of interest. If the flux is high enough the output of the photomultiplier can be displayed on an oscilloscope. If it is very weak a sampling system can be used, the reference signal being derived from the source used for generating the light pulse.

If the open-gate time is short compared to the length of the light pulse, adjustable delays can be used to strobe the sampling period with respect to the signal. Fig. 68 shows the principle of this, and Fig. 69 the block diagram of a circuit. As the measurement covers several periods, it is essential that the light pulse remains the same shape throughout.

Instead of gating the measuring circuit, the photomultiplier itself can be gated by, for example, electronically switching its supply voltage. Fig. 70 shows a switching circuit, in which a pulse at the cathode is used

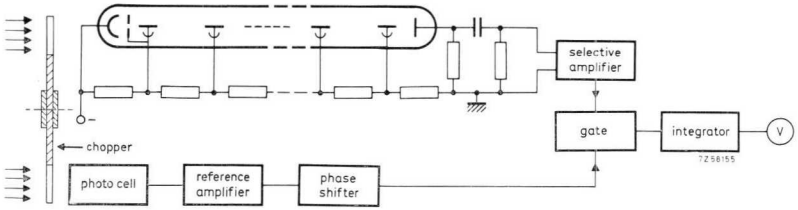

Fig. 67. Block diagram of a synchronous system for measuring a continuous luminous flux.

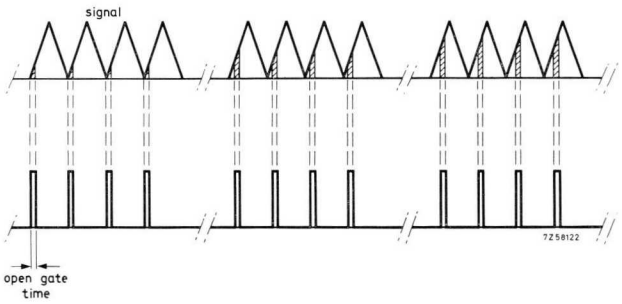

Fig. 68. Sampling principle in which the open-gate time can be varied with respect to the signal.

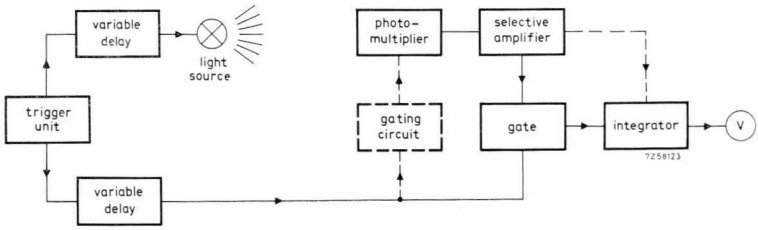

Fig. 69. Block diagram of a sampling system for spectrometry.

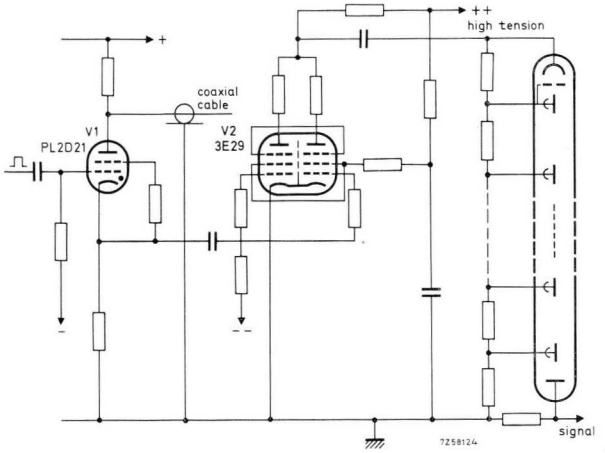

Fig. 70. Basic circuit for gating the high tension supply of a photomultiplier.

to "open" the photomultiplier. With a positive pulse on its grid V_1 conducts and the open coaxial cable in its anode circuit forms a driving pulse. The length of the cable sets the pulse length and thus the time for which the photomultiplier is open. The positive pulse at the control grid of V_2 produces a negative-going anode pulse whose amplitude depends on the supply voltage. The cathode of the photomultiplier is capacitively coupled to the anode of V_2 and thus receives a pulse that is negative with respect to the anode; the photomultiplier is thus "opened" and able to detect a signal.

A drawback of the system is that the steep flanks of the driving signal reach the anode via the anode-to-dynode capacitances, and may seriously interfere with the results. This can be avoided to a great extent by switching only the voltage between two dynodes instead of the entire supply. The dynodes chosen should have low capacitance with respect to the anode, and should considerably influencing the gain. The dynodes of the first stages are commonly used, as in Fig. 71.

A negative-going pulse at the control grid cuts-off V_1, consequently the anode voltage and thus also the dynode voltage rise with respect to the cathode potential and the photomultiplier is "opened". The operating point of tube V_1 should be so chosen that, when it is conducting, the dynode voltage is about 20 V negative of the cathode. Photoelectrons

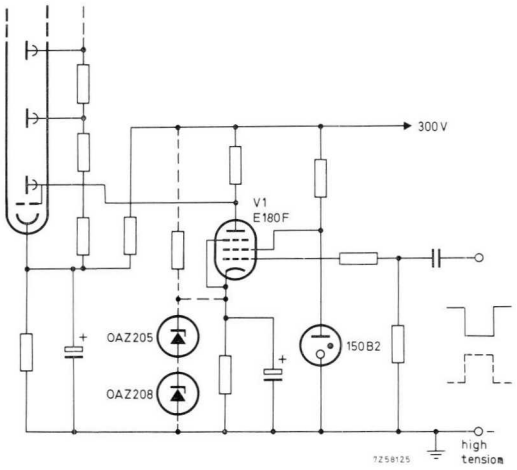

Fig. 71. Basic circuit for gating a photomultiplier via a dynode. (For the circuit in broken line, see text.)

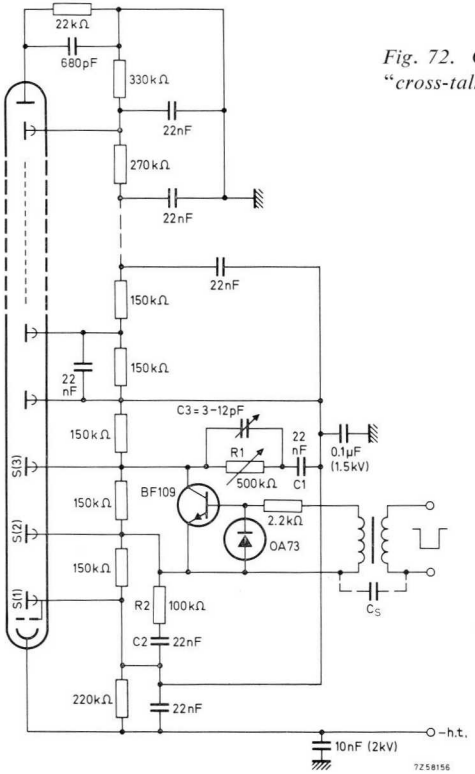

Fig. 72. Gating circuit with compensation for "cross-talk" between dynode and anode.

emitted by the cathode while the photomultiplier is inoperative are thus rapidly returned to the cathode, and do not interfere with the measurement when the photomultiplier is "open".

Sometimes photomultipliers must be protected against bright flashes occurring just before the measurement. The circuit of Fig. 71 can easily be modified to this end by replacing the bypassed cathode resistor of tube V_1 with a fixed cathode bias to hold the tube cut off. The driving pulse must now be a positive-going one, as shown by the broken line in Fig. 71; voltage regulator (zener) diodes are substituted for the bypassed cathode resistor.

In Fig. 72 a transistor is used to short-circuit the bleeder resistor between dynodes $S(2)$ and $S(3)$.[13] The n-p-n transistor is bottomed by a positive-going pulse on its base, the polarity of the driving pulse being reversed by the isolating transformer. The voltage between $S(2)$ and $S(3)$

drops, and the gain of the photomultiplier is reduced by a factor of about 100. Although the photomultiplier is not completely inoperative, the difference in gain is usually enough for sampling. Resistor R_1 with capacitor C_3 compensates the steep flanks of the driving pulse, which may reach the anode.

Wide-band Circuits for Photomultipliers

The high resolution of photomultipliers makes them particularly suitable for detecting high-frequency modulated light, as with flying-spot scanners widely used for slide reproduction in television studios. The principle of a black-and-white system is shown in Fig. 73. A very thin pencil of light traces a raster on each slide. The image on the slide modulates the light which is then converted into an electric signal by the photomultiplier. A system for colour television is shown in Fig. 74 where a dichroic mirror splits the light into the three fundamental colours. Signal-to-noise ratio is obviously important here and, from section 3.4.5, three ways are open to improve it:

— reducing the bandwidth,

— reducing the dark current,

— raising the secondary emission factor of the first stage.

The signal-to-noise ratio cannot be improved by reducing the bandwidth as this is set by the television system. However, photomultipliers can be selected in respect of dark current, and secondary emission factor can be raised by using the maximum permissible voltage between cathode and first dynode, which also improves collection efficiency.

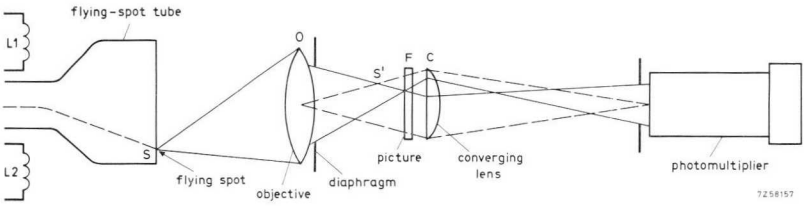

Fig. 73. Flying spot method for scanning black and white diapositives.

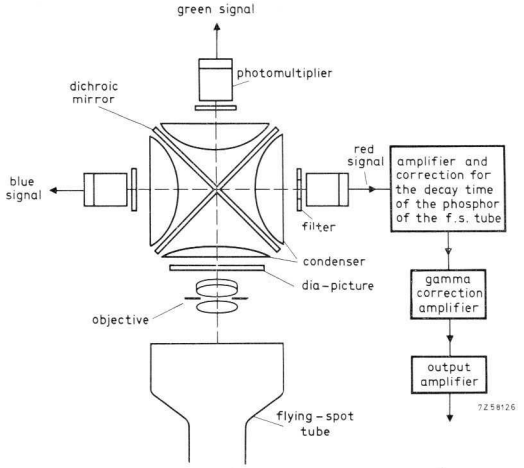

Fig. 74. Flying spot method for scanning colour diapositives.

Another way is to increase the cathode signal current (see eq. (117)), which depends on cathode sensitivity and the amount of incident light. The phosphor of the flying-spot scanner and the spectral sensitivity of the photomultipliers should be such that the product of cathode sensitivity and luminous flux is a maximum for each of the three colour channels. In practice this means using photomultipliers with an *S*11-type photocathode for the blue and green channels, and one with an *S*20-type photocathode for the red channel. The spread in spectral sensitivity of the photomultipliers could be important to the colour fidelity of the channels. Some considerations concerning spectral requirements are dealt with in Appendix III.

As a broad bandwidth is essential, the anode capacitance, the wiring capacitance and the input capacitance must be reduced to a minimum. With a load resistance of 470 Ω and assuming the total capacitance to be 20 pF yields a 3 dB bandwidth of:

$$B_{3dB} = 1/2\pi \cdot 470 \times 20 \times 10^{-12} \simeq 17 \text{ MHz}, \qquad (126)$$

which is much more than is needed for colour television. To keep the wiring capacitances as low as possible, the preamplifier should be mounted close to the photomultipliers. Cathode followers (also mounted close to the photomultipliers) will reduce the anode impedance and match the output to a coaxial cable. If the match is perfect, the cable can be of any length as its capacitance has no effect.

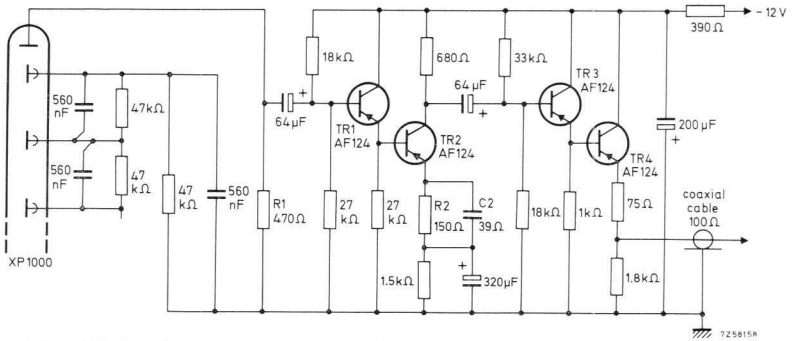

Fig. 75 Wide-band circuit for matching the photomultiplier impedance to a cable with a characteristic impedance of 100 Ω.

Fig. 75 shows a circuit used for flying-spot scanning. The video signal produced across R_1 is fed to the amplifying transistor TR_2 via emitter follower TR_1. Resistor R_2 with capacitor C_2 compensate the higher frequencies. The double emitter follower, TR_3 and TR_4, reduces the output impedance to 100 Ω to match the coaxial cable. Transistors are used in the impedance matching network because they allow a much lower output impedance than is practicable with tubes. Transistors, however, have some disadvantages: their input impedance is lower than that of tubes and their input capacitance for high frequencies depends on the operating point of the transistor. The pentode cathode follower shown in Fig. 76 combines high input impedance with a low input capacitance. By screening the lead towards the control grid and connecting the screen to the cathode, the wiring capacitance can be reduced to a minimum.

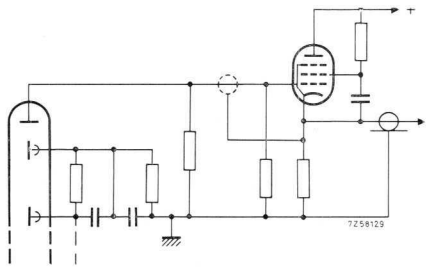

Fig. 76. Pentode cathode follower with high input impedance and low input capacitance.

In most applications in which photomultipliers cope with high frequency signals, the associated circuit sets a limit to the bandwidth. Conventional photomultipliers have a bandwidth ranging from d.c. up to about 100 MHz. Special types, such as the XP1020 series and the XP1210 reach bandwidths of 250 MHz and 350 MHz respectively. They have a coaxial anode terminal (characteristic impedance 100 Ω for the XP1020 and 50 Ω for the XP1021 and XP1210), and dynode connections of the XP1210 are disc shaped, which reduces their inductance, prevents ion and light feedback, and, moreover, ruggedizes the photomultiplier.

4.1.2 Pulse Amplitude and Pulse Frequency Measuring Circuits

The photomultiplier characteristics of interest in pulse operation (dark current pulse spectrum, single electron spectrum and single photon efficiency) have been mentioned in sections 3.3.3 and 3.4.3. In general, pulsed operation implies a measuring circuit for recording pulse amplitudes and/or pulse frequencies.

As the multiplier system of a photomultiplier is, in principle, a charge amplifier, the signal at the anode also assumes the form of a charge, and the pulses must be integrated over a certain time. The choice of time constant is mainly dictated by:

— the information required (pulse amplitude and/or pulse frequency),
— the pulse shape demanded by the associated equipment.

For pulse height analysis the time constant must be long with respect to the transit time spread of the electrons (see section 3.4.3). However, too long a time constant will degrade the resolution of the system. Pulse height analysis is used mainly in nucleonics where the photomultiplier is used to measure ionizing radiation (see "General Aspects of Scintillation Counting").

Photon counting is often used in measuring very low light levels. Since this procedure is based on the single-electron principle, the pulse height is less important. Usually the only requirement imposed is that the top of the pulse should lie between thresholds so chosen that the signal-to-noise ratio is optimum (see section 3.4.5). The number of pulses per unit time must, however, be measured with the utmost accuracy.

The minimum radiant flux that can be measured is determined by the number of background pulses of the photomultiplier. The maximum is set by the resolution and consequently by the bandwidth of the equipment.

Photon Counting

Measuring light by photon counting has distinct advantages over d.c. current measurement: as it is based on the principle that only single electrons leave the cathode (see section 3.4.3), absolute radiant flux can be measured, provided the wavelength of the light and the quantum efficiency of the photocathode are known. It is a particular advantage that the gain of the multiplier system has little effect on the results and need not be known.

The radiant power (in watts) incident on the cathode can be calculated from the expression:

$$\Phi = \eta_q N_s hc/\lambda, \tag{127}$$

where η_q is the quantum efficiency of the cathode,
N_s is the number of anode pulses per second attributable to single photoelectrons,
h is Planck's constant (6.624×10^{-34} Js),
c is the speed of light (3×10^{17} nm/s),
λ is the wavelength of the light expressed in nm.

If the number of photons per unit time can be measured so, too, can their distribution in time, which may be important in studying light emitted by lasers. By using a time to pulse-height converter the intervals between the appearance of photons can be converted into a pulse height difference that can be discriminated by a pulse height analyser.

The photomultiplier should meet the following requirements:
— low background (see section 3.4.4),
— high and stable quantum efficiency,
— stable collection efficiency of the multiplier system,
— a typically distinct single-electron spectrum (see section 3.4.3).

Fig. 82 is the block diagram of a photon counter. To prevent the single electron pulses piling up, the radiant flux incident on the cathode is reduced by a filter of known density. Piling up may cause pulses normally below the threshold to exceed it and thus falsify the count. The linear

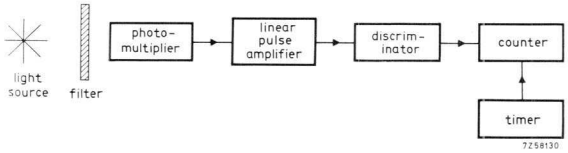

Fig. 77. Essential parts of a photon counter composed.

pulse amplifier raises the signal to a level suitable for the discriminator unit, with which one or more thresholds can be incorporated in the circuit. The counter records the number of pulses passed by the discrimintor in a predetermined time.

The maximum count rate depends on the bandwidth of the various circuits, and is usually about 10^7 to 10^8 pulses per second. In principle, the finite resolution of the photomultiplier limits the maximum count rate, but this depends on the transit time spread of the electron bunches in the multiplier system which is about 1 to 2 ns, so that usually it is the ancillary equipment that limits the bandwidth.

Fig. 78 is a block diagram of a system for studying the distribution of photons as a function of time. The beam of photons is split by a semi-transparent mirror; if two photons leave the semi-transparent mirror simultaneously, there is 50% chance that both photomultipliers will receive one.

Assuming the quantum efficiency of the photomultipliers to be 25%, about 3% of the photon pairs will result in a pulse at the anodes of both photomultipliers. The pulses are amplified and fed to a fast coincidence AND gate circuit, which passes them only if both arrive within a pre-

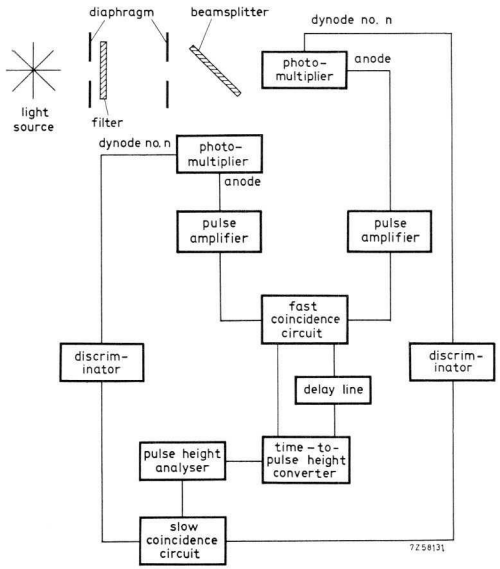

Fig. 78. Circuit for measuring the distribution of photons as a function of time.

determined time. One pulse starts the time-to-height converter; the other passes through a delay line and stops the converter. This converter supplies a pulse the height of which is proportional to the delay of the delay line. The pulse height is subsequently measured by the pulse-height analyser.

Photons that are not simultaneous produce pulses of different heights at the output of the time-to-height converter because it is stopped earlier or later than by coincident photons.

The pulse-height analyser gives the distribution of the photons as a function of time. The length of the delay line determines in which channel of the pulse-height analyser coincident photons are recorded, in other words it determines the zero point of a scale that shows the time distribution of photons.

Interference by dark current pulses can be limited by making the pulse-height analyser open only for pulses that appear within a given time interval and whose heights lie within given limits.

This is done by taking signals from one of the final dynodes of both photomultipliers and feeding them via discriminators to a slow coincident circuit (see Fig. 83). Apart from polarity the pulses at the dynodes correspond to those at the anode, if both occur within an interval determined by the resolution of the slow coincidence circuit, an output pulse is produced that can be used to open the pulse height analyser.

General Aspects of Scintillation Counting

Photomultipliers used with scintillators that convert ionizing radiation into light pulses, are known as scintillation counters. The pulse rate is a measure of the radiation intensity. If the pulse amplitude is proportional to the particle or quantum energy, the energy spectrum of the radiation can be found by measuring the pulse rate of each of a broad range of amplitudes (gamma ray spectrometry). The sensitivity of the scintillation counter (lower limit of detection about 100 nc/cm^3) allows very weak samples to be used, which greatly reduces the risk of radiation damage (especially in medical investigations).

Scintillators are substances that emit flashes of light of very short duration (1 μs to 1 ns) when irradiated by ionizing radiation. Mostly this is a case of fluorescence, caused by fast electrons. A good scintillator should be efficient in absorbing incident radiation energy, and in converting it into luminous energy. The photons should reach the photocathode without loss, and the emission spectrum of the scintillator should match the

spectral response of the photocathode. The decay time of the light pulse must be very short, especially where very intense radiation is to be measured. Finally, in many measurements photons should be produced in proportion to the energy of the incident particles or quanta.

In the light of these demands it is hardly surprising that there are no universal scintillators: for any particular application the most suitable must be chosen. Scintillators may be organic or inorganic, solid, liquid or gaseous. Solid scintillators most widely used are plastic scintillators and crystalline scintillators, the last named in the form of single crystals, polycrystalline layers, or powder uniformly distributed in a plastic carrier.

The energy efficiency can reach 20% to 30% with zinc sulphide or cadmium sulphide activated with copper or silver (for alpha radiation). The decay time ranges from about 10 μs to 1 μs. Organic scintillators usually have a much lower energy efficiency, but a much shorter decay time (ranging from 10 ns to 1 ns).

An adapter must be used between scintillator and photomultiplier to prevent reflection at the interface. If the scintillator can be placed directly against the cathode window, the gap between should be filled with a silicone grease or oil with a refractive index intermediate between that of the photomultiplier window and the scintillator glass. Moreover, the kinematic viscosity should be above 5×10^4 cSt (silicone oil may be up to 10^6 cSt).

If the scintillator cannot be placed directly against the photocathode window (it may not be flat), a light guide of acrilate or similar material may be used. The gaps at both interfaces should, as before, be filled with silicone oil or grease. The light guide must transmit light well, and its side(s) should be polished to ensure total internal reflection (see Fig. 79).

The light pulses, especially those from plastic scintillators, are so short that they cannot be converted into electrical pulses without being distorted. Fortunately this is not objectionable, provided that the amplitude of the electrical pulses is proportional to that of the light pulse, and that the counting error due to the finite time resolution is not excessive. For spectrometry care must also be taken that the spread of the amplitudes is not unduly increased. The output pulse shape is determined by the shape of the light pulses, the transit-time spread in the photomultiplier, and the time constant of the output circuit. Since little can be done to alter the shape of the light pulse and the transit-time spread, the anode circuit and associated amplifiers and measuring equipment must be carefully designed.

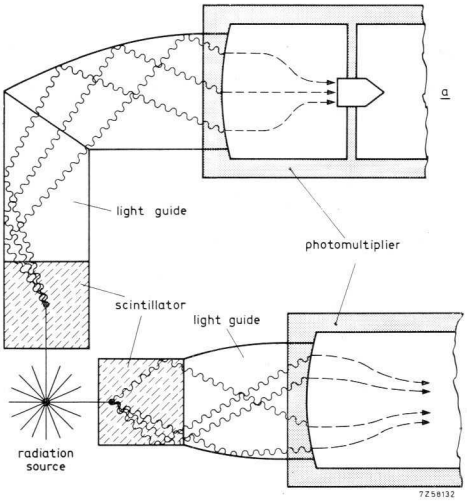

Fig. 79. Arrangement of light guides between scintillator and photomultiplier.

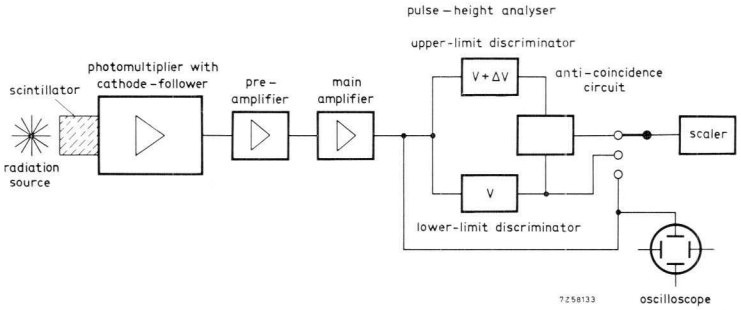

Fig. 80. Block diagram of equipment for scintillation counting and gamma ray spectrometry.

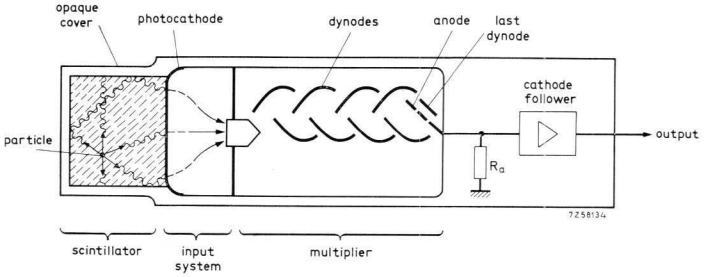

Fig. 81. Sketch of a scintillation counter.

A complete scintillation counter comprises a scintillator, a photomultiplier with cathode follower, a preamplifier, a main amplifier, and measuring and counting equipment, as shown in Fig. 80.

The passband of the amplifier must be so chosen as to avoid pulse distortion. The output pulse from the amplifier is fed to an oscilloscope for studying the pulse form, and to a discriminator and scaler for counting the number of pulses or (for spectrometry) to a pulse-height analyser.

Let us now discuss the shape of the output pulse and the factors that influence it. Taking particles of average energy W_1 penetrating the scintillator (see Fig. 81) and transferring to it average energy W_2. Part of their energy will be released by the scintillator in the form of N_p photons of energy W_p. The energy efficiency of the scintillator is then:

$$\eta_0 = N_p W_p / W_2,$$

whence

$$N_p = \eta_0 W_2 / W_p. \tag{128}$$

Of the N_p protons produced in the scintillator, $N_{p(1)}$ strike the photocathode, the optical transmission factor being:

$$\eta_1 = N_{p(1)} / N_p. \tag{129}$$

$N_{p(1)}$ photons produce on average N_e electrons at the photocathode, the quantum efficiency of which is:

$$\eta_q = N_e / N_{p(1)}. \tag{130}$$

The collection efficiency of the input system is:

$$\eta_c = N_{e(1)} / N_e, \tag{131}$$

(where $N_{e(1)}$ is the number of electrons reaching the first dynode). Knowing the gain G of the photomultiplier, we can put the number of electrons reaching the anode as:

$$N_{ea} = N_{e(1)} G = (W_2 / W_p) \eta_0 \eta_1 \eta_q \eta_c G. \tag{132}$$

The charge at the anode is therefore:

$$Q = (W_2 / W_p) \eta_0 \eta_1 \eta_q \eta_c G e. \tag{133}$$

For convenience we can introduce the constant:

$$\Gamma = \eta_0 \eta_1 \eta_q \eta_c / W_p, \tag{134}$$

known as the transformation factor of the scintillation counter. It is a mean value because all the factors involved are mean values; it has the dimension of a reciprocal energy. Eq. (133) may thus be rewritten:

$$Q = \Gamma W_2 G e. \tag{135}$$

Assuming the fluorescent radiation of the scintillator to decay exponentially with time constant τ_0, the charge of each pulse at the anode is:

$$Q = \int_0^\infty i_a(t) \cdot \mathrm{d}t = \int_0^\infty i_{a\,\max} \cdot \exp(-t/\tau_0) \cdot \mathrm{d}t = i_{a\,max} \tau_0, \tag{136}$$

neglecting the transit time spread. Since $i_{a\,\max} = Q/\tau_0$, the anode current is:

$$i_a = -(Q/\tau_0) \cdot \exp(-t/\tau_0). \tag{137}$$

This current divides between the load resistor R_L and the parallel capacitance C_a;

$$i_a = i_R + i_C. \tag{138}$$

Denoting the voltage drop across R_L by $v(t)$ yields:

$$v/R_L + C_a \cdot \mathrm{d}v/\mathrm{d}t = i_a = -(Q/\tau_0) \cdot \exp(-t/\tau_0). \tag{139}$$

Integrating and substituting τ_1 for the time constant $R_L C_a$, yields the following expression for the output pulse of the photomultiplier:

$$v(t) = -(Q/C_a)\{\tau_1/(\tau_0 - \tau_1)\}\{\exp(-t/\tau_0) - \exp(-t/\tau_1)\}. \tag{140}$$

By this expression if W_2 and G are constant, the amplitude of the output pulse is proportional to the total charge Q, which increases with transformation factor Γ, as has been seen from eq. (135). This equation can be given a more general form by introducing the factors $\varkappa^* = \tau_1/\tau_0$, and $x = t/\tau_0$. Eq. (140) can then be written:

$$V(\varkappa) = -(Q/C_a)\{\varkappa/(1 - \varkappa)\} \exp(-x) [1 - \exp\{-x(1 - \varkappa)/\varkappa\}]. \tag{141}$$

Fig. 82 shows the variation of the voltage pulse across the load resistance R_L at several values of $\varkappa$. The curves are referred to the maximum value of v, for $\varkappa \to \infty$ and $x \to \infty$. Fig. 83 shows the amplitude of the pulse as a function of $\varkappa$.

* The symbol $\varkappa$ as used on pages 110-116 corresponds to the symbol κ in Figs. 82-91.

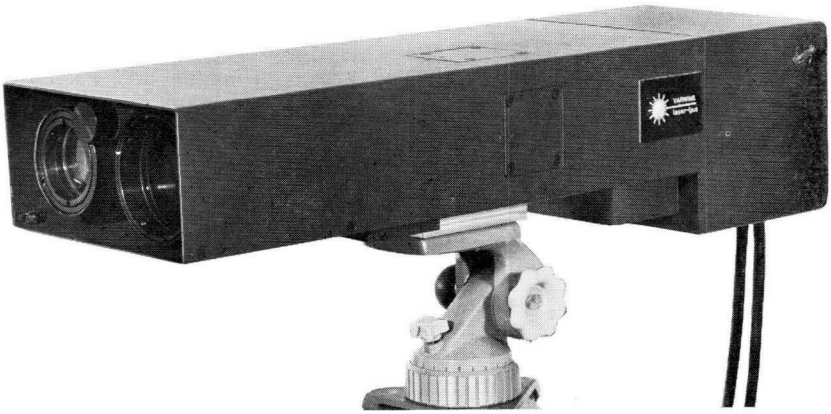

Transmitter/Receiver of ruby laser rangefinder using XP1117 photomultiplier (by courtesy of L. M. Ericsson, Sweden).

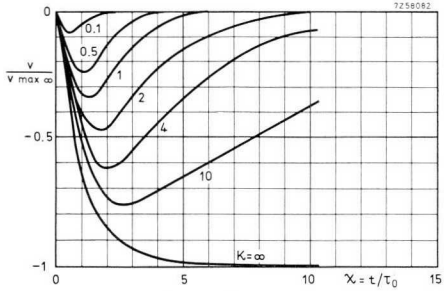

Fig. 82. Output pulses of a photomultipier for several values of $\varkappa = \tau_1/\tau_0$ at constant gain.

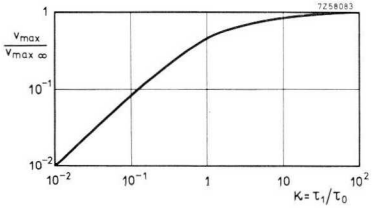

Fig. 83. Relative pulse amplitude as a function of $\varkappa$ at constant gain.

It follows from Fig. 82 that the pulse duration decreases with $\varkappa$, that is, as $\tau_1 = R_L C_a$ becomes smaller with respect to τ_0. The amplitude of the output pulses also decreases with $\varkappa$, so it is difficult to decide from Figs 82 and 83 what the best value of the time constant τ_1 will be.

To gain an insight into the advantages and disadvantages of a given value of $\varkappa$, we shall assume the amplification to be so varied that the amplitude is kept constant at $v_{\max\,\infty}$. Fig. 84 illustrates the dependence of v on x, with $\varkappa$ as parameter, at constant $v_{\max\,\infty}$. Both the pulse rise time and the pulse duration are seen to increase with $\varkappa$. The pulse rise time t_r, that is, the time the pulse takes to rise from 10% to 90% of its maximum value, is plotted as a function of $\varkappa$ in Fig. 85. The pulse duration t_p, measured at half height, is plotted as a function of $\varkappa$ in Fig. 86. In both graphs the time is referred to the constant τ_0.

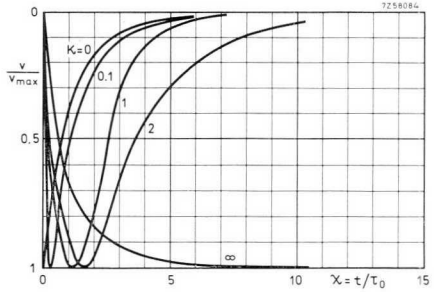

Fig. 84. Form of the output pulses at several values of $\varkappa$ when of the gain is so adjusted that pulse amplitude is independent of $\varkappa$.

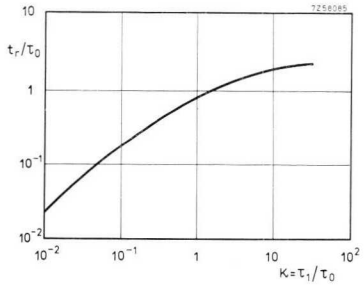

Fig. 85. Relative pulse rise time as a function of $\varkappa$.

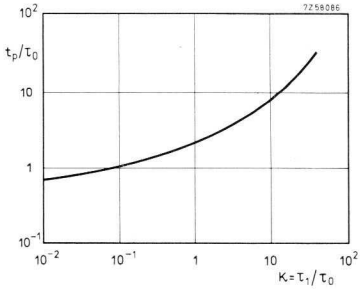

Fig. 86 Relative pulse duration as a function of $\varkappa$.

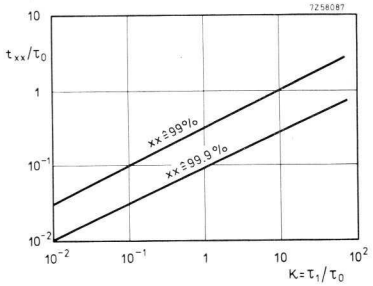

Fig. 87 Relative duration of the pulse peak t_{xx}/t_0 as a function of $\varkappa$ for two different percentages of the peak value.

Fig. 87 finally shows the pulse-peak duration t_{xx} as a function of $\varkappa$. The duration t_{xx} is understood to be the time during which v exceeds a certain percentage of its peak value. To render this graph generally applicable, t_{xx} is also referred to the time constant τ_0 of the scintillator. Curves are shown for 99% and 99.9% of the peak value.

The following example will illustrate the situation. If $\tau_0 = 10^{-7}$ s, the time t_{xx} for which the pulse amplitude exceeds 99% of its maximum value amounts to:

$$t_{xx} = 3\times10^{-8}\text{ s} \quad \text{when} \quad \varkappa = 1, \quad \text{i.e. } R_L C_a = 10^{-7}\text{ s};$$
$$t_{xx} = 3\times10^{-9}\text{ s} \quad \text{when} \quad \varkappa = 0.01, \quad \text{i.e. } R_L C_a = 10^{-9}\text{ s}.$$

It should be kept in mind that at low values of $\varkappa$ (e.g. less than 0.1) the transit time spread of the photomultiplier ceases to be negligible. This will not only distort the pulses but also increase the amplitude spread, as only a small fraction of the electrons occur during the rise of the pulse. For gamma spectrometry, therefore $\varkappa$ should be much larger than unity, the output pulses can then be clipped by, for example, a clipping cable.

In three special cases, namely when τ_1 is much longer than, equal to, or much shorter than τ_0, eq. (141) simplifies considerably.

If τ_1 is much longer than τ_0 ($\varkappa$ approaching infinity in Fig. 87), eq. (141) reduces to:

$$v(t) = -(Q/C_a) \cdot \exp(-t/\tau_1) - \exp(-t/\tau_0), \tag{142}$$

the pulse amplitude being:

$$v_{\max} = -Q/C_a, \tag{143}$$

and the pulse rise time (measured here from zero to maximum):

$$t_r' = \tau_0 \cdot \ln(\tau_1/\tau_0). \tag{144}$$

If τ_1 equals τ_0 ($\varkappa = 1$ in Fig. 87), eq. (141) becomes:

$$v(t) = -(Q/C_a)(t/\tau_0) \cdot \exp(-t/\tau_0), \tag{145}$$

the pulse amplitude being:

$$v_{\max} = -Q/C_a e, \tag{146}$$

and the pulse rise time:

$$t_r' = \tau_0. \tag{147}$$

If, τ_1 is much shorter than τ_0 (e.g. $\varkappa = 0.1$ in Fig. 87), eq. (141) becomes:

$$v(t) = -(R_L Q/\tau_0) \cdot \exp(-t/\tau_0) \cdot \{1 - \exp(-t/\tau_0)\}, \tag{148}$$

the pulse amplitude being:

$$v_{\max} = -R_L Q/\tau_0, \tag{149}$$

and the pulse rise time:

$$t_r' = \tau_0 \cdot \ln(\tau_0/\tau_1). \tag{150}$$

Figs 88 and 89 show the influence of transit time spread. A measure of the spread is given by t_p, the time for which the anode pulse is above half-height with an infinitely short light pulse. The output pulse is seen to become flatter and broader as $\varkappa$ decreases and t_p/τ_0 increases.

Another quantity to be taken into account is the signal-to-noise ratio. This is also a function of $\varkappa$, as shown by Fig. 90. It passes through a maximum at $\varkappa = 1$, that is, when $R_L C_a = t_0$.

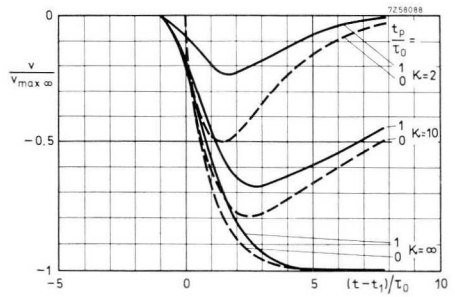

Fig. 88. Distortion of the anode voltage pulses due to spread in transit time, with ϰ as parameter.

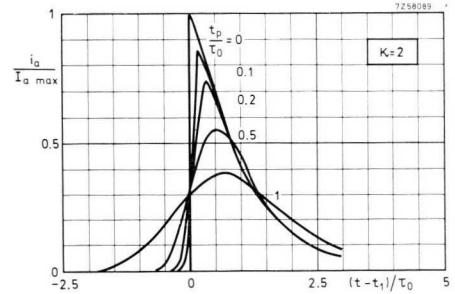

Fig. 89. Form of the anode current pulse, referred to $I_{a\,max}$, as a function of the spread in transit time, with t_p/t_0 as parameter

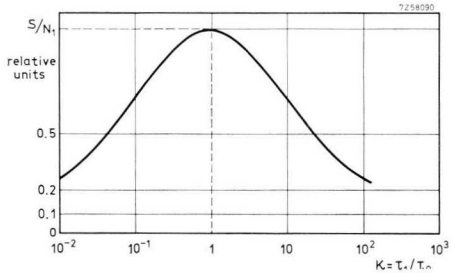

Fig. 90. Signal-to-noise ratio as a function of ϰ.

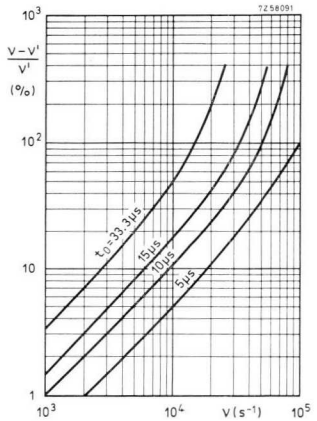

Fig. 91. Relative counting error $(\nu - \nu')/\nu'$ as a function of the observed number of pulses, with the dead time t_0 of the counting circuit as parameter.

A final important characteristic is the dead time, that is, the time following a pulse, for which the counter is unresponsive to further pulses. The dead time depends on the properties of the scintillator, the photomultiplier, the amplifier, and — last but not least — the scaler. Dead time can be kept short making $\varkappa$ small and by using a broadband amplifier. However, this is of little use if the dead time of the scaler is long.

Dead time causes a number of pulses to be missed. If the actual frequency is ν, the measured frequency ν', and the dead time t_0, the total inactive time per second will be $\nu' t_0$, and a fraction $\nu\nu' t_0$ of the pulses per second will be skipped. In other words, $\nu' = \nu - \nu\nu' t_0$ pulses will be recorded. The relative counting error is thus given by:

$$(\nu - \nu')/\nu' = \nu' t_0/(1 - \nu' t_0). \tag{151}$$

This error is plotted in Fig. 91 as a function of ν for several values of t_0.

Measuring Soft Beta Radiation with Liquid Scintillators

As mentioned previously, there are no universal scintillators. In most cases the scintillator is solid, which means that the radioactive substance will be outside the scintillator which receives only a fraction of the ioinzing particles. This fraction depends on:

— the geometric relation of radioactive substance to scintillator,
— the absorption of the scintillator window.

With liquid scintillators the radioactive substance can be dissolved in the scintillator so that every ionizing particle dissipates its energy in the scintillator and produces a corresponding signal. For some kinds of radiation, for example beta radiation, the efficiency is much higher than with solid scintillators.

Since the decay time of scintillations in liquid scintillators is extremely short, radioactive phenomena of very short duration can be studied. With a short decay time fast coincident techniques can be used with advantage, the influence of background of both photomultipliers can be kept very low. Refrigerating the photocathodes will also help reduce background.

The main conditions imposed on photomultipliers used with liquid scintillators are:

— the photocathode should have a high quantum efficiency,

— the background should be low,

— the output pulse should have a short rise time,

— transit time fluctuations should be small.

The count rate resulting from coincident background pulses in a coincidence circuit is given by:

$$N_0 = 2N_{01}N_{02}t, \tag{152}$$

where N_{01} is the background of the first photomultiplier,
N_{02} is the background of the second photomultiplier,
t is the resolution of the coincidence circuit.

The resolution depends partly on the transit time fluctuations of the photomultipliers. The electron-optical input system and dynode structure of the 56DUVP photomultiplier, which is designed for liquid scintillation counting, allow a resolution of $t = 10^{-8}$ s to be attained, the count rate of coincident background pulses being negligible.

Aside from soft beta radiation, liquid scintillators are often used in measuring hard radiation of great penetration, for example, cosmic radiation. In that case advantage is taken of the possibility of manufacturing liquid scintillators of considerable volume.

Cerenkov Counters

All transparent media emit Cerenkov light if traversed by a charged particle moving faster than the speed of light in the medium. The emission is similar in character to a shock wave. If the speed of the particle is

constant, the angle (to the direction of travel) at which the light is emitted is given by:

$$\cos \Phi = c/un, \tag{153}$$

where c is the speed of light in vacuum (3×10^{10} cm/s),
u is the speed of the charged particle.
n is the index of refraction of the medium.

The emitted light is polarized and the number of photons N_p emitted during an interval $\Delta\nu$ depends on the charge Z of the particle and the angle of emission ϕ:

$$N_p = (4\pi Z^2 e^2/hc^2)\Delta\nu \sin^2 \phi \tag{154}$$

per centimetre travel in the medium.

Within the spectral sensitivity range of photomultipliers the number of photons per frequency interval is constant. For a high photoelectric current the integral of the quantum efficiency as a function of the wavelength should be as large as possible. Moreover, the absorption of the material that carries the photocathode should be as low as possible. Photomultipliers with a quartz window are therefore recommended for this application. Cerenkov radiation is mainly used to detect single particles, advantage being taken of the good time resolution of the radiator. This means that the transit time spread of the photomultiplier should be small. As with liquid scintillation counting, coincidence circuits can minimize the influence of the background.

4.2 Refrigerating Photomultipliers

The change of sensitivity with temperature can be serious (section 2.2.1) and must be taken into acount when photomultipliers are mounted in heat dissipating equipment. Thermionic emission of the photocathode has been dealt with in section 1.1.3, and the temperature dependence of the anode dark current was mentioned briefly in section 2.2.2.

In some applications it is worth refrigerating the photomultiplier. The dark current can thus be greatly reduced, so that extremely low light levels can be accurately measured. Allowance must be made, however, for changes in the spectral sensitivity of the photocathode. In the following subsections we shall discuss the results of some measurements made with refrigerated photomultipliers.

4.2.1 Temperature Dependence of the Dark Current

Fig. 92 shows the results of tests with a single specimen of the XP1000 photomultiplier (S11-type photocathode). They are typical of this type of tube and in good agreement with the results usually obtained.

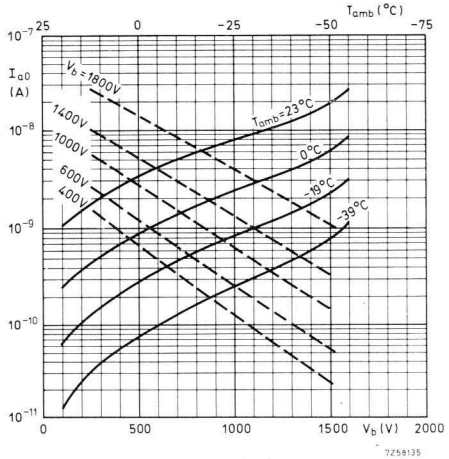

Fig. 92. Temperature dependence of the anode dark current of a XP1000 photomultiplier The solid curves give $I_{a0} = f(V_b)$ with T_{amb} parameter (lower scale); the broken curves give $I_{a0} = f(T_{amb})$ with V_b as parameter (upper scale).

The curves show the anode dark current I_{a0} as a function of the supply voltage V_b, with ambient temperature T_{amb} as parameter, and I_{a0} as a function of T_{amb} with V_b as parameter. From the last named we can derive the relationship between anode dark current and a change of the ambient temperature from T_1 to T_2:

$$I_{a0(1)}/I_{a0(2)} \simeq 10^{0.025(T_1-T_2)}, \tag{155}$$

in which $I_{a0(1)}$ and $I_{a0(2)}$ denote the anode dark current at temperatures T_1 and T_2 respectively.

Similar measurements were made on a series of 150CVP photomultipliers (S1 photo-cathode) with the (mean) results shown in Fig. 93, the relationship between anode dark current and temperature is in this case:

$$I_{a0(1)}/I_{a0(2)} \simeq 10^{0.067(T_1-T_2)}, \tag{156}$$

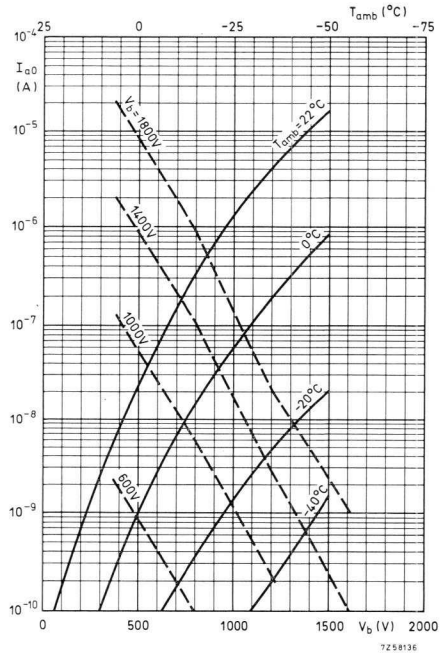

Fig. 93. Temperature dependence of the anode dark current of a 150CVP photomultiplier, using the same notation as in Fig. 92.

It should be recognizedthat eqs (155) and (156) have been found empirically, so their validity is confined to the temperature range studied (+25 °C to −40 °C).

Photomultipliers with a T-type (S20) cathode have been found to obey the following law:

$$I_{a0(1)}/I_{a0(2)} \simeq 10^{0.040(T_1-T_2)} \tag{157}$$

Comparison of eqs (155), (156) and (157) shows that temperature dependence of the dark current is greatest with the S1 and S20 cathodes. As might be expected, considering their lower work functions, dark currents of the S-1 and S-20 are much more temperature dependent than with S-11.

4.2.2 Temperature Dependence of the Spectral Sensitivity

The influence of temperature on the spectral sensitivity of the photocathode depends on the properties of the cathode semiconductor. In section 1.1.2 dealing with the photoelectric effect it was shown that distinction should be made between volume and surface effects. The essential temperature dependent parameters are:[14]

Volume Effect

— the average escape depth of the electrons, which increases as the temperature decreases;
— the resistance of the photocathode, which increases rapidly as the temperature decreases.

Surface Effect

— the Fermi level, which in the case of n-type semiconductors increases as the temperature decreases, but with p-type semiconductors decreases with temperature;
— the forbidden zone, which widens with decreasing temperature; the change is in the order of 10^{-4} eV/degK.

Semiconductor theory, confirmed by experiment,[14] shows that the temperature coefficient of a photocathode (the change in sensitivity expressed in per cent per degK) attributable to these factors, is negative for a volume effect and positive for a surface effect. In general, volume effect prevails with $\lambda < 5000$ Å and surface effect with $\lambda > 6000$ Å. For intermediate wavelengths both effects occur to about the same extent. Figs 94 and 95

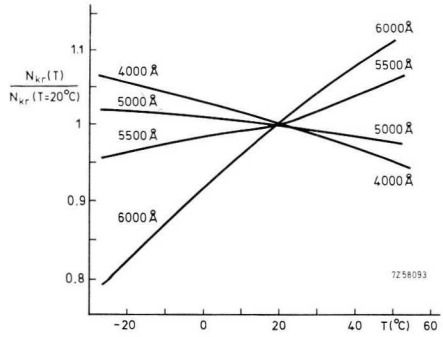

Fig. 94. Relative spectral sensitivity of an S11 cathode as a function of temperature.

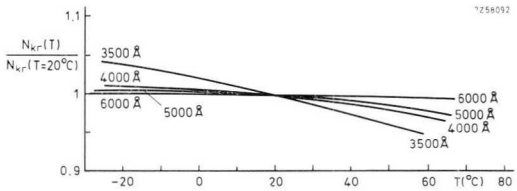

Fig. 95. Relative spectral sensitivity of an S20 cathode as a function of temperature.

illustrate the influence of temperature on the spectral sensitivity for S11 and S20 photocathodes respectively, both agree well with theory. Fig. 95 illustrates the low temperature dependence of the S20 cathode.

Since the resistance of the photocathode rises rapidly as the temperature drops, potential variations are apt to occur at the surface of the cathode, particularly at low temperatures. These may affect the collection efficiency of the first dynode and introduce additional transit time variations.

4.2.3 Temperature Dependence of the Gain

Fig. 96 gives an idea of the influence of temperature changes on the gain of an XP1000 photomultiplier. Usually the gain changes are low, less than a few tenths per cent per degK (see section 2.2.3). Fig. 96 has been plotted as a function of the supply voltage, with temperature as parameter, the gain being derived from:

$$G = I_a/I_k. \tag{158}$$

Both I_a and I_k have also been plotted in this graph. To reduce the effect of changes in spectral sensitivity on the gain, a colour filter with its maximum transmission at 4800 Å and a half-peak width of 900 Å was used. When the temperature was cycled between $+10$ °C and -34 °C the gain was found to display a hysteresis effect. Similar tests on other photomultipliers of the same type revealed a similar effect but not always in the same direction.

As shown by Fig. 96, the gain variation due to temperature changes is so small (about 0.3% per degC) that it can usually be disregarded. A supply voltage change of 0.03% will produce the same change in gain, it is clear how stringent the supply regulation must be before temperature need give concern.

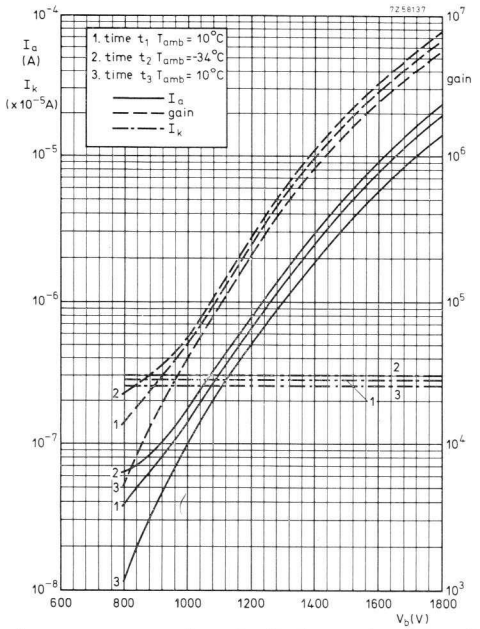

Fig. 96. Influence of temperature on the gain G, the anode current I_a, and the cathode current I_k of an XP1000 photomultiplier.

4.2.4 Refrigerating Photomultipliers

Depending on the desired temperature, various techniques discussed in literature can be used for cooling photomultipliers. The form and construction of a cryostat are governed by the application of the photomultiplier and the requirements imposed on the available volume and flexibility. This explains why a universal construction is not practicable. The main points to which due attention must be paid are:

— condensation of water vapour on the tube base and cathode window must be avoided at all costs;
— the heat resistance between the photomultiplier and ambience should be as high as possible.

Fig. 97 shows by way of example a cryostat that cools mainly the cathode part of a photomultiplier. Liquid nitrogen can be used as the cooling medium. Condensation is prevented by evacuating the space which houses the cooling body and the photomultiplier. This space is sealed by O-rings.

The support of the "cold finger", which fits around the photomultiplier, is made of heat-insulating material. The outside of the cooling body is polished to minimize heat radiation and hence wastage of liquid nitrogen.

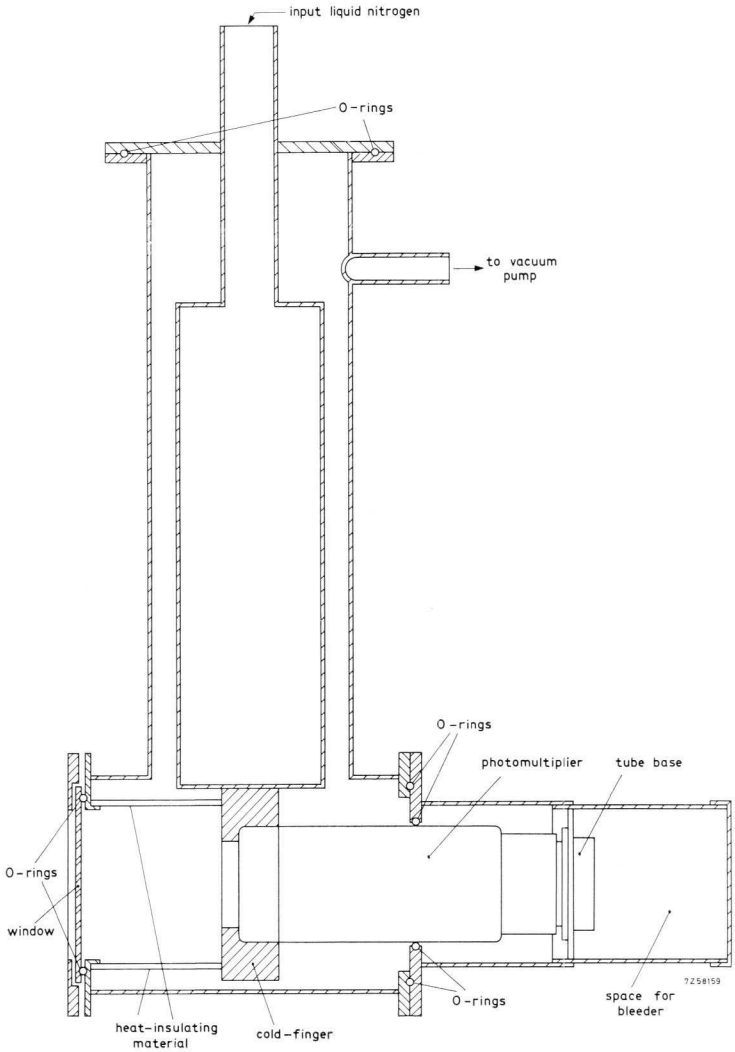

Fig. 97. Example of a cryostat for photomultipliers.

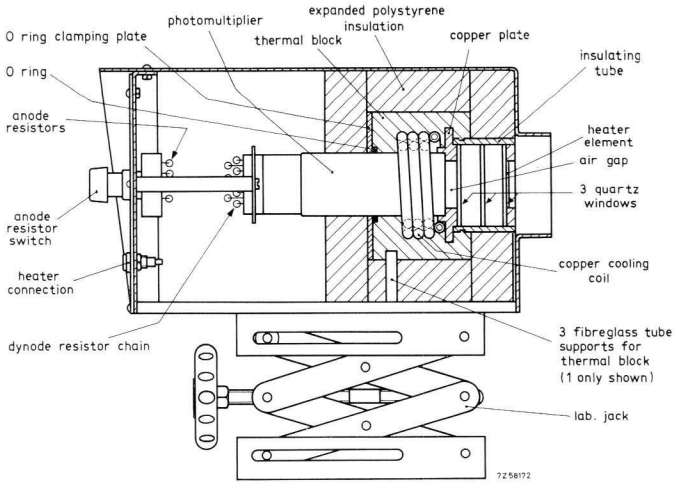

Fig. 98. Construction of the cooting unit.

Fig. 98 shows a very practical refrigerator that has been used to cool a 150 CVP photomultiplier to a temperature of —45 °C. If an ordinary thermostat is included the temperature can be adjusted to a higher value. The unit is based on an ordinary domestic refrigeration unit with a two stage condensor and a compressor; it can be mounted on castors for mobility.

Refrigerant is circulated through a double-wound copper coil that surrounds the photomultiplier and is imbedded in an eutectic alloy heat sink. The whole is thermally insulated by expanded polystyrene. So that the photocathode is evenly cooled, the window and a centimetre or so of the tube itself are cooled. A snug fit between heat sink and tube is ensured by shaping a copper plate to fit between them and giving it a smear of silicone grease on assembly.

Condensation on the photocathode window is prevented by cementing three circles of quartz glass into a tube of the same material to form a compound window. Each of the two chambers thus formed is dried by a little silica gel inserted before sealing. The front window is heated by a small element. The photomultiplier base is protected from condensation by wiring the resistors of the bleeder chain direct onto the socket: These dissipate about a third of a watt which is enough to prevent condensation without adversely affecting the cooling.

The photomultiplier housing and refrigeration unit are interconnected by flexible tubing covered with an insulating layer of rubber and synthetic material. Details of the construction are shown in Fig. 99.

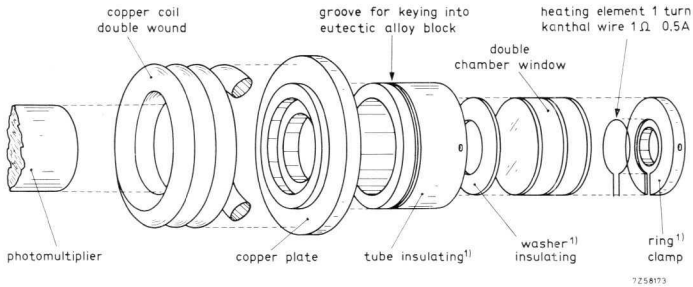

Fig. 99. Detail of the cooling unit and triple window.

Appendix

I Some Photometric Concepts

The spectral energy distribution of a light source $\Phi = f(\lambda)$, is determined by its properties: All the luminous energy of a sodium lamp, for example, is emitted at one characteristic wavelength (5890 Å); such light is monochromatic. Other light sources, for example fluorescent lamps, emit light at several discrete wavelengths as well as a continuous spectrum. A normal incandescent lamp with a tungsten filament emits only a continuous spectrum, the energy emitted by the filament per unit time depending on the material and the temperature of the filament.

If the properties of a helical or ribbon filament correspond to those of a "black body", its emitted energy can be calculated from the Stefan-Boltzmann law:

$$P = \sigma T^4, \tag{A1}$$

in which $\sigma = 5.669 \times 10^{-12}$ W·cm^{-2}·°K^{-1} and T is the temperature in °K. By Planck's law of radiation the energy can be expressed as a function of wavelength:

$$P(\lambda) = (2\pi hc^2/\lambda^5)/\{\exp(hc/\lambda kT) - 1\},$$

where h is the Planck constant (6.624×10^{-34} Js),
c is the speed of light (2.9979×10^{14} cm/s),
k is the Boltzmann constant (1.38×10^{-23} Ws/°K),
λ is the wavelength in cm.

$P(\lambda)$ is the power in W/cm^2·cm, in a solid angle of 2π steradians, per cm^2 surface area of the radiator, per cm wavelength interval. The constants $2\pi hc^2$ and hc/k are the first and second radiation constants respectively:

$$c_1 = 3.7413 \times 10^{-12} \text{ Wcm}^2$$

and

$$c_2 = 1.4380 \text{ cm°K}. \tag{A3}$$

In Fig. *A*1 the relative radiation energy P_{rel} of a black body is plotted as a function of wavelength with the temperature T as parameter. Using the Wien displacement law the curves can be derived from one another by multiplying the wavelength by T/T' and the ordinate by $(T'/T)^5$, where T' is the new temperature. The wavelength at which the radiation energy reaches a maximum is given by the relationship:

$$\lambda_{max} = 2898/T, \tag{A4}$$

in which λ is in μm and T in °K.

The radiation energy for radiators that are not ideal can be calculated if the emission factor as a function of the wavelength is known. The emission factor $e(\lambda)$ is defined as the ratio of the radiation output at a specific wavelength to that of an ideal black body, both at the same temperature.

As the radiation properties of tungsten are best known and closely approximate those of a black body, it is commonly used as a calibration light source for the visible range. Fig. *A*2 compares the relative spectral energy distribution of a black body at 2854 °K with that of a lamp with a tungsten ribbon filament. The black body temperature that has the maximum of its spectral energy distribution at the same wavelength as the source considered is called the colour temperature; the black body temperature to produce the same radiation intensity is the luminance temperature. Standard light sources have been laid down in the" International Lighting Dictionary" (3rd edition, C.I.E.); of these the "white *A* standard" is used for measurements on photosensitive elements. The standard light source has the spectral emission of a black body at 2854 °K, see Table *A*1. It is best approximated by a tungsten filament at 2800 °K.

Usually the emitted luminous flux is expressed in watts. In photometry however, it is customary to work with the total visible radiation, expressed in lumens. Luminous flux Φ is derived from the expression:

$$\Phi = 682 \int_0^\infty E(\lambda)V(\lambda) \cdot \mathrm{d}(\lambda), \tag{A5}$$

in which $E(\lambda)$ is the luminous flux in watts as a function of λ, and $V(\lambda)$ the standardized luminosity curve (Fig. *A*3) as laid down by the C.I.E. (see Table in Appendix II). The constant 682 has the dimension of lumens per watt, which gives 1 W = 682 lm for the wavelength at which the luminosity curve passes through a maximum (5550 Å).

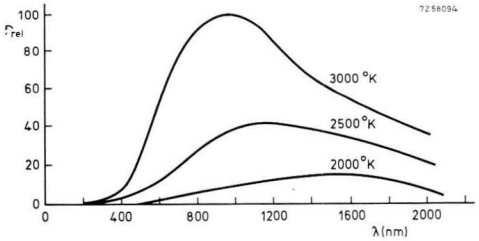

Fig. A1. Relative radiation energy of a black body as a function of the wavelength, with the absolute temperature as parameter.

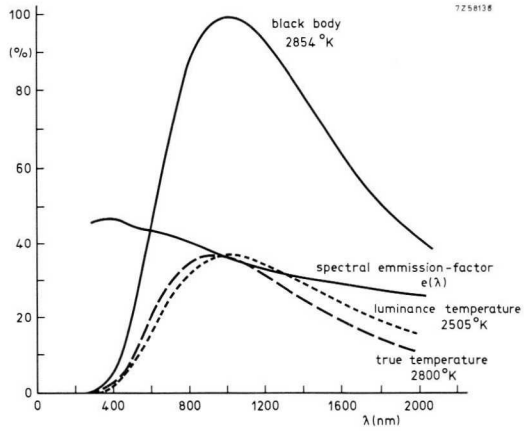

Fig. A2. Relative spectral energy distribution of a tungsten light source, derived from the product of the black body curve and the spectral emission factor e(λ).

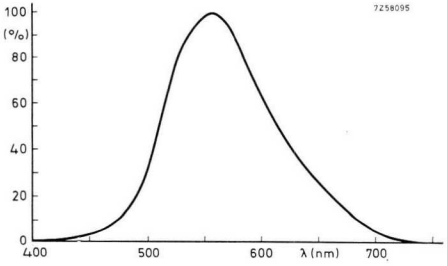

Fig. A3. Standardized luminosity curve.

Table A I
Relative energy distribution of a black body at a colour temperature of 2854 °K.

λ	E	λ	E	λ	E	λ	E	λ	E
0.30 μm	0.1%	0.50 μm	20.5%	0.70 μm	68.0%	0.90 μm	96.3%	1.10 μm	98.4%
0.31 μm	0.2%	0.51 μm	22.7%	0.71 μm	70.2%	0.91 μm	97.0%	1.11 μm	98.0%
0.32 μm	0.3%	0.52 μm	24.9%	0.72 μm	72.2%	0.92 μm	97.5%	1.12 μm	97.7%
0.33 μm	0.6%	0.53 μm	27.2%	0.73 μm	74.2%	0.93 μm	98.0%	1.13 μm	97.3%
0.34 μm	1.0%	0.54 μm	29.4%	0.74 μm	76.1%	0.94 μm	98.5%	1.14 μm	96.8%
0.35 μm	1.6%	0.55 μm	31.8%	0.75 μm	78.0%	0.95 μm	98.8%	1.15 μm	96.4%
0.36 μm	2.2%	0.56 μm	34.3%	0.76 μm	79.8%	0.96 μm	99.2%	1.16 μm	96.0%
0.37 μm	2.8%	0.57 μm	36.8%	0.77 μm	81.5%	0.97 μm	99.4%	1.17 μm	95.4%
0.38 μm	3.4%	0.58 μm	39.3%	0.78 μm	83.1%	0.98 μm	99.6%	1.18 μm	94.8%
0.39 μm	4.2%	0.59 μm	41.8%	0.79 μm	84.5%	0.99 μm	99.8%	1.19 μm	94.3%
0.40 μm	5.0%	0.60 μm	44.4%	0.80 μm	86.0%	1.00 μm	99.90%	1.20 μm	93.8%
0.41 μm	6.2%	0.61 μm	46.9%	0.81 μm	87.4%	1.01 μm	99.95%	1.21 μm	93.2%
0.42 μm	7.3%	0.62 μm	49.4%	0.82 μm	88.7%	1.02 μm	99.95%	1.22 μm	92.5%
0.43 μm	8.5%	0.63 μm	51.8%	0.83 μm	89.8%	1.03 μm	99.90%	1.23 μm	92.0%
0.44 μm	9.8%	0.64 μm	54.3%	0.84 μm	91.0%	1.04 μm	99.8%		
0.45 μm	11.4%	0.65 μm	56.7%	0.85 μm	92.9%	1.05 μm	99.6%		
0.46 μm	13.0%	0.66 μm	59.0%	0.86 μm	93.2%	1.06 μm	99.5%		
0.47 μm	14.8%	0.67 μm	61.4%	0.87 μm	94.0%	1.07 μm	99.3%		
0.48 μm	16.7%	0.68 μm	63.7%	0.88 μm	94.8%	1.08 μm	99.0%		
0.49 μm	18.5%	0.69 μm	66.0%	0.89 μm	95.6%	1.09 μm	98.7%		

The *illumination* E of a plane A is defined as the luminous flux per square metre and is expressed in lux (1 lx = 1 lm/m^2):

$$E = \mathrm{d}\Phi/\mathrm{d}A. \tag{A6}$$

The solid angle in which the light is emitted is expressed in steradians, and is defined as follows. A beam of light originating in a point source in the centre of a spherical space with a radius of 1 m has a solid angle of 1 sr if a surface area of 1 m^2 of the sphere is illuminated by the beam. If, at a distance r from the point source, the area of the spherical surface is S, the solid angle, expressed in sr, amounts to:

$$\omega = S/r^2. \tag{A7}$$

A sphere contains 4π sr.

The luminous flux emitted in a given direction per unit solid angle is defined as the luminous intensity I of the light source and is expressed in candelas (1 cd = 1 lm/sr):

$$I = \mathrm{d}\Phi/\mathrm{d}\omega. \tag{A8}$$

The candela is defined as follows. A black body at the freezing point of platinum (1769 °C) radiates light in a direction normal to the plane of the radiator with an intensity of 60 cd per cm^2.

The brightness to the human eye in a given direction is called the *luminance* B. The luminance of a surface element that radiates diffused light is understood to be the luminous intensity of that element, considered as a point source in the direction of observation, per unit of the apparent size of that element, as seen from that direction. The luminance, expressed in nits (1 nt = 1 cd/m^2), is given by:

$$B = I_\alpha/\Delta A \cos \alpha, \tag{A9}$$

in which I_α denotes the luminous intensity in the direction of observation, and α the angle between this direction and the normal to the surface.

With a perfect diffuser the luminance will be the same in all directions, which gives:

$$B = I_0/\Delta A = I_\alpha/\Delta A \cos \alpha = \text{constant}, \tag{A10}$$

whence

$$I_\alpha = I_0/\cos \alpha, \tag{A11}$$

in which I_0 denotes the luminous intensity in the direction normal to the surface element. Eq. (A11) is known as the *law of Lambert* for a perfect diffuser.

The relation between the several units in which luminance is frequently expressed, are given in Table *A* II.

Table A II

unit	nt	cd/ft^2	cd/in^2	ft-L	L	sb	apo-sb
1 nt	1	0.0929	6.45×10^{-4}	0.2919	$10^{-4}\pi$	10^{-4}	π
1 cd/ft^2	10.76391	1	6.94×10^{-3}	π	3.382×10^{-3}	1.076391×10^{-3}	33.82
1 cd/in^2	1550	144	1	452.4	0.4869	0.155	4869
1 ft-L	3.426259	$1/\pi$	2.211×10^{-3}	1	1.076391×10^{-3}	3.426259×10^{-4}	10.76391
1 L	$10^4/\pi$	295.7	2.054	929	1	$1/\pi$	10^4
1 sb	10^4	929	6.452	2919	π	1	$10^4\pi$
1 apo-sb	$1/\pi$	0.02957	2.054×10^{-4}	0.0929	10^{-4}	$(1/\pi)10^{-4}$	1

II Some Colorimetric Concepts[15]

Virtually all colours occurring in nature can be reproduced by additively mixing three spectral primaries, that is, by combining them so that they simultaneously reach the same part of the retina of the observer. In colorimetry the following primaries are used:

$$\left.\begin{array}{ll} \text{red}, & \lambda = 7000\ \text{Å}, \\ \text{green}, & \lambda = 5461\ \text{Å}, \\ \text{blue}, & \lambda = 4358\ \text{Å}. \end{array}\right\} \quad \text{(A12)}$$

The quantities of red (R), green (G) and blue (B) needed to reproduce a given colour by additive mixing are termed the chromaticity coordinates. The chromaticity coordinates R, G and B over the full spectrum for a light intensity of 1 lm are plotted in Fig. *A*4. As can be seen the coordinates are in some cases negative, which means that additive mixing of these primaries cannot reproduce the related colour.

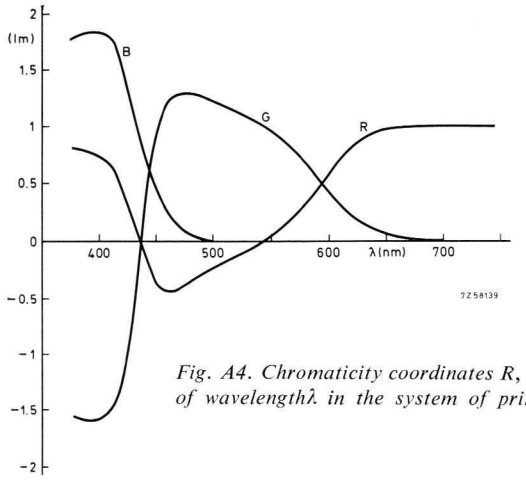

Fig. A4. Chromaticity coordinates R, G and B of 1 lm of the primaries of wavelength λ in the system of primaries according to eq. (A12).

The chromaticity coordinates of a non-chromatic light sample having a spectral energy distribution $E(\lambda)$ are given by:

$$\left.\begin{array}{l} R = 682 \int R(\lambda) \cdot E(\lambda) \cdot V(\lambda) \cdot \mathrm{d}(\lambda), \\ G = 682 \int G(\lambda) \cdot E(\lambda) \cdot V(\lambda) \cdot \mathrm{d}(\lambda), \\ B = 682 \int B(\lambda) \cdot E(\lambda) \cdot V(\lambda) \cdot \mathrm{d}(\lambda), \end{array}\right\} \quad \text{(A13)}$$

where R, G and B are in lumens, and in which $R(\lambda)$, $G(\lambda)$ and $B(\lambda)$ are the functions represented on Fig. A4. $V(\lambda)$ is the luminosity curve (cf. Fig. A3), and the factor 682 accounts for the luminous efficiency in lm/W.

The sum

$$R + G + B = L, \tag{A14}$$

gives the luminance of the sample and can be measured directly by an instrument whose spectral sensitivity corresponds to the luminosity curve $V(\lambda)$. The chromaticity coordinates R, G and B could be measured with instruments having spectral sensitivities corresponding to $R(\lambda) \cdot V(\lambda)$, $G(\lambda) \cdot V(\lambda)$ and $B(\lambda) \cdot V(\lambda)$ respectively. However, because the first two functions would require a partly negative sensitivity, which cannot be realized, the C.I.E. have developed a chromaticity coordinate system in which negative values do not occur. In place of the coordinate R, G and B, are three mutually independent linear combinations of R, G and B with coefficients such that one combination represents the luminance $L = R + G + B$. The new chromaticity coordinates X, Y and Z, called the tristimulus values, are related to R, G and B by the following expressions:

$$\left.\begin{aligned} X &= 2.7689\,R + 0.38159\,G + 18.801\,B, \\ Y &= \quad R + \quad G + \quad B, \\ Z &= \quad 0.01237\,G + 93.060\,B. \end{aligned}\right\} \tag{A15}$$

The coordinate Y thus defines the luminance L. Analogous to eq. (A13), we may express the X, Y and Z coordinates of the chromaticity $E(\lambda)$ by:

$$\left.\begin{aligned} X &= 682 \int \bar{X}(\lambda) \cdot E(\lambda) \cdot \mathrm{d}(\lambda), \\ Y &= 682 \int \bar{Y}(\lambda) \cdot E(\lambda) \cdot \mathrm{d}(\lambda), \\ Z &= 682 \int \bar{Z}(\lambda) \cdot E(\lambda) \cdot \mathrm{d}(\lambda), \end{aligned}\right\} \tag{A16}$$

in which

$$\left.\begin{aligned} \bar{X}(\lambda) &= [2.7689\,R(\lambda) + 0.38159\,G(\lambda) + 18.801\,B(\lambda)]\,V(\lambda), \\ \bar{Y}(\lambda) &= [\quad R(\lambda) + \quad G(\lambda) + \quad B(\lambda)]\,V(\lambda), \\ \bar{Z}(\lambda) &= [\quad 0.01237\,G(\lambda) + 93.060\,B(\lambda)]\,V(\lambda). \end{aligned}\right\} \tag{A17}$$

The functions $\bar{X}(\lambda)$, $\bar{Y}(\lambda)$ and $\bar{Z}(\lambda)$, termed the spectral distribution curves for a constant energy spectrum, are plotted in Fig. *A*5, their numerical values are given in Table *A* III.

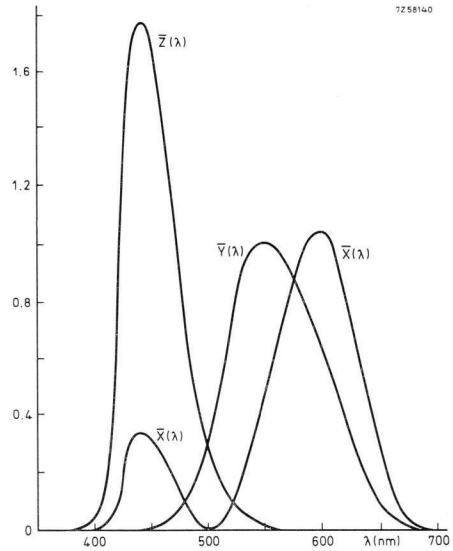

Fig. A5. Spectral distribution curves $\bar{x}(\lambda)$, $\bar{y}(\lambda)$ and $\bar{z}(\lambda)$ for a constant energy spectrum.

The coordinates X, Y and Z of a sample of light with spectral energy distribution $E(\lambda)$ can be found with measuring instruments whose spectral sensitivities correspond to $\bar{x}(\lambda)$, $\bar{y}(\lambda)$ and $\bar{z}(\lambda)$ respectively. Samples with the same coordinate ratio $X : Y : Z$ have the same chromaticity, but may differ in luminance. Luminance is defined by the coordinate Y which means that two quantities are sufficient for defining the chromaticity; it is customary to take two of the three quantities x, y and z, given by:

$$\left.\begin{aligned} x &= X/(X + Y + Z), \\ y &= Y/(X + Y + Z), \\ z &= Z/(X + Y + Z), \end{aligned}\right\} \qquad \text{(A18)}$$

$x + y + z$ being unity. We can now represent any chromaticity by a point in a plane with coordinates x and y. The resultant chromaticity diagram is shown in Fig. *A*6, one boundary of which is formed by the locus of points representing pure colours, the other is the purple boundary, which is a straight line between the ends of the spectrum locus. The centre of the diagram corresponds to white with coordinates $(x, y) = (0.33, 0.33)$. Proceeding from the boundary towards white, the saturation decreases from maximum to zero.

TABLE A.III

Tristimulus values for equal energy as functions of the wavelength. The value of

λ (μm)	$\overline{X}$	$\overline{Y}$	$\overline{Z}$	λ (μm)	$\overline{X}$	$\overline{Y}$	$\overline{Z}$
0.380	0.0014	0.0000	0.0065	0.480	0.0956	0.1390	0.8130
0.385	0.0022	0.0001	0.0105	0.485	0.0580	0.1693	0.6162
0.390	0.0042	0.0001	0.0201	0.490	0.0320	0.2080	0.4652
0.395	0.0076	0.0002	0.0362	0.495	0.0143	0.2586	0.3533
0.400	0.0143	0.0004	0.0679	0.500	0.0049	0.3230	0.2720
0.405	0.0232	0.0006	0.1102	0.505	0.0024	0.4073	0.2123
0.410	0.0435	0.0012	0.2074	0.510	0.0093	0.5030	0.1582
0.415	0.0776	0.0022	0.3713	0.515	0.0291	0.6082	0.1117
0.420	0.1344	0.0040	0.6456	0.520	0.0633	0.7100	0.0782
0.425	0.2148	0.0073	1.0391	0.525	0.1096	0.7932	0.0573
0.430	0.2839	0.0116	1.3856	0.530	0.1655	0.8620	0.0422
0.435	0.3285	0.0168	1.6230	0.535	0.2257	0.9149	0.0298
0.440	0.3483	0.0230	1.7471	0.540	0.2904	0.9540	0.0203
0.445	0.3481	0.0298	1.7826	0.545	0.3597	0.9803	0.0134
0.450	0.3362	0.0380	1.7721	0.550	0.4334	0.9950	0.0087
0.455	0.3187	0.0480	1.7441	0.555	0.5121	1.0002	0.0057
0.460	0.2908	0.0600	1.6692	0.560	0.5945	0.9950	0.0039
0.465	0.2511	0.0739	1.5281	0.565	0.6784	0.9786	0.0027
0.470	0.1954	0.0910	1.2876	0.570	0.7621	0.9520	0.0021
0.475	0.1421	0.1126	1.0419	0.575	0.8425	0.9145	0.0018

$\overline{Y}(\lambda)$ corresponds to the luminosity curve.

λ (μm)	$\overline{X}$	$\overline{Y}$	$\overline{Z}$	λ (μm)	$\overline{X}$	$\overline{Y}$	$\overline{Z}$
0.580	0.9163	0.8700	0.0017	0.680	0.0468	0.0170	0.0000
0.585	0.9786	0.8163	0.0014	0.685	0.0329	0.0119	0.0000
0.590	1.0263	0.7570	0.0011	0.690	0.0227	0.0082	0.0000
0.595	1.0567	0.6949	0.0010	0.695	0.0158	0.0057	0.0000
0.600	1.0622	0.6310	0.0008	0.700	0.0114	0.0041	0.0000
0.605	1.0456	0.5668	0.0006	0.705	0.0081	0.0029	0.0000
0.610	1.0026	0.5030	0.0003	0.710	0.0058	0.0021	0.0000
0.615	0.9384	0.4412	0.0002	0.715	0.0041	0.0015	0.0000
0.620	0.8544	0.3810	0.0002	0.720	0.0029	0.0010	0.0000
0.625	0.7514	0.3210	0.0001	0.725	0.0020	0.0007	0.0000
0.630	0.6424	0.2650	0.0000	0.730	0.0014	0.0005	0.0000
0.635	0.5419	0.2170	0.0000	0.735	0.0010	0.0004	0.0000
0.640	0.4479	0.1750	0.0000	0.740	0.0007	0.0003	0.0000
0.645	0.3608	0.1382	0.0000	0.745	0.0005	0.0002	0.0000
0.650	0.2835	0.1070	0.0000	0.750	0.0003	0.0001	0.0000
0.655	0.2187	0.0816	0.0000	0.755	0.0002	0.0001	0.0000
0.660	0.1649	0.0610	0.0000	0.760	0.0002	0.0001	0.0000
0.665	0.1212	0.0446	0.0000	0.765	0.0001	0.0000	0.0000
0.670	0.0874	0.0320	0.0000	0.770	0.0001	0.0000	0.0000
0.675	0.0636	0.0232	0.0000	0.775	0.0000	0.0000	0.0000

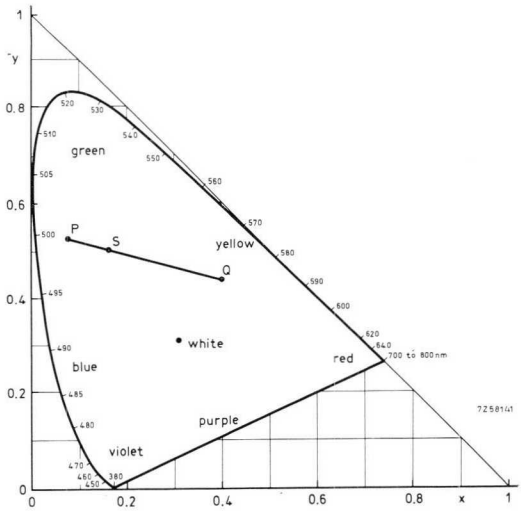

Fig. A6. Chromaticity diagram.

The coordinates of point P with luminance Y_P are:

$$\left.\begin{aligned} X_P &= (x_P/y_P)Y_P, \\ Y_P &= Y_P, \\ Z_P &= \{1-(x_P+y_P)/y_P\}Y_P \end{aligned}\right\} \qquad \text{(A19)}$$

The coordinates of point Q with luminance Y_Q are:

$$\left.\begin{aligned} X_Q &= (x_Q/y_Q)Y_Q, \\ Y_Q &= Y_Q, \\ Z_Q &= \{1-(x_Q+y_Q)/y_Q\}Y_Q. \end{aligned}\right\} \qquad \text{(A20)}$$

The coordinates of the mixture are obtained by simply adding these coordinates, hence:

$$X_S = X_P + X_Q, \quad Y_S = Y_P + Y_Q, \quad Z_S = Z_P + Z_Q, \qquad \text{(A21)}$$

in which $Y_S = Y_P + Y_Q$ gives the luminance of the mixture.

Point S can also be found by the "centre of gravity rule". Imagine a mass $X_P + Y_P + Z_P$ at point P and a mass $X_Q + Y_Q + Z_Q$ at point Q; their centre of gravity S is then the chromaticity to be found; it will

always be situated on the line that links P and Q. It can be derived from eqs ($A19$) and ($A20$) that:

$$X_P + Y_P + Z_P = Y_P/y_P, \tag{A22}$$

and

$$X_Q + Y_Q + Z_Q = Y_Q/y_Q. \tag{A23}$$

Several investigations have shown that the colour differences perceptibe to the human eye are not identical for all colours[16]. If the least perceptible colour difference for various colours are plotted in the chromaticity diagram they do not appear as equal distances.

The results of MacAdam's colour discrimination measurements have been plotted in Fig. $A7$, the axes of the ellipses having been exaggerated by a factor of 10 for the sake of clarity. These axes correspond to the standard deviation of measuring results obtained from investigation on the colour discrimination of the human eye. The least colour difference than can be perceived is expressed in terms of the Just Noticeable Differences (J.N.D.s).

That the distances between equal colour differences do not correspond to equal distances in the C.I.E. chromaticity diagram is a nuisance that several investigators have sought a transformation of the diagram to overcome.[16] MacAdam has suggested a fairly simple transformation:[17]

$$\left.\begin{aligned} u &= 2x/(6y - x + 1.5), \\ v &= 3y/(6y - x + 1.5), \end{aligned}\right\} \tag{A24}$$

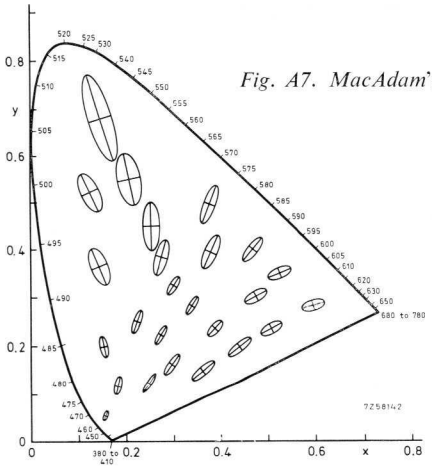

Fig. A7. MacAdam's colour discrimination measurements.

in which x and y are the coordinates of the C.I.E. diagram, and u and v the corresponding coordinates of that due to MacAdam. This "uniform chromaticity chart" is shown in Fig. *A*8.

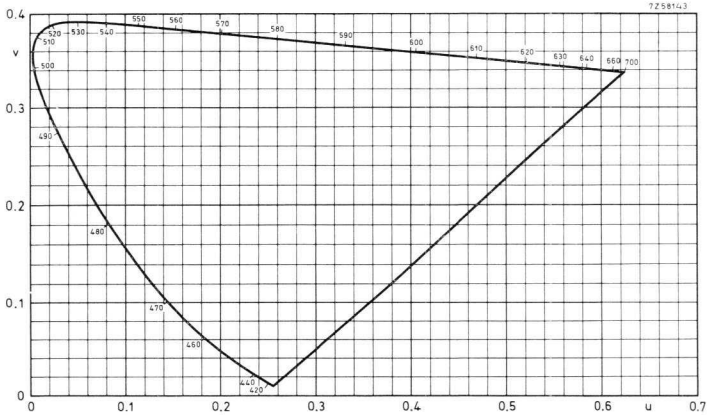

Fig. A8. Uniform chromaticity scale according to MacAdam.

The magnitude of a colour shift, expressed in J.N.D.s can be calculated from the expression:

$$\text{J.N.D.} = 260\ \{(u_1 - u_2)^2 + (v_1 - v_2)^2\}^{\frac{1}{2}}, \qquad \text{(A25)}$$

where u_1, v_1 are the coordinates of the original chromaticity and u_2, v_2 those of the new one.

III Influence of Spectral Sensitivity Spread in Colour Television

To gain an insight into the influence of the spread in spectral sensitivity of the photomultiplier, we shall briefly discuss

— how the spectral sensitivity curves of the colour channels are fixed;
— the factors that influence them;
— how deviation from the ideal curve can be expressed vectorially in a chromaticity diagram.

The requirements imposed on the spectral sensitivity of the three colour

channel depends on the three primary colours. They must fulfil the following conditions:

— the triangle formed by their coordinates must cover the largest possible area of the chromaticity diagram;
— the colours must be such that they can be conveniently reproduced by available phosphors.

These arguments have led to the choice of the following colour points:

red with coordinates $(x, y) = (0.67, 0.33)$,
green with coordinates $(x, y) = (0.21, 0.71)$,
blue with coordinates $(x, y) = (0.14, 0.08)$.

These points are indicated in the chromaticity diagram shown in Fig. *A*9 (see Appendix II). The colour range lying within or on the lines joining the points (hatched area in Fig. *A*9) can be reproduced by the system. Practically all natural colours and most artificial colours are reproducible.

The spectral sensitivity of the three colour channels also depend on the normalization of the amplitude of the colour signals required for obtaining white light. The signals S_r, (red) S_g, (green) and S_b, (blue) needed to produce white are usually taken as unity. The colour point for the white light radiated by a picture tube usually lies in the vicinity of "standard white C", corresponding to point C in Fig. *A*9 with coordinates $x = 0.310$ and $y = 0.316$. Taking as a starting point a given luminance L for standard white C, the luminance contribution l_r, l_g and l_b of each colour channel can be derived by eqs (*A*19) and (*A*15) and by applying the additively rule. Taking into account the normalization of the colour signals for standard white C, we thus find:

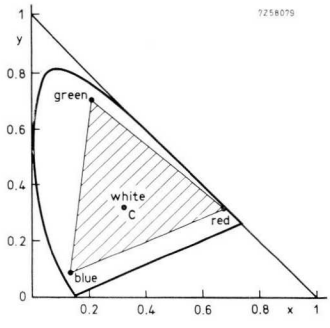

Fig A9. Colour points for flying spot scanning.

$l_r = 0.298L$, corresponding to $S_r = 1$,
$l_g = 0.588L$, corresponding to $S_g = 1$,
$l_b = 0.114L$, corresponding to $S_b = 1$.

Assuming the reproducing equipment to be linear i.e., that luminous flux produced is proportional to the amplitudes of S_r, S_g and S_b, this yields:

$$l_r = 0.298LS_r, \quad l_g = 0.588LS_g, \quad l_b = 0.114SB_b. \qquad \text{A 26}$$

By substituting eq. (A26) in eq. ((*A*16) we find the colour coordinates X Y and Z as functions of S_r, S_g and S_b. From this, for exact colour rendition the signals S_r, S_g and S_b as functions of the wavelength should satisfy the following:

$$\begin{aligned}(L/k)S_r(\lambda) &= 1.92\bar{X}(\lambda) - 0.535\,\bar{Y}(\lambda) - 0.29\bar{Z}(\lambda),\\ (L/k)S_g(\lambda) &= -0.984\bar{X}(\lambda) + 2.00\,\bar{Y}(\lambda) - 0.0247\bar{Z}(\lambda),\\ (L/k)S_b(\lambda) &= 0.0588\bar{X}(\lambda) - 0.119\,\bar{Y}(\lambda) + 0.901\bar{Z}(\lambda),\end{aligned} \qquad \text{A 27}$$

in which $\bar{X}(\lambda)$, $\bar{Y}(\lambda)$ and $\bar{Z}(\lambda)$ denote the tristimulus values for a constant energy spectrum, as represented in Fig. *A*5 and in Table *A* III. Fig. *A*10 shows the spectral sensitivities for the three colour channels, calculated from eq. *A* 27. It is seen from this graph that in several wavelength ranges a negative sensitivity is required. Since this cannot easily be realized, and since neglecting the negative parts of the curves does not lead to serious errors in colour rendition, they are usually disregarded. The positive parts of the curves are determined by:

— the spectral composition of the light from the flying spot tube;
— the spectral properties of the dichroic mirror;
— the spectral sensitivity of the photomultipliers.

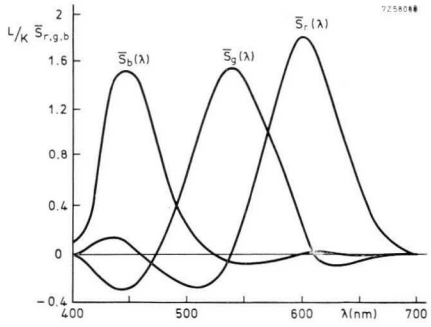

Fig. A10. Calculated spectral sensitivities of the three colour channels.

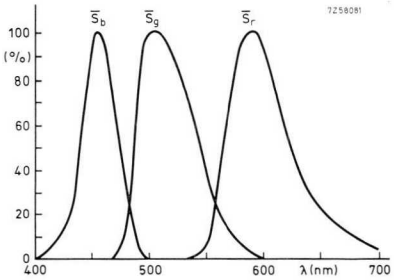

Fig. A11. Relative spectral sensitivities of the three colour channels in a flying spot scanner, as encountered in practice.

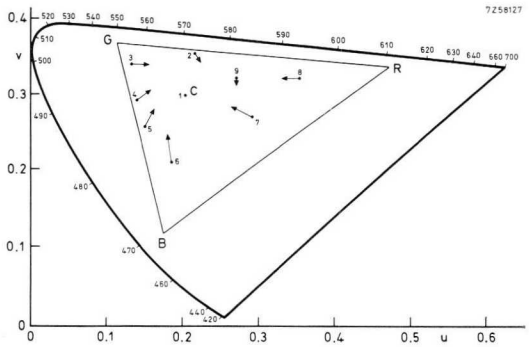

Fig. A12. Colour shifts attributable to differences between the practical and theoretical sensitivity.

Filters may be used to correct deviations from the positive parts of the curves of Fig. *A*10. Fig. *A*11 shows the relative spectral sensitivities encountered in practice.

Fig. *A*12 shows the colour shifts caused by the differences between practical and theoretical sensitivities, plotted on the "MacAdam's uniform chromaticity chart" (see Appendix II). The tails of the arrows are on the *u*-*v* coordinates of the original colour and the heads on the coordinates of the reproduced colour. These shifts expressed in "Just Noticeable Differences" (J.N.D.) will be found in column "J.N.D.2" in Table *A* IV. The table quotes the number of J.N.D.s caused by a spectral sensitivity shift in the photomultiplier in the red channel. The

spectral sensitivity curves of this photomultiplier, on which the columns "J.N.D.1", "J.N.D.2" and "J.N.D.3" are based, are shown in Fig. *A*13. The spread appears to have little influence on the colour errors present.

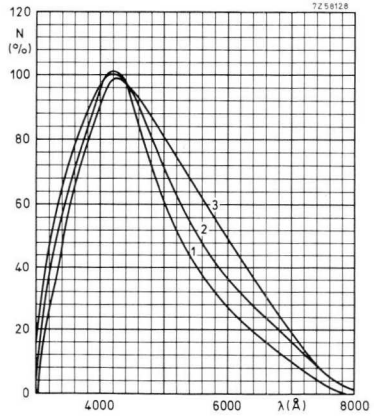

Fig. A13. Possible spread of the spectral sensitivity of the photomultiplier in the "red" channel.

In general, it may be concluded that the spectral sensitivities of the three colour channels are determined mainly by the dichroic mirror, but that in the red channel the influence of the flying spot tube is quite considerable.

Table A IV

	(*x*,) *y* coord.		(*u*,)*v* coord.		J.N.D.		
	x	*y*	*u*	*v*	1	2	3
1 white C	0.310	0.316	0.201	0.307	0.13	0.13	0.13
2 greenish-yellow	0.407	0.457	0.212	0.357	3.63	3.63	3.63
3 green	0.260	0.459	0.130	0.347	6.36	6.46	6.38
4 blue green	0.217	0.313	0.135	0.297	5.41	5.46	5.48
5 blue	0.207	0.237	0.151	0.262	6.21	6.25	6.21
6 purplish-blue	0.207	0.157	0.188	0.212	10.47	10.48	10.46
7 purplish-pink	0.362	0.231	0.287	0.275	8.22	8.29	8.55
8 pink	0.503	0.317	0.347	0.328	5.75	5.92	6.16
9 red	0.633	0.269	0.262	0.325	2.22	2.26	2.28

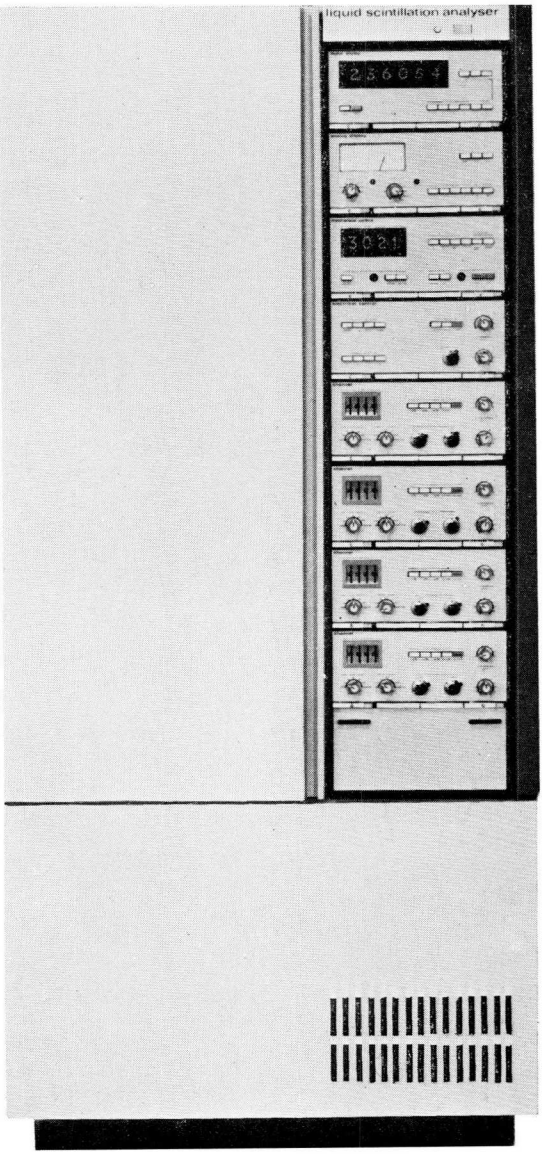

Analyser used in liquid scintillation counting.

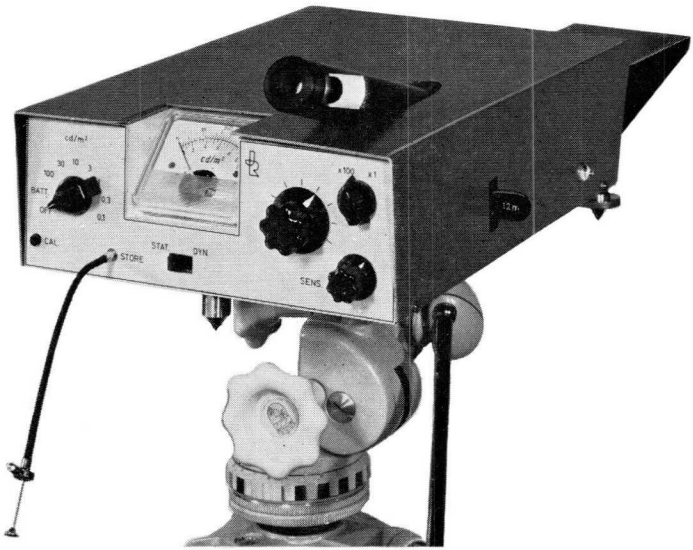

Luminence meter using XP1110 photomultiplier. It is used for measuring the luminence of road surfaces.

Bibliography

1 Document 39 (Central Office) 228 and Publication 306-1 of the International Electrotechnical Commission, June 1969.

2 W. E. SPICER and F. WOOTEN, Photoemission and Photomultipliers, Proc. I.E.E.E. Aug. 1963, pp. 1119-1126.

3 H. FRÖHLICH and R. A. SACK, Light Absorption and Selected Photo-Effect in Absorbed Layers, Proc. Phys. Soc. (London) **59**, pp. 30-33, Jan. 1947.

4 MAYER and THOMAS, Z. Phys. pp 147-149, 1957.

5 W. E. SPICER, Photoemissive, Photoconductive and Optical Absorption Studies of Alkali-Antimony Compounds, Phys. Rev. **112**, pp 114-122, Oct. 1958.

6 R. BARBIER, Etude de l'activation du bruit des photocathodes sous l'influence de la lumière.

7 A. MAYER, Das Frequenzverhalten von magnetischen Abschirmröhren, Frequenz **22**, pp 24-27, 1968.

8 ALDERS VAN DER ZIEL, Noise, Prentice-Hall, Inc.,

9 E. BREITENBERGER, Scintillation Spectrometer Statistics, Prog. Nucl. Phys. **4**, pp 56-94, 1956.

10 J. R. PRESCOTT, A Statistical Model for Photomultipliers Single-Electron Statistics, Nucl. Instr. and Meth. **39**, pp 173-179, 1966.

11 Document 39 (Central Office) 228 of the International Electrotechnical Commission, June 1969.

12 M. H. SWEET, Electronics, p. 105, November, 1946.

13 U. J. ROOSE, Ein rückwirkungsfreien Dynodengate für Photomultiplier, Nucl. Instr. and Methods **36**, pp. 333-334, 1965.

14 ARDALAN ABDUL HAMID, Comportement en température des couches photoémissives en cas de photomultiplicateurs utilisés dans les compteurs à scintillations, Rapport C.E.A. - R.2995, Centre d'Etudes Nucléaires de Saclay, 1966.

15 F. W. DE VRIJER, Fundamentals of Colour Television, Philips techn. Rev. **19**, pp. 86-97, 1957 (No. 3).

16 H. D. MURRAY, Colour in Theory and Practice, Chapman and Hall Ltd., London, 1952.

17 D. L. MACADAM, Projective Transformations of I.C.I. Colour Specifications, J. Opt. Soc. Am. **29**, p. 370, 1939; Chapman and Hall Ltd. London, 1952.

List of the Main Symbols

W	kinetic energy of an electron
h	Planck constant
ν	frequency
c	speed of light
λ	wavelength
ϕ	work function of an electron
ν_0	threshold frequency
λ_0	threshold wavelength
η_q	quantum efficiency
α_{tot}	total optical absorption of a material
α_{pe}	part of the total absorption that causes photoemission
α_c	part of the total absorption that causes photoconduction
l_0	mean escape depth of an electron from a material
T	temperature
e	charge of an electron
k	Boltzmann constant
N_{kr}	radiant cathode sensitivity
m	mass of an electron
E	electric field strength
V_b	supply voltage
V_s	interdynode voltage
δ	secondary emission factor
G	gain
n	number of dynodes
N_e	number of electrons
Φ	luminous or radiant flux
τ	time interval
N_p	number of photons
η_c	collection efficiency
I	d.c. current
Q	charge
B	magnetic induction
H	magnetic field strength
μ	permeability
P	power or energy
N_k	cathode luminous sensitivity
E	illumination
A	surface area
D	index for drift
SH	index for shift
I_{a0}	d.c. anode dark current
Δf	bandwidth
σ	standard deviation
σ^2	variance
v	relative variance
η_{sp}	single photon detection efficiency
N_s	number of signal pulses
N_0	number of dark current pulses (background)
N_a	anode luminous sensitivity
N_{ar}	anode radiant sensitivity
i	varying current

Technology relating to the products described in this publication is shared by the following firms.

Argentina
FAPESA I.y.C.
Melincué 2594
Tel. 50-9941/8155
BUENOS AIRES

Australia
Philips Electrical Pty. Ltd.
Miniwatt Electronics Division
20, Herbert St.
Tel. 43-2171
ARTARMON, N.S.W.

Austria
WIVEG
Prinz Eugenstrasse 32
Tel. 65 16 21
1041 WIEN

Belgium
M.B.L.E.
80, rue des Deux Gares
Tel. 23 00 00
BRUXELLES 7

Brazil
IBRAPE S.A.
Rua Manoel Ramos Paiva 506
Tel. 93-5141
SAO PAULO

Canada
Philips Electron Devices
116 Vanderhoof Ave.
Tel. 425-5161
TORONTO 17, Ontario

Chile
Philips Chilena S.A.
Av. Santa Maria 0760
Tel. 39 40 01
SANTIAGO

Columbia
SADAPE S.A.
Calle 19, No. 5-51
Tel. 422-175
BOGOTA D.E. 1

Denmark
Miniwatt A/S
Emdrupvej 115
Tel. 69 16 22
KØBENHAVN NV

Finland
Oy Philips A.B.
Elcoma Division
Kaivokatu 8
Tel. 10 915
HELSINKI 10

France
R.T.C.
La Radiotechnique-Compelec
Avenue Ledru Rollin 130
Tel. 797-99-30
PARIS 11

Germany
VALVO G.m.b.H.
Valvo Haus
Burchardstrasse 19
Tel. (0411) 33 91 31
2 HAMBURG 1

Greece
Philips S.A. Hellénique
Service Division
54, Av. Syngrou
ATHENES

Hong Kong
Philips Hong Kong Ltd.
Components Dept.
St. George's Building, 21st Fl.
Tel. K—42 82 05
HONG KONG

India
INBELEC Div. of
Philips India Ltd.
Band Box Building
254-D, Dr. Annie Besant Road
Tel. 45 33 86,
Worli, BOMBAY 18 (WB)

Indonesia
P.T. Philips-Ralin Electronics
Elcoma Division
Djalan Gadjah 18
Tel. 44 163
DJAKARTA

Ireland
Philips Electrical (Ireland) Pty.
Newstead, Clonskeagh
Tel. 69 33 55
DUBLIN 6

Italy
Philips S.p.A.
Sezione Elcoma
Piazza IV Novembre 3
Tel. 69.94
MILANO

Japan
I.D.C.C. Ltd.
Kokusai Building, 7th floor
Marunouchi
Tel. (213) 6751.7
TOKYO

Mexico
Electrónica, S.A. de C.V
Varsovia No. 36
Tel. 5-33-11-80
MEXICO 6, D.F.

Netherlands
Philips Nederland N.V.
Afd. Elonco
Boschdijk, VB
Tel. (040) 43 33 33
EINDHOVEN

New Zealand
EDAC Ltd.
70-72 Kingsford Smith Street
Tel. 873 159
WELLINGTON

Norway
Electronica A/S
Middelthunsgate 27
Tel. 46 39 70
OSLO 3

Peru
CADESA
Av. Abancay 1176
Tel. 7 73 17
LIMA

Portugal
Philips Portuguesa S.A.R.L.
Rua Joaquim Antonio de Aguiar 66,
Tel. 68 31 21/9
LISBOA

South Africa
EDAC (Pty) Ltd.
South Park Lane
New Doornfontein
Tel. 24/6701-2
JOHANNESBURG

Spain
COPRESA S.A.
Balmes 22
Tel. 2 32 03 00
BARCELONA 7

Sweden
ELCOMA A.B.
Lidingövägen 50
Tel. 08/67 97 80
10250 STOCKHOLM 27

Switzerland
Philips A.G.
Edenstrasse 20,
Tel. 051/44 22 11
CH-8027 ZUERICH

Taiwan
Philips Taiwan Ltd.
Tel. 55 97 42
TAIPEI

Turkey
Türk Philips Ticaret A.S.
EMET Department
Gümüssuyu Cad. 78-80
Tel. 45.32.50
Beyoglü, ISTANBUL

United Kingdom
Mullard Ltd.
Mullard House
Torrington Place
Tel. 01-580 6633
LONDON W.C. 1

United States
Amperex Electronic Corp.
Electron Tubes Div.
Tel. 516 WE 1-6200
HICKSVILLE N.Y

Uruguay
Luzilectron S.A.
Rondeau 1567, piso 5
Tel. 9 43 21
MONTEVIDEO

Venezuela
C.A. Philips Venezolana
Elcoma Department
Colinas de Bello Monte
Tel. 72.01.51
CARACAS

Printed in The Netherlands 2IC33 ③⑤㉒ 9399 243 05201